MATHEMATICAL MODELLING OF TUMOUR-IMMUNE COMPETITION AND TUMOUR GROWTH: DISCRETE AND CONTINUUM APPROACHES

Fiona Ruth Macfarlane

A Thesis Submitted for the Degree of PhD
at the
University of St Andrews

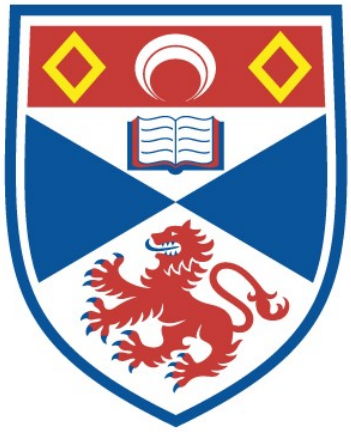

2019

Mathematical modelling of tumour-immune competition and tumour growth: Discrete and continuum approaches

Fiona Ruth Macfarlane

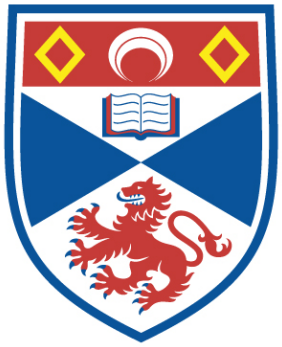

University of
St Andrews

This thesis is submitted in partial fulfilment for the degree of

Doctor of Philosophy (PhD)

at the University of St Andrews

March 2019

Abstract

The ability of the human immune system to detect and remove cancer cells is exploited in the development of immunotherapy techniques. However, further understanding of these mechanisms is required and can be achieved through the use of mathematical models. In this thesis, we develop a simple individual-based model of cell movement and illustrate the ability of our model to qualitatively reproduce the migration patterns of immune cells that have been observed in single cell tracking experiments. We then extend the model to describe the spatio-temporal interactions between dendritic cells, cytotoxic T cells and a solid tumour. Through further extension of the model, we explicitly consider the immune recognition of evolving tumour antigens. Computational simulations of our models further clarify the conditions for the onset of a successful immune action against cancer cells and may suggest possible targets to improve the efficacy of immunotherapy. Mathematically, individual-based models can be limited in their amenability to different analysis techniques which are better suited to continuum models. To overcome this, we aim to derive the continuum version of our described individual-based models. However, due to the complexity of the biological mechanisms included, we first consider a simpler biological situation. We develop an individual-based model describing the spatial dynamics of multicellular systems whereby cells undergo pressure-driven movement and pressure-dependent proliferation. From this, we formally derive nonlinear partial differential equations that are commonly used to model the spatial dynamics of growing cell populations. Through systematic comparison of both models, we demonstrate that the results of computational simulations of the individual-based model faithfully mirror the qualitative and quantitative properties of the solutions to the corresponding partial differential equations. This method could be adapted to more complex individual-based models, such as those we describe in this work.

Candidate's declaration

I, Fiona Ruth Macfarlane, do hereby certify that this thesis, submitted for the degree of PhD, which is approximately 29,000 words in length, has been written by me, and that it is the record of work carried out by me, or principally by myself in collaboration with others as acknowledged, and that it has not been submitted in any previous application for any degree.

I was admitted as a research student at the University of St Andrews in September 2015.

I received funding from an organisation or institution and have acknowledged the funder(s) in the full text of my thesis.

Date Signature of candidate

Supervisor's declaration

I hereby certify that the candidate has fulfilled the conditions of the Resolution and Regulations appropriate for the degree of PhD in the University of St Andrews and that the candidate is qualified to submit this thesis in application for that degree.

Date Signature of supervisor

Permission for publication

In submitting this thesis to the University of St Andrews we understand that we are giving permission for it to be made available for use in accordance with the regulations of the University Library for the time being in force, subject to any copyright vested in the work not being affected thereby. We also understand, unless exempt by an award of an embargo as requested below, that the title and the abstract will be published, and that a copy of the work may be made and supplied to any bona fide library or research worker, that this thesis will be electronically accessible for personal or research use and that the library has the right to migrate this thesis into new electronic forms as required to ensure continued access to the thesis.

I, Fiona Ruth Macfarlane, have obtained, or am in the process of obtaining, third-party copyright permissions that are required or have requested the appropriate embargo below.

The following is an agreed request by candidate and supervisor regarding the publication of this thesis:

Printed copy

No embargo on print copy.

Electronic copy

No embargo on electronic copy.

Date Signature of candidate

Date Signature of supervisor

Underpinning Research Data or Digital Outputs

Candidate's declaration

I, Fiona Ruth Macfarlane, understand that by declaring that I have original research data or digital outputs, I should make every effort in meeting the University's and research funders' requirements on the deposit and sharing of research data or research digital outputs.

Date Signature of candidate

Permission for publication of underpinning research data or digital outputs

We understand that for any original research data or digital outputs which are deposited, we are giving permission for them to be made available for use in accordance with the requirements of the University and research funders, for the time being in force.

We also understand that the title and the description will be published, and that the underpinning research data or digital outputs will be electronically accessible for use in accordance with the license specified at the point of deposit, unless exempt by award of an embargo as requested below.

The following is an agreed request by candidate and supervisor regarding the publication of underpinning research data or digital outputs:

No embargo on underpinning research data or digital outputs.

Date Signature of candidate

Date Signature of supervisor

Acknowledgements

I would like to take this opportunity to first and foremost thank God for the blessings he has given and for being my strength and guide in all things.

Furthermore, I would like to thank several people for their help and support in the completion of this thesis. Firstly, I would like to thank my supervisors, Mark Chaplain and Tommaso Lorenzi, for insightful discussions, their support and their guidance over the course of my PhD. I am grateful for the time and energy they have given to support my work. Moreover, I wish to thank the entire St Andrews Math Biology (StAMBio) research group, the wider School of Mathematics and Statistics and my fellow PhD students for their encouragement. In particular, I am grateful to Linnéa Franßen for being a great officemate and friend. I would like to thank her for always encouraging and reassuring me in work and life matters.

My family have always been a great support throughout my life, and I would especially like to thank my dad, Colin, and my siblings: Christine, Peter, Susan and Alastair, for their constant love and encouragement in everything that I do. Furthermore, I am grateful to my wider Gate Church and Girls' Brigade families for their friendship, wisdom and support. In particular, I would like to thank my small group and those within the young adult ministry for their friendship, words and prayers which have been a great comfort in the good times and the hard times. I would also like to thank my friends, Caitlin and Aimée for their support and for making me keep in touch throughout our PhD journeys.

Finally, I would not have embarked upon an academic career if it had not been for the encouragement of my late mother. I would like to express my sincere gratitude for her wisdom, example, love and limitless support. Although I still cannot believe she is not here for the final part of my PhD journey, I know that she will always be watching and hope that she would be proud.

Funding

The funding for this work was provided by the University of St Andrews School of Mathematics and Statistics, 2015 Doctoral Training Grant (DTG) funded provided by the Engineering and Physical Sciences Research Council (EPSRC).

Contents

Chapter 1

Introduction

Cancer is defined as '*a disease caused by uncontrolled division of abnormal cells in a part of the body*' (Oxford University Press, 2019). With over two hundred types of cancer, each with their own causes, symptoms and treatment options, research into this group of diseases is continually expanding and becoming more diverse. The prevalence of these diseases is vast, in particular, in the UK around 50% of the population will be diagnosed with some form of cancer in their life (Cancer Research UK, 2018). Furthermore, over 18 million new cases of cancer and over 9 million deaths due to cancer were reported globally in 2018 (Bray et al., 2018; Ferlay et al., 2018), see Figure 1.1. Consequently, most, if not all, of the UK (and global) population will be, directly or indirectly, affected by cancer over their lifetime.

Traditionally, chemotherapy treatments, radiotherapy treatments and surgery have been administered to manage and treat a wide range of cancers. However, side effects of these treatment approaches can be severe. For example, they can include: sustained damage to healthy cells, nausea, fertility issues, hair loss and psychological issues (Carelle et al., 2002; Coates et al., 1983). More recently, the focus of cancer therapy research has turned to developing targeted and more personalised treatment

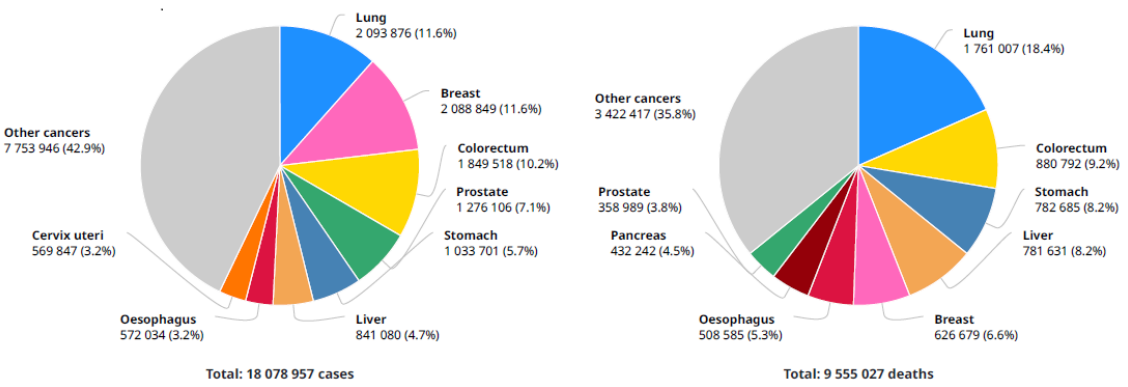

Figure 1.1: Global cancer incidence rates and mortality rates (2018). *The left pie chart shows the number of new cases worldwide of different types of cancer in 2018 for both sexes and all ages. The right pie chart shows the number of cancer deaths worldwide for different types of cancer in 2018 for both sexes and all ages.*

Figure adapted from the Global Cancer Observatory website (Ferlay et al., 2019) taking data from (Bray et al., 2018; Ferlay et al., 2018). © International Agency for Research on Cancer 2019

against cancers. The development of these new treatment approaches relies on the understanding of the key mechanisms, or hallmarks (Hanahan and Weinberg, 2011), which underpin this group of diseases. One key hallmark is the ability of cancer cells to evade the immune response, which naturally suggests that the immune system can also control cancer to a limited extent.

The immune system is a complex collection of cells, structures and processes which allow for the destruction of harmful foreign substances that invade the human body. Additionally, the immune system can retain memory of these substances to allow for a prompt response in the event of re-exposure. A notable aspect of the immune system is the ability to target only the harmful substances and not healthy cells within the body. This makes the immune system a potentially useful mechanism for controlling and treating cancers. Consequently, immunotherapy techniques have been, and continue to be, developed to utilise these properties and offer a more

personalised form of cancer treatment (Coulie et al., 2014; Fesnak et al., 2016; Gotwals et al., 2017). However, the development and testing of new therapy techniques can be an expensive and time-consuming process.

Mathematical modelling has been used previously to describe complex biological interactions including tumour-immune competition. These models allow for a greater understanding of these interactions and can be used to distinguish the key underlying mechanisms. Furthermore, mathematical models allow for the time-efficient and inexpensive testing of potential treatment ideas that, upon success, can be further investigated by experimentalists and clinicians. In this work, we aim to use mathematical modelling techniques to investigate the dynamical interactions occurring between the cells of the immune system and a solid tumour, including biologically relevant parameters where possible.

In Chapter 2, we begin with an overview of the key biological and immunological mechanisms involved in the recognition and removal of solid tumours and provide a short review of current immunotherapy techniques. We specifically focus on the role of dendritic cells and cytotoxic T lymphocytes which can recognise, and respond to, antigens expressed by tumour cells. Following this, a summary of the previously used and currently used mathematical modelling techniques within the field of mathematical oncology is given in Chapter 3. In particular, we highlight models and techniques used to describe the biophysical properties of cells and tumour-immune interactions. Following these background chapters, we provide the main body of this work.

To capture the experimentally observed migration patterns of immune cells we develop an individual-based random walk model for cell motion in Chapter 4. In particular, we consider a homogeneous cell population (*i.e.* all cells exhibit the same phenotype) and allow the cell population to perform one of two random walks: a

Lévy walk or Brownian motion. Through observations of the resulting cell trajectories, we compare both stochastic models. We illustrate the ability of our model to reproduce qualitatively the spatial trajectories of immune cells in the tumour microenvironment observed in experimental data of single cell tracking. In correspondence with experimental findings, a Lévy walk appears to capture the movement of inactive immune cells, whereas Brownian motion can describe the movement of antigen-activated immune cells. Utilising these properties of immune cell motion we develop the model further to consider the immune response to a solid tumour.

In Chapter 5, we extend the individual-based model to describe the interactions between dendritic cells, cytotoxic T lymphocytes and tumour cells. We exploit the random walk methods described in Chapter 4 to capture the movement of inactive and active immune cells, *i.e.* the movement of both inactive and active dendritic cells and cytotoxic T lymphocytes, in the tumour microenvironment. Furthermore, we consider the activation process of immune cells, the proliferation of cancer cells, and the destruction of cancer cells by the immune cells. The resulting computational simulations of our model further clarify the conditions for the onset of successful immune action against cancer cells and may suggest possible targets to improve the efficacy of cancer immunotherapy. For the sake of simplicity, in the model we consider a homogeneous tumour whereby all cancer cells exhibit the same phenotype. However, solid tumours can be heterogeneous where each cancer cell can have a unique antigen profile. In the following chapter we address this by extending the individual-based model further to explicitly include tumour antigen expression and further investigate the role of antigens within the immune response to cancer.

We describe, in Chapter 6, the expanded individual-based model where each cancer cell is characterised by an antigen profile which can vary over time due to either epimutations or mutations. Once again, the immune response against the

cancer cells is initiated by dendritic cells that recognise the tumour antigens and present them to cytotoxic T cells. Consequently, T cells become activated against a particular tumour antigen and can only remove cancer cells which express a sufficient level of the corresponding antigen. Computational simulations of the model highlight the required conditions for the emergence of tumour clearance, dormancy or escape. Furthermore, the model allows us to assess the impact of antigenic heterogeneity of cancer cells on the efficacy of immune action. The results suggest that epimutations, which alter the antigen profile of tumour cells, ultimately dictate the outcome of tumour-immune competition. The results further indicate which other processes can control the outcome of tumour-immune competition, and therefore suggest which mechanisms may be exploited in the development of new immunotherapy techniques.

One potential limitation, in terms of mathematical interest, of individual-based models is their lack of amenability to mathematical analysis. To overcome this we aim to derive the continuum counterparts of the individual-based models introduced in this work. However, due to the inclusion of a Lévy walk and other complex mechanisms, we begin by considering a simpler cell population model in Chapter 7. We present a simple stochastic individual-based model describing the spatial dynamics of multicellular systems whereby cells undergo pressure-driven movement and pressure-dependent proliferation. We show that nonlinear partial differential equations commonly used to model the spatial dynamics of growing cell populations can be formally derived from the branching random walk that underlies our discrete model. Moreover, we carry out a systematic comparison between the individual-based model and its continuum counterparts, both in the case of one single cell population and in the case of multiple cell populations with different biophysical properties. The outcomes of our comparative study demonstrate that the results of computational simulations of the individual-based model faithfully mirror the qual-

itative and quantitative properties of the solutions to the corresponding nonlinear partial differential equations. Although the model is not applied to a specific biological case, the methodology and results obtained could be used to describe tumour growth and invasion into healthy tissue.

Chapter 8 concludes this thesis with an overview of the mathematical models we have developed and the main findings of our work. We finish by considering the future directions and potential applications of the modelling techniques we have developed.

Chapter 2

Biological overview of the immune response to cancer

2.1 Overview

In this chapter we introduce the key biological mechanisms involved in the immune response to cancer. We begin by considering the human immune system and, specifically, how its separate components can work together. In this thesis, we will focus on two immune cell types: dendritic cells (DCs) and cytotoxic T lymphocytes (CTLs) and how they interact with each other to remove harmful cells and material from the body. Additionally, we will describe some of the key aspects of tumour growth and development, such as the expression of tumour antigens, and the ways in which the immune system can control these processes. We will conclude the chapter by considering some of the properties of cancer which allow for the evasion of the immune response and the immunotherapy techniques which have been developed to target these aspects.

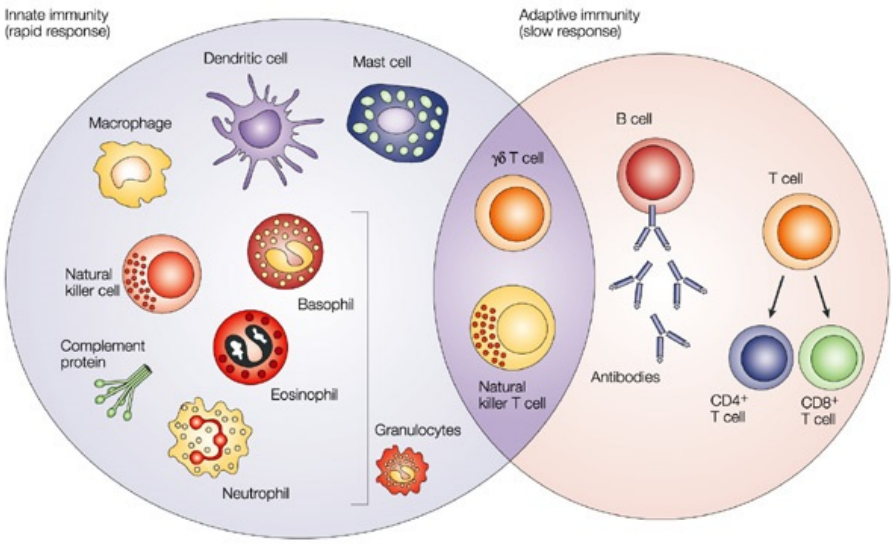

Figure 2.1: Cellular components of the human immune response. *The figure displays the key cell types involved in the innate and adaptive branches of the human immune response. In this work, we focus on dendritic cells and how they activate the adaptive immune response, namely CD8+ T cells (*i.e. *cytotoxic T lymphocytes), to launch an attack against cancer cells.*

Reprinted with permission from Macmillan Publishers Ltd: [Nat Rev Cancer] (Dranoff, G. (2004). Cytokines in cancer pathogenesis and cancer therapy. Nat Rev Cancer, 4(1), 11-22.), copyright (2004) (Dranoff, 2004)

2.2 Immunology

The human immune system is a complex collection of cells, structures and processes that work in conjunction to eliminate foreign and harmful material from within the body. The immune system consists of two branches: the innate immune response and the adaptive immune response, which both incorporate multiple cell types, as shown in Figure 2.1.

The role of the innate immune response is to identify and attempt to remove foreign material from the body. Cells which are involved in the innate response can exhibit a range of phenotypes and perform a range of functions and they include:

natural killer (NK) cells, macrophages and dendritic cells (DCs). Specifically, NK cells can induce the death of target cells without requiring activation by other cells via cell lysis (*i.e.* disintegration) which results in cell debris within the microenvironment (Messerschmidt et al., 2016). Macrophages and DCs, on the other hand, are phagocytic, which means that they can engulf and remove harmful particles or cells that have been marked for removal by antibodies (Chaplin, 2010). The destruction and removal of target cells by NK cells, DCs and macrophages can be limited, however their recognition of, and interactions with, foreign cells can initiate the adaptive immune response (Messerschmidt et al., 2016).

Almost all cells within the human body express protein antigens on their cell surface through major histocompatibility complex (MHC) molecules allowing them to be recognised by the immune system (Brown et al., 2014). DCs and macrophages can act as antigen presenting cells (APCs) where they can collect and present these antigens to the adaptive immune cells (Weinberg, 2007a). The APCs can collect antigens through the recognition of signals from phagocytosed cells, or living target cells, where they then produce recognition receptors to allow for antigen collection. Inflammatory or anti-inflammatory cytokines may also be released by the immune cells to aid in the collection of antigens (Harshyne et al., 2001).

Once collected, the APCs can process the antigen and load them on to MHC molecules on their cell surface (Chaplin, 2010). In particular, dendritic cells can recognise and present multiple type of antigen (Coico and Sunshine, 2015). Once the APCs have processed the antigen they move to the lymph nodes to present the antigen to adaptive immune cells, specifically T cells (Laoui et al., 2016; Parlato et al., 2017). It is interesting to note that T cells cannot bind to unprocessed antigens which are not attached to MHC molecules.

Naive T lymphocytes within the lymph node can be activated via the antigen

presenting cells. APCs present the antigen through an antigen-MHC complex on their cell surface which can bind to the T cell receptor (TCR) on the surface of the lymphocytes (Chaplin, 2010; Rohrs et al., 2019). The activation process relies on co-stimulatory (*e.g* CD28) and co-inhibitory (*e.g* CTLA-4, PD-1) molecules (Keir et al., 2008; Chen and Flies, 2013). Subsequently, the T cells can mature into different subtypes including cytotoxic T lymphocytes, T helper (T_h) cells and memory T cells (Weinberg, 2007a) depending on the antigen-MHC complex and other complementary molecules. If a dendritic cell, carrying an antigen, meets an inactive T cell the binding affinity of the T cell to the antigen-MHC complex plays a critical role in the activation of the T cells (Łuksza et al., 2017). If the binding affinity of the T cell is too low they cannot interact with the APC. On the other hand, if the binding affinity is too high then the immune cells may be able to bind to nonharmful cells causing autoimmune reactions (Engelhardt et al., 2012; Tan et al., 2015). CD8 glycoproteins on the surface of naive T cells strengthen the interaction with the APC and results in the maturation to CD8+ T cells, also known as cytotoxic T lymphocytes (CTLs) (Chaplin, 2010). Through this interaction with APCs, CTLs become activated and subsequently can recognise and destroy any cells or particles that express the target antigen (Weinberg, 2007a). However, T cells only produce one type of antigen receptor and therefore can only target cells expressing that particular antigen (Brenner et al., 2008; Coico and Sunshine, 2015). Not all target cells will express the same target antigens and therefore, it has been suggested that, a repertoire of T cells activated against a range of antigens will result in a more successful immune response (Chaplin, 2010). The activated T cells will then travel to the site of infection, or the site of the target cells (Halle et al., 2016), where they can then recognise these cells through the interaction of their TCR with an antigen-MHC complex on the surface of the target cell (Messerschmidt et al., 2016).

Once the T cell has recognised the target cell, there are two mechanisms which can be used to cause apoptosis (programmed cell death). These are the perforin-granzyme mechanism or the Fas-FasL mechanism, which may be used independently or together to remove harmful cells. The former mechanism is where perforin is injected directly into the target cell, through a synapse, creating small holes in the cell membrane. Subsequently, granzyme B can enter the target cell through these small holes and activate the apoptotic cascade within the target cell (Basu et al., 2016; Lawrence, 2016; Messerschmidt et al., 2016). The second mechanism that the CTL can use to cause apoptosis utilises necrosis factors like the Fas ligand (FasL). Generally, FasL is present on the cell surface of the CTL which allows direct contact between the CTL and cells that produce the Fas receptor. Most cells will produce Fas receptors on their cell surface. Once FasL or sFasL binds to the Fas receptor, they aggregate to form an adaptor protein known as FADD (Fas associated death domain) which can trigger apoptosis, resulting in target cell death (Hersey and Zhang, 2001).

After all target cells are removed, CTLs must be deactivated or removed to prevent any damage being done to normal cells. This response has three stages: an inactivation phase, a self-apoptosis stage, and the formation of a subset of memory cells (Klebanoff et al., 2006). The deactivation process prevents the risk of autoimmune diseases occurring and the formation of a memory population allows for a faster response if the same antigen is recognised in future.

In this thesis, we focus on DCs and CTLs in particular and how they interact together through the antigen presentation process. We utilise the properties of these cell types in the individual-based models described in Chapter 4, Chapter 5 and Chapter 6.

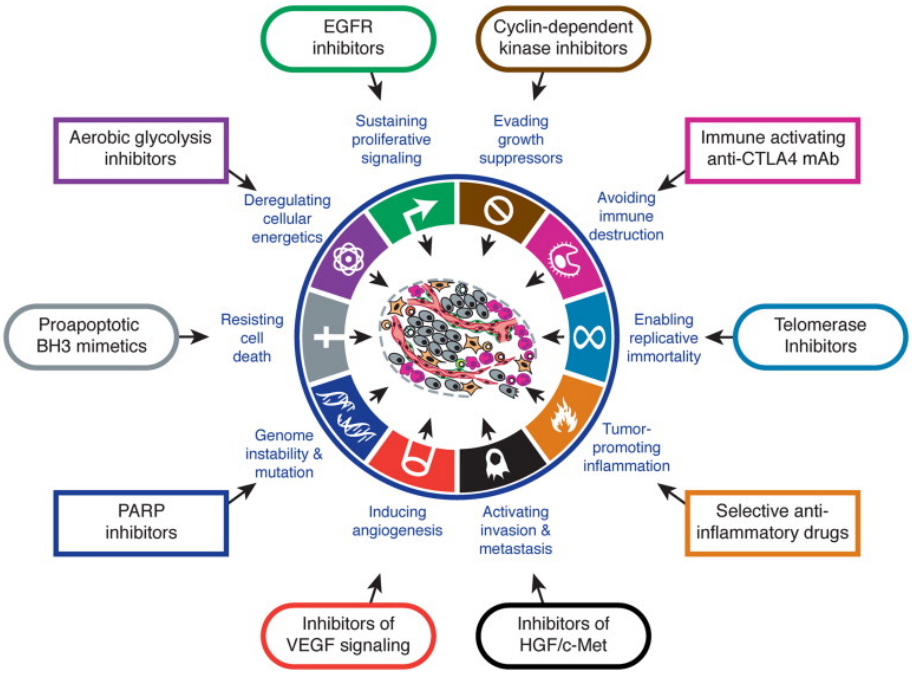

Figure 2.2: The ten hallmarks of cancer and their potential treatment options. *The figure describes the ten key characteristics of a tumour and highlights therapies which target each characteristic. In this work we specifically focus on the ability of the immune system to control the tumour and subsequently, the ability of tumours to evade immune destruction.*

Reprinted from Cell, 144 (5), D Hanahan, RA Weinberg, Hallmarks of Cancer: The Next Generation, 646-674, Copyright (2011), with permission from Elsevier (Hanahan and Weinberg, 2011)

2.3 Tumour development

Hanahan and Weinberg (2011) (re)defined the ten hallmarks, or key characteristics, of cancer, which are displayed in Figure 2.2. These include the ability of cancer cells to sustain/enhance replication and growth (cell proliferation), avoid growth suppressors, avoid the immune response, be able to divide/replicate indefinitely, recruit immune cells to cause inflammation, invade another area of the body (formation of metastasis), create new blood vessels (angiogenesis), mutate, resist cell death (apoptosis) and alter their metabolic processes to avoid the need for oxygen.

Mutations, or epimutations, within healthy cells, which alter the antigen expressed by the cell, can lead to the emergence of cancer cells. Through cell division, the altered cells cluster together to form a growing tumour. In the early stages of tumourigenesis, cancer cells stay close to the original site of the tumour (Hanahan and Weinberg, 2011). However, once the tumour has developed and is large enough it can begin to create a blood supply through angiogenesis. This allows single cells to leave the tumour mass and travel to other sites of the body, through the blood stream, and form metastasis (Weinberg, 2007b). Furthermore, the process that leads human cells to induce their own cell death depends on the shortening of the telomeres at the end of chromosomes through each cell division. Therefore, once the telomeres shorten significantly the cell can no longer replicate and will initiate apoptosis leading to cell death. However, most cancer cells express high levels of telomerase, an enzyme that prevents the shortening of the telomeres allowing for a longer or infinite survival of cells (Shay et al., 2001). In our work we focus on tumours in the early stages of development (*i.e.* small pre-angiogenic tumours).

Cancer cells within the tumour can exhibit a distinct set of phenotypes and antigens making the tumour heterogeneous. These tumour antigens dictate which genes and proteins that the tumour cell expresses. There are three main types of tumour antigen: (i) tumour associated antigens (TAAs), (ii) tumour specific antigens (TSAs) or (iii) cancer-testis antigens (CTAs). Tumour associated antigens are over expressed in cancer cells but can also be found in normal healthy cells, whereas tumour specific antigens are only expressed by cancer cells. Furthermore, cancer-testis antigens are expressed in cancer cells but also in the normal reproductive tissues at low levels (Yarchoan et al., 2017). One potential drawback to the development of new cancer therapies is the ability to identify these tumour antigens. Recently, with this aim extensive cell-based studies have been carried out and used to successfully

identify tumour antigens (Brown et al., 2014; Joglekar et al., 2019).

Furthermore, through epimutations or mutations the antigen profile of cancer cells may evolve over time. Epimutations are spontaneous '*heritable changes in gene expression that leave the sequence of bases in the DNA unaltered*' (Oey and Whitelaw, 2014), whereas mutations take place during cell division and may cause the antigen profile of one progeny cell to be different from that of the parent cell. One of the first epimutations to be identified, in cancer cells, was the loss of DNA methylation at the CpG dinucleotides. DNA methylation is an important mechanism in gene regulation where the addition of methyl groups to DNA can repress gene expression (Coulie et al., 2014). In normal cells 70-80% of all CpG dinucleotides are methylated. However, hypomethylation in cancer cells can lead to gene activation, mismatch repair, chromosomal instability and mechanisms of viral effects in cancer (Feinberg and Tycko, 2004). Generally, epimutations are reversible and occur much more frequently than mutations, which are generally not reversible (Feinberg, 2004; Peltomäki, 2012).

Notably, one tumour antigen gene family of interest are the melanoma associated genes (MAGE) which are cancer-testis antigens. MAGE-A genes are frequently expressed in cancers of different types and originating from different tissues and are linked to poor prognosis. In regards to DNA methylation, MAGE genes are methylated in normal cells but in cancer cells are not, allowing for their activation and expression (Boon et al., 2006; Chalitchagorn et al., 2004; Chinnasamy et al., 2011; Müller-Richter et al., 2009; Zajac et al., 2017). Demethylation becomes more prominent as the cancer develops, suggesting that these epigenetic events are important in tumour progression (Coulie et al., 2014). Furthermore, MAGE-A proteins are involved in processes which reduce apoptosis of tumour cells and enhance tumour proliferation, therefore benefiting tumour progression if they are

expressed (Van Tongelen et al., 2017). Common cancers that they are expressed in are melanomas (Boon et al., 2006; Connerotte et al., 2008; Coulie et al., 2014; Urosevic et al., 2005), oesophageal cancers (Zajac et al., 2017), lung, breast, prostate and colorectal carcinomas (Coulie et al., 2014) and head and neck cancers (Hartmann et al., 2016; Müller-Richter et al., 2009). Moreover, there can be high variability of specific antigen expression between patients with the same cancer and even within samples from the same patient (Hartmann et al., 2016; Müller-Richter et al., 2009; Urosevic et al., 2005). In this thesis, we focus on these MAGE-A antigens in particular and how their expression varies over time through epimutations. These mechanisms are utilised in the individual-based model described in Chapter 6.

2.4 Tumour immunology

Early experimental studies highlighted that immunodeficient mice were more likely to develop cancers than those with a healthy immune system (Hanahan and Weinberg, 2011). Furthermore, the presence of T lymphocytes within the tumour microenvironment can be used as a marker to predict the success of cancer treatments (Spranger and Gajewski, 2018). These findings indicate that the immune system is capable of controlling and preventing tumour development. The mechanisms of the immune response against cancer have been studied in depth to provide an understanding of the key mechanisms involved. In general, tumour cells are poor antigen presenting cells (Dhodapkar et al., 2008) and therefore innate immune cells are required to act as antigen presenting cells (APCs) to initiate a successful response against tumours. Specifically, dendritic cells (DCs) can collect tumour antigens to become activated APCs (Bianca et al., 2012; Dhodapkar et al., 2008; Harshyne et al., 2003). The activated DCs can then subsequently activate cytotoxic

T lymphocytes (CTLs) to initiate a response against the tumour. Since tumour cells express MHC (Algarra et al., 2000), they can be recognised by the activated T cells, which may result in tumour cell death (Boissonnas et al., 2007; Christophe et al., 2015; Engelhardt et al., 2012; Phan and Rosenberg, 2013; Spranger, 2016). Notably, cancer cells normally produce Fas receptors at higher levels than noncancer cells, making them more susceptible to removal by CTLs through the Fas-FasL mechanism (Modiano and Bellgrau, 2016).

In recent years, cell imaging techniques have improved greatly permitting single cell tracking of immune cells and tumour cells in real time in both *in vitro* and *in vivo* situations. This allows for a greater understanding of cell movement, velocity and spatial distributions within the tumour microenvironment. These imaging techniques generally involve the labelling of cells with fluorescent proteins, or genetically engineering cells to produce specific reporter proteins (Liu and Li, 2014). For example, Boissonnas et al. (2007) used individual cell tracking to study the movement of CTLs, *in vivo*, in the presence and absence of a tumour antigen, and verified a change in their patterns of migration between these situations. In the case where no antigen was present, the cells moved actively in a search-like pattern. On the other hand, when the tumour antigen was present, the cells switched to a more restricted form of movement. Engelhardt et al. (2012) discovered similar results when studying the movement of DCs in response to a solid tumour, where the change in movement was linked to the presence or absence of tumour antigen.

Overall, many experimental studies have concluded that the immune system is able to remove early stage tumours and cancer cells, however through antigenic changes and other evolutionary mechanisms the disease can adapt to evade the immune response through a process known as immunoediting (Aguirre-Ghiso, 2007).

2.5 Immunoediting

2.5.1 Tumour dormancy

At the initial stages of immunoediting the tumour can undergo a period of dormancy where there is no change in size of the tumour. There are three types of dormancy: (i) tumour mass dormancy, (ii) cellular dormancy or (iii) immunological dormancy. In more detail, tumour mass dormancy is where the tumour does not grow due to the environmental conditions, such as lack of blood flow or nutrients. On the other hand, cellular dormancy is where the tumour cells do not undergo growth phases (Aguirre-Ghiso, 2007; Wang and Lin, 2013). Furthermore, immunological dormancy is where the tumour is maintained at a reduced size by the immune system (Manjili, 2018; Yeh and Ramaswamy, 2015). During tumour dormancy, mutations and epimutations can allow the tumour cells to become less susceptible to the immune response (Teng et al., 2008). This accumulation of favourable changes within the tumour cells may result in relapse and a more aggressive disease. Additionally, single cells may migrate away from the dormant tumour and form a secondary tumour (*i.e.* metastasis) (Gomis and Gawrzak, 2017). We describe the biological settings required for the onset of tumour dormancy in the individual-based model described in Chapter 6.

2.5.2 Immune evasion

It is clear that some tumour cells must evade the immune response to develop a solid tumour and eventually cause damage within the body. There are several mechanisms that tumour cells can use to do this. Generally, if tumour-infiltrating CTLs are present along with chemokines, such as interferons, the tumour cells generally use immune suppression pathways to inhibit and attack the immune response. If

tumour-infiltrating CTLs are not present, then cancer cells are more likely to use evasion mechanisms that allow them to avoid physical interaction with the immune cells (Gajewski et al., 2013). In the remainder of this sub-section we highlight some of these key evasion mechanisms used by the tumour to avoid immune destruction.

It has been shown that both genetic and epigenetic mutations within tumour cells can aid in immune resistance and immune evasion (Sadikovic et al., 2008). These mutations may alter the antigens expressed by the tumour cells, potentially preventing CTLs from recognising them as they no longer express the targeted antigen. Even if tumour cells produce the target antigen, they are generally expressed in low numbers with around 50 copies per cell (Tan et al., 2015), which can prevent immune recognition. Similarly, if the antigen profiles of the cancer cells are still similar enough to healthy cells, the cancer cells may not be recognised by the immune system (Messerschmidt et al., 2016).

Tumour cells can evade cell-cell recognition by immune cells through manipulating the binding process. The binding between the MHC molecule and the tumour antigen is the first step in antigen recognition. However tumour cells can cause genetic or epigenetic downregulation of MHC molecules within themselves preventing presentaion of the antigen (Agrawal and Kishore, 2000; Boon et al., 2006; Garrido et al., 2010; Igney and Krammer, 2002; Leone et al., 2013). This may limit the ability of the immune cells to recognise the tumour cells and allows the tumour cells to survive. Furthermore, tumour antigen and T cell receptor binding is generally weak and even a slight reduction in affinity, through tumour mutation or T cell exhaustion, can lead to the immune cells not being activated by the APCs (Mckeithan, 1995; Messerschmidt et al., 2016; Tan et al., 2015).

After the CTLs are activated, the tumour cells can use direct contact mechanisms to prevent apoptosis and downregulate the immune response. For example, increased

expression of PD-L1 (programmed death ligand 1) allows the tumour cell to bind to the PD-1 (programmed death 1) receptor on the immune cells causing immune cell death or inhibition (Gajewski et al., 2013; Restifo et al., 2016). Similarly, the Fas ligand and receptor response can be inhibited by either tumour cells downregulating the level of Fas receptors on their cell surface, or by producing FasL and sFasL themselves. The FasL produced can then bind to Fas receptors on the immune cells causing the immune cells to undergo apoptosis (Stewart and Abrams, 2008; Modiano and Bellgrau, 2016).

With the aim of targetting the immune resistant mechanisms of cancer, immunotherapy techniques have been developed as a method of treatment to allow for a stronger immune response.

2.6 Cancer treatment and therapies

Traditional treatments for cancer include chemotherapy and radiotherapy, which have proven to be beneficial in many cases and are used widely to treat most types of cancer. However these methods can have potentially severe side effects. For example, the damage caused to healthy cells as well as the cancer cells can result in further illness or even fatalities (Carelle et al., 2002; Coates et al., 1983). Targeted therapies, like immunotherapy, may be able to reduce the damage to normal cells. Generally, immunotherapies aim to boost the natural immune system in the body and specifically within the microenvironment of the tumour. There are three main types of immunotherapy: cancer vaccines; antibody therapies; and adoptive cell therapies.

2.6.1 Cancer vaccines

The successful HPV preventive cancer vaccine (Einstein et al., 2009), led to research into the development of other vaccines to be used a preventative measures, as well as treatment choices for cancer. There are currently a small number of FDA (American Food and Drug Association) approved cancer vaccines for public use. In particular, the Sipuleucel-T protocol exposes immune cells of prostate cancer patients to the protein PAP (prostatic acid phosphotase), which induces the maturation of dendritic cells and, upon reinjection, a more successful immune response (American Cancer Soceity, 2018). Furthermore, the Bacille Calmette-Guerin (BCG) vaccine has been approved for use in early stage bladder cancers or melanomas. The BCG bacterium can infect human tissue and induce an immune response without causing tissue damage. It is generally used post-surgery and has been shown to reduce tumour recurrence in 50-70% of patients (Bunimovich-Mendrazitsky et al., 2015). Recently, clinical trials where nanoparticles carrying tumour RNA are injected into the patient have proven to enhance CD8+ T cell activity in both mouse and human experiments, although the treatment is not yet approved (Bialkowski et al., 2016; Kranz et al., 2016).

2.6.2 Antibody therapies

Antibody-based therapies involve the administration of drugs to target specific proteins within the cancer cells. Multiple types of tumour antigen have been identified through experimental research which allows these to become targets for immunotherapy. However, when targeting TAAs care must be taken as healthy cells may be recognised as foreign and destroyed along with the cancer cells. The drugs administered for treatment may be attached to radioactive particles or used in con-

junction with chemotherapy drugs. Approved treatments include drugs that: target growth factors in head and neck cancers (American Cancer Soceity, 2018); inhibit the anti-apoptosis mechanism in leukaemia (Delbridge et al., 2016; Hua et al., 2016; Leverson, 2016); inhibit programmed death receptor 1 (PD-1) in melanoma and lymphoma (Huang et al., 2017; Littman, 2015; Moreno et al., 2015) and combine PD-1 inhibition with other antibody treatments (Keir et al., 2008; Larkin et al., 2015; Postow et al., 2015).

A particular therapy approach utilizing monoclonal antibodies is to increase the expression of particular tumour antigens. For example, Yarchoan et al. (2017) found experimentally that a higher expression of tumour antigens led to the tumour being increasingly recognised by the immune system. It has also been shown experimentally that epigenetic alterations can be both beneficial and detrimental to tumour development, small levels of alteration can increase the tumour's evolutionary fitness. However, too much alteration leads to increased immune recognition (Chen and Mellman, 2017). These properties have been exploited through treatment approaches, in particular it was shown that 5-aza-2'-deoxyctidine and histone deacetylase inhibitors could increase the expression of MAGE genes through decreased methylation of their promoters, allowing for the recognition of tumour cells (Chinnasamy et al., 2011; Wischnewski et al., 2006).

Although using monoclonal antibodies is a promising method of treating a variety of cancers there is a potential for resistance and tumour recurrence to occur (Restifo et al., 2016). Furthermore, some of these drugs can have severe side effects such as risk of autoimmune diseases and can even enhance cancer progression (Champiat et al., 2016; Kato et al., 2017). The main cause of this resistance or relapse is thought to be evolution of the antigenic profiles of the cancer cells. For example, in a PD-1 therapy trial 10% of patients showed resistance due to loss of tumour

antigens through mutation (Anagnostou et al., 2017). T cell therapies can lead to inflammation of the tissue, promoting the mutation of cancer cells, like melanoma cells, to become more resistant to T cell induced death (Baar et al., 2016).

2.6.3 Adoptive cell therapy

Adoptive T cell therapy: Adoptive T cell therapies rely on T cells from the patient, or from donor patients, to be modified and then (re)injected into the patient's blood stream (Fesnak et al., 2016). The use of the patient's own T cells, allows this therapy to become more adaptable for each patient, *i.e.* personalised. These therapies were shown to be of potential use through mouse models, demonstrating that immunity could be acquired adoptively (Billingham et al., 1954). The standard method is that cells are removed from the body, modified and undergo incubation with cytokines to allow for expansion *ex vivo* (outwith the body). For example, the cells may be activated against a certain antigen. They are then transferred back into the patient and are able to initiate a specific immune response against the cancer (Gross and Eshhar, 2016; Weinberg, 2007a). Traditionally, adoptive T cell therapies have been used to treat B-cell malignancies and have proved beneficial with high response rates (Brentjens et al., 2013; Davila et al., 2014; Grupp et al., 2013; Maude et al., 2014). However, there is a large amount of work on the development of therapies against solid tumours (Andersen et al., 2016; Frigault and Maus, 2016; Gross and Eshhar, 2016; Ikeda, 2016; Johnson et al., 2015; Perez et al., 2015).

Adoptive cell therapies which target solid tumours have, generally, been nonspecific in the past, targeting common antigens such as EGFR (epidermal growth factor receptor) and its variants (Feng et al., 2016; Johnson et al., 2015; Morgan et al., 2012; O'Rourke et al., 2016) and NY-ESO-1 (New York oesophageal squamous cell carcinoma 1) (Rapoport et al., 2015; Robbins et al., 2011, 2015). However, not all

patients respond well to treatment, or at all, and those who do respond can experience a limited effect (Dudley et al., 2001; Feng et al., 2016; Mackensen et al., 2006). Additionally, by targeting common antigens there is a risk of attacking healthy cells.

However, germline cells do not contain MHC and therefore cannot produce antigens that T cells could then recognise. Hence, there is little risk of T cells recognising normal cells when targeting cancer-testis antigens, (*e.g.* the MAGE antigens) (Boon et al., 2006; Connerotte et al., 2008). This makes cancer-testis antigens a useful target in immunotherapy. Clinical trials of treatments which target MAGE-A antigens have proven somewhat successful, for example, targetting MAGE-A3 has been found to be successful in mouse model tests (Chinnasamy et al., 2011) and in treating human melanoma cases (Connerotte et al., 2008; Lu et al., 2015; Zhang et al., 2003). Additionally, MAGE-A4 has also been a successful target in oesophageal cancers (Kageyama et al., 2015; Zhang et al., 2002). However, these can lead to partial responses and when similar methods have been applied to a wider range of cancers, severe side effects, such as cardiogenic shock and neural toxicity, lead to fatalities. It is thought that these deaths were caused by the high affinity of the receptors for normal human antigens (Linette et al., 2013; Morgan et al., 2013). Further studies have enhanced T cells that target MAGE genes *in vitro* (Gerdemann et al., 2011; Graff-Dubois et al., 2002).

An effective modification to T cells, in the adoptive therapy setting, is the attachment of chimeric antigen receptors (CARs) which allow T cells to better recognise and destroy cancer cells. A CAR is a recombinant protein combined with a specific tumour associated antigen that can activate other T cells (Sadelain et al., 2013). These CARs can be used universally, regardless of the patient's MHC profile, as the CAR-T cells do not require activation through antigen presentation. Furthermore, CAR-T cells have been shown to be functional up to four years after a single treat-

ment, and even over ten years in some cases (Porter et al., 2015; Scholler et al., 2012). There have been extensive experiments and clinical trials based on CAR-T cell therapies with successful initial results, however very few have been approved as viable options for cancer treatment. In particular, Phase I trials using CAR-T cells to treat non-Hodgkins lymphoma (NHL), chronic lymphocytic lymphoma (CLL) and acute lymphoblastic leukaemia (ALL) proved successful, with overall response rates of over 60% (Gross and Eshhar, 2016). Similar trials targeting ALL also had high remission rates of around 90% (Bonini and Mondino, 2015; Walker and Enderling, 2016). Furthermore, when used to treat leukaemia, clinical trial results highlighted that one CAR-T cell can kill up to 1000 leukaemia cells, with the CAR-T cell levels expanding over 1000 times *in vivo* (*i.e.* within the body). These highly effective CAR-T cells also survived in the body for at least 6 months after insertion, allowing for prolonged defense against cancer and also allowed for stronger binding to tumour associated antigens (Kalos et al., 2011; Tan et al., 2015).

However, there have been safety concerns and a potential risk of CAR-T cells attacking non-tumour cells that express the target antigen has been suggested. This could explain situations where CAR-T cell treatments became fatal (Morgan et al., 2010). To combat this, mechanisms have to be put in place to prevent the CAR-T cells from attacking normal cells. 'Suicide switches' allow the modified T cells to be deactivated or destroyed when exposed to certain molecules or drugs (Ikeda, 2016). Contrastingly, modifying the receptors so that they are only active in the presence of certain drugs has also been investigated (Rodgers et al., 2016; Wu et al., 2015).

The standard protocol of adoptive cell therapy is to inject the enhanced cells into the blood, where they then travel through the blood stream to the lungs and later the liver and spleen. However, some issues with extravasation from the blood vessels and intravasation into tumours have been found (Frigault and Maus, 2016; Kershaw

et al., 2006). Solid cancers can be difficult to infiltrate, as cells must overcome abnormal vasculature that can restrict their movement. This could potentially be overcome by combining adoptive cell therapy with other techniques such as: those that target growth factors (Gotwals et al., 2017; Yong et al., 2017) or using viruses to reduce the cancer mass (VanSeggelen et al., 2015; Walker et al., 2016). By injecting the adoptive cells directly into the tumour, if possible, the restriction on these cells moving to the site of tumour would also be reduced (Gross and Eshhar, 2016).

Another potential limitation to using T cell and CAR-T cell therapies is that these modified cells can also be immunosuppressed by the tumour, through the mechanisms described in the previous section (Beatty and Moon, 2014). In particular, CAR-T cells can be suppressed by tumour cells via the PD-1 and PD-L1 mechanism, and by using a PD-1 monocloncal antibody a more successful immune response can be initiated (John et al., 2013). Additionally, to combat this there is an aim to develop CAR-T cells that would be resistant to PD-L1 suppression (Ren et al., 2017). Notably, the expression of PD-L1 by tumour infiltrating cells can be a strong predictor of clinical response to immunotherapies (Hui et al., 2017; Perez et al., 2015).

A further limitation to T cell therapies may be that only one antigen is focused on. However, clinical trials using multiple TCRs in adoptive T cell therapy, to target multiple tumour antigens, have proved successful (Verdegaal et al., 2016). Furthermore, it has been shown that targeting only specific antigens within a tumour could lead to untargeted antigens becoming prevalent (Łuksza et al., 2017) and therefore it would be beneficial for a T cell population to be able to target more than one tumour antigen.

Dendritic cell therapy: Using a similar approach to adoptive T cell therapy, dendritic cells can be removed from the body and expanded or activated using tumour antigens *ex vivo*. This may subsequently induce an enhanced response by T lymphocytes, once the DCs are reinjected into the patient. For example, several clinical trials where extracted DCs of melanoma patients were pulsed with tumour antigens proved successful in inducing an enhanced CTL response (Carreno et al., 2015; Schreibelt et al., 2016; Tel et al., 2013; Wilgenhof et al., 2011, 2016). In particular, Gerdemann et al. (2011) produced high affinity CTL populations through dendritic vaccines that were capable of targeting multiple tumour antigens. The enhanced cells showed improved responses *in vitro* when using heterogeneous human lymphoma samples.

2.6.4 The role of interdisciplinary research

Immunotherapy techniques can take an extensive amount of time to develop and test. Once an initial hypothesis is set, it can be several attempts before a successful and viable result is obtained. Computational and mathematical oncology modelling can be useful in removing some of the 'testing time' and providing more accurate predictions of the model. If we can predict whether a certain treatment will have a beneficial effect on a certain type of cancer, this can then be developed further, thereby hopefully reducing the time to develop immunotherapies. We briefly review a selection of the mathematical and computational methods used previously to model tumour growth and the immune response to cancer in the following chapter.

Chapter 3

Review of modelling strategies

3.1 Overview

In this chapter, we provide a short review of the mathematical modelling approaches which have previously been used to describe cell motion, tumour growth and tumour-immune competition. We begin with a discussion on the multiple scales considered in modelling and some of the general approaches to mathematical modelling biological phenomena.

3.2 Methods of mathematical modelling

Biological processes exhibit multiscale properties where interactions occur across various spatial and temporal scales. Generally, there are three spatial scales potentially considered in modelling: the molecular scale, the microscopic scale and the macroscopic scale. Intracellular processes, such as mutations and cell signalling, may occur at the molecular scale, *i.e.* nm-μm. Whereas, extracellular interactions, *e.g.* interactions between cells, may occur at the microscopic scale, *i.e.* μm-mm. Furthermore, tissue level processes may occur at the macroscopic scale, *i.e.* mm-

cm (Deisboeck et al., 2011). All of these processes and mechanisms may also occur across various temporal scales, *e.g.* ns, μs, s, mins, hrs, days, years. The scale that is considered within mathematical descriptions of these processes depends on the level of detail required. Often, the dynamics from each scale can feed into the description and cause variation in the mechanisms of other scales. In these situations it is important to consider multiscale models, where these multiscale properties of the biological system are described.

Furthermore, mathematical models can have discrete or continuous approaches and can relate to discrete and continuous biological mechanisms. Although, discrete models can be stochastic and capture small scale dynamics, they are less tractable towards mathematical analysis. Continuous models are, generally, less computationally expensive than discrete models and allow for the investigation of large cell densities. By using hybrid models with both discrete and continuous parts a better understanding of the situation as a whole can be obtained, but these can also be computationally expensive due to complexity (Lowengrub et al., 2009). Various mathematical methods are used to model biological phenomena including differential equations, stochastic models and combinations of these. In these models there can be a correlation between the complexity of the model and the biological relevance, although often, due to limitations of mathematical methods, a balance between these must be found.

3.2.1 Differential equations

Differential equations are used to describe the change of continuous variables over time and/or space. Ordinary differential equation (ODE) models consider the change over either time or space, and can vary in complexity from a simple one variable model to multi-variable systems. However, ODEs cannot incorporate both spatial

and temporal dynamics, which can both be important in biological processes. On the other hand, partial differential equations (PDEs) can be used to describe the change in variables which depend on both space and time and therefore can be used to describe the spatio-temporal dynamics of biological systems (Eftimie et al., 2011).

3.2.2 Discrete models

Computational models can be used to describe discrete properties of biological systems in multiple dimensions. These models can be grid (lattice) based or be described on an non-uniform grid (mesh) (Macklin and Edgerton, 2010; Van Liedekerke et al., 2015). Generally, a set of rules that describe the potential mechanisms or interactions that each individual can undergo are defined. These rules depend on the probability of events occurring and allow for the observation of any patterns in the dynamics of the biological system (An et al., 2009). Individual-based (IB) models, or agent-based models (ABM), track each individual over time and allow them to move or interact with other individuals independently (Grimm and Railsback, 2005). Although we will focus on these individuals being cells in our work, particles, animals and social interactions can also be modelled in this way. Specifically, cellular automata (CA) models are a type of grid based IB model where, often, only one cell can occupy each grid position through volume exclusion. The cell's movement and interactions with other cells within the system then depends on the rules of the model and the number of cells occupying the neighbouring grid positions of the cell (Wolfram, 1983). Lattice gas CA (LGCA) models are similar, however, multiple cells may occupy one grid position. Contrastingly, cellular potts models use multiple grid positions to describe the location of one cell (Lowengrub et al., 2009). Other methods can include more physical representations of cells via masses and springs models (Murray et al., 2009). The development of multiple modelling approaches

has led to the development of many computational tools and packages that can be used to implement these models, and a review of several of these tools can be found in Metzcar et al. (2019). Although using previously developed software can be beneficial, in this work we develop our own computational techniques to allow for deeper understanding and control over the model.

3.2.3 Multiscale and hybrid models

In recent years, it has become more common to combine discrete and continuous models to provide a more in-depth description and analysis of the biological systems. By combining computational models with differential equations a greater understanding of the biological relevance can be obtained through both the dynamics of the system emerging. Additionally, through this hybrid approach a wider range of tools can be used to analyse the model.

In this thesis, we will develop individual-based (IB) modelling techniques to describe tumour-immune competition in Chapter 4, Chapter 5 and Chapter 6, and consider the derivation of a PDE model from an IB model of cell populations in Chapter 7.

3.3 Modelling random walks

In both differential equation and computational models the movement of organisms or cells can be described through random walk methods. The theory of random walks was studied and developed independently in the areas of biology (Brown, 1828), probability theory (Bernoulli, 1713), finance (Bachelier, 1900) and physics (Pearson, 1905; Rayleigh, 1880). In particular, the rigorous connection between the microscopic dynamics of particles and the macroscopic processes of diffusion was

described in the seminal work of Einstein (1905).

One of the first types of walks to be described is Brownian motion, where cells have equal probability of moving in any direction at any time. The Brownian discrete random walk can be used to formally derive the standard, continuous, diffusion equation (Nava-Sedeno et al., 2017). However, issues arise with the diffusion equation due to the implied infinite, and unrealistic, propagation speed of cells (Zaburdaev et al., 2015). In an attempt to overcome these issues several methods were introduced, such as, the use of ballistic cones defining the maximal velocity of particles (Taylor, 1922), persistent Brownian motion with finite velocity (Furth, 1920) and the development of the telegraph equation which included an additional second order time derivative (Bakunin, 2003; Davydov, 1934). The continuous time random walk (CTRW) was introduced by Montroll and Weiss (1965) to include waiting times of cells which allowed for the derivation of anomalous diffusion, where the spreading of cells was slower than standard (*i.e.* Fickian) diffusion, also known as subdiffusion. Furthermore, situations where particles can spread faster then Brownian motion, also known as superdiffusion, were observed in turbulent flows (Richardson, 1926).

To allow for the inclusion of superdiffusive behaviour, random walk methods were developed to allow particles and cells to travel for longer periods of time in a given direction. To achieve this, Lévy stable distributions (Gnedenko and Kolmogorov, 1954; Lévy, 1937) were considered and Lévy flights were introduced (Mandelbrot, 1982). These consist of instant jumps characterised by infinite mean squared flight lengths which allow particles to travel a longer distance, faster (Dybiec and Gudowska-Nowak, 2017). However, infinite propagation speeds are still possible and this form of motion (Shlesinger et al., 1986) is generally not biologically realistic. Lévy walks, on the other hand, impose finite propagation speeds on cells (Shlesinger et al., 1982) and have two general approaches. Firstly, cells still exhibit waiting times. However,

once the waiting time has elapsed the cells move with a constant speed in the required direction towards their destination (Klafter and Zumofen, 1994; Zaburdaev and Chukbar, 2002). The second method is more commonly used, and eliminates the waiting time of cells allowing them to move continuously (Humphries et al., 2013; Klafter and Zumofen, 1994; Shlesinger et al., 1986; Zumofen and Klafter, 1993). More formally, a Lévy walk is a scale invariant motion characterised by a power-law run length distribution function:

$$L(s) \sim s^{-(\alpha+1)},$$

where $0 < \alpha < 2$ is a scaling factor and s is the length of a step that they will take in the chosen direction. Therefore, the frequency of steps of length s will be proportional to $s^{-(\alpha+1)}$ (Matthäus et al., 2011).

Since their introduction, Lévy walks have been used to successfully describe and capture the migration patterns of a wide range of organisms, such as; soil amoebae (Levandowsky et al., 1997), eukaryotic cells (Li et al., 2008), bacteria (Zaburdaev et al., 2014) and even humans (Rhee et al., 2011; Raichlen et al., 2014). For example, Matthäus et al. (2011) considered a model of the chemotaxis signalling pathway of *E. coli* and demonstrated that stochastic fluctuations and the specific design of the signalling pathway together enable the generation of Lévy walks. The *E. coli* exhibited a chemotactic run and tumble motion, where the flagella of the bacteria rotated counter clockwise, formed a bundle and propelled the cell in a straight line. If the flagella rotated clockwise the bundle opened and the bacteria randomly changed their angle without forward propagation. Furthermore, recent literature, based on experimental data, suggests that T cells may move in a superdiffusive or Lévy like motion (Agliari et al., 2014; Fricke et al., 2016; Harris et al., 2012; Krum-

mel et al., 2016; Weninger et al., 2014). We note that, although Lévy processes have been investigated through more generalised one dimensional continuous mathematical models (Fedotov, 2016; Fedotov and Korabel, 2017; Gan et al., 2015; Golovin et al., 2008; Hanert, 2012; Stage et al., 2016), it has been suggested that stochastic individual-based models may be more appropriate methods of capturing these complex migration patterns (Nava-Sedeno et al., 2017). In Chapter 4 of this thesis, we will develop an individual-based model of Brownian and Lévy walk methods to describe immune cell motion.

3.3.1 Mathematical models of cell population migration and growth

As mentioned above, random walks can be used to model cell migration and from these methods continuous descriptions of the cell population can be obtained. One particular area of interest, is the use of nonlinear partial differential equation models to describe the movement and growth of populations of cells. For example, models that describe the evolution of cellular densities in response to pressure gradients generated by population growth have been particularly popular (Ambrosi and Mollica, 2002; Ambrosi and Preziosi, 2002; Araujo and McElwain, 2004; Bresch et al., 2010; Byrne, 2010; Byrne and Chaplain, 1995, 1996, 1997; Byrne and Drasdo, 2009; Byrne et al., 2003; Byrne and Preziosi, 2003; Chaplain et al., 2006; Chen et al., 2001; Ciarletta et al., 2011; Greenspan, 1976; Lowengrub et al., 2009; Perthame, 2014; Preziosi, 2003; Ranft et al., 2010; Roose et al., 2007; Sherratt and Chaplain, 2001; Ward and King, 1999, 1997). Models of this form have been widely used to complement empirical research in developmental biology and cancer research.

Further to the biological and clinical insights into the underpinnings of tissue

development and tumour growth they can provide, these continuum models exhibit a range of interesting qualitative behaviours. For example, travelling-wave solutions with composite shapes and discontinuities (Tang et al., 2014). Moreover, in analogy with reaction-diffusion systems arising in the mathematical modelling of other biological and ecological problems (Dancer et al., 1999; Mimura et al., 2000), these models can give rise to sharp interfaces, which bring about spatial segregation between cell populations with different biophysical properties (Lorenzi et al., 2017).

A key advantage of continuum models for the spatial dynamics of growing cell populations over their individual-based counterparts, *i.e.* discrete models that track the dynamics of individual cells (Drasdo, 2005; Van Liedekerke et al., 2015) is that they are amenable to mathematical analysis and they are computationally inexpensive. Mathematical analysis enables a complete exploration of the model parameter space, which ultimately allows more in-depth conclusions to be drawn. Furthermore, compared to individual-based models, continuum models offer the possibility to carry out numerical simulations at the level of larger portions of tissues or even of whole organs, while keeping computational costs within acceptable bounds.

However, continuum models are defined at the scale of whole cell populations and, as such, they are usually formulated on the basis of phenomenological considerations, which can hinder a precise mathematical description of crucial biological and physical aspects. On the contrary, stochastic individual-based models that describe the dynamics of single cells in terms of algorithmic rules can be more easily tailored to capture fine details of cellular dynamics, thus making it possible to achieve a more accurate mathematical representation of multicellular systems. Furthermore, individual-based models are able to reproduce the emergence of population-level phenomena that are induced by stochastic fluctuations in single-cell biophysical properties, which are relevant in the regime of low cellular densities and cannot

easily be captured by continuum models. Therefore, it is desirable to derive continuum models for the spatial dynamics of cell populations as the appropriate limit of individual-based models for spatial cell movement and proliferation, in order to have a clearer picture of the modelling assumptions that are made and guarantee that they correctly reflect the essentials of the underlying application problem.

For this reason, the derivation of continuum models formulated in terms of partial differential equations or partial integrodifferential equations from underlying individual-based models has attracted the attention of a considerable number of mathematicians and physicists. This is generally done by considering the limit of the discrete models as the dependent variables go to a certain value, usually 0 or ∞. Examples in this active field of research include the derivation of continuum models of chemotaxis from velocity-jump process (Hillen and Painter, 2009; Othmer et al., 1988; Hillen and Othmer, 2000; Painter and Sherratt, 2003) or from self-attracting reinforced random walks (Stevens, 2000; Stevens and Othmer, 1997); the derivation of diffusion and nonlinear diffusion equations from underlying random walks (Othmer and Hillen, 2002; Penington et al., 2011, 2014), from systems of discrete equations of motion (Fozard et al., 2010; Murray et al., 2009, 2012), from discrete lattice-based exclusion processes (Binder and Landman, 2009; Dyson et al., 2012; Fernando et al., 2010; Johnston et al., 2017, 2012; Landman and Fernando, 2011; Lushnikov et al., 2008; Simpson et al., 2010) or from cellular automata (Deroulers et al., 2009; Drasdo, 2005; Simpson et al., 2007); and, most recently, the derivation of nonlocal models of cell-cell adhesion from position-jump processes (Buttenschoen et al., 2018). In Chapter 7 of this thesis, we develop a simple individual-based model of growing cell populations and formally derive the corresponding continuous PDE model.

3.4 Mathematical oncology

Mathematical oncology is an ever increasing field and many models have been developed and used to describe the growth, development and treatment of cancer. Within these mathematical models specific areas of tumour development, or specific hallmarks of cancer, can be investigated. These include models of tumour and immune interactions. In this section we will discuss some of the key models, from the literature, that have been developed previously to describe tumour development and the immune response to cancer.

3.4.1 Mathematical modelling of cancer growth and development

In particular, partial differential equations have been used in various cases to understand the spatial aspects of the mechanisms of cancer. In this regard, reaction-diffusion equations have been used in cancer models to describe: cancer invasion (Chaplain and Lolas, 2006; Gatenby and Gawlinski, 1996; Peng et al., 2017; Ramis-Conde et al., 2008); spherical tumour growth in the presence of nutrients, growth factors and inhibitors (Byrne and Chaplain, 1995; Chaplain, 1995; Chaplain et al., 2001; Ferreira et al., 2002); angiogenesis (Ambrosi et al., 2004; Anderson and Chaplain, 1998; Bauer et al., 2007); cell adhesion (Ambrosi et al., 2009; Ambrosi and Preziosi, 2009; Armstrong et al., 2006); or combinations of these mechanisms (de Pillis et al., 2006b). Generally, individual-based (IB) models have been used to describe mechanisms such as: tumour growth and development (Enderling et al., 2009; Poleszczuk et al., 2016; Wang et al., 2015); cell adhesion and variance in tumour cell movement (Frascoli et al., 2016).

Furthermore, many mathematical models have consider tumour heterogeneity

and the role of tumour antigens (Balachandran et al., 2017; Cho and Levy, 2017; Lorz et al., 2015). In particular, tumour antigen expression and the effects of epigenetic and genetic events have been modelled through differential equation models (Cho and Levy, 2017; Lorenzi et al., 2016; Lorz et al., 2015; Johnston et al., 2007, 2017; Tomasetti and Levy, 2010), stochastic computational models (Bouchnita et al., 2017; Ghaffarizadeh et al., 2018; Manem et al., 2014) or hybrid approaches (Anderson et al., 2006). For example, Asatryan and Komarova (2016) developed ordinary differential equation (ODE) models to investigate the effects of genetic instability on the competition between sub-populations within a heterogenous tumour. Their model highlighted several patterns of genetic instability which corresponded to different stages of tumour development.

3.4.2 Modelling of tumour-immune dynamics

The use of mathematical modelling to capture the specific interactions between the immune system and cancer has been widely examined over the past few decades. The majority of the models use ordinary differential equations or integro-differential equations (IDEs) to describe cellular level dynamics, with many of them focusing on tumour cells interacting with cytotoxic T lymphocytes (Bunimovich-Mendrazitsky et al., 2008; Cattani et al., 2010; Delitala and Lorenzi, 2013; Frascoli et al., 2014; Kolev, 2003; Kuznetsov and Knott, 2001; Lin Erickson et al., 2009; Lorenzi et al., 2015). These nonspatial models can vary in complexity and include specific aspects of the immune system such as: the specific chemicals involved in the apoptosis cascade (Calzone et al., 2010; Eissing et al., 2004; Fussenegger et al., 2000; Galante et al., 2012; Legewie et al., 2006; Lejeune et al., 2008); the tumour antigen recognition process (Cattani and Ciancio, 2012; De Boer et al., 1985); cooperation between immune cell types (de Pillis and Radunskaya, 2003; de Pillis et al., 2005;

Fishman and Perelson, 1993); and the immune cells' ability to attack the cancer cells (Bellomo and Delitala, 2008; Takayanagi and Ohuchi, 2001; Wilkie and Hahnfeldt, 2013). From nonspatial models, the effect of immune evasion by the cancer cells has been well described, with the parameter values of the models being derived either from experimental data or estimated logically. Many models which focus on tumour immune competition are based on the pivotal work of Kuznetsov et al. (1994), where the authors developed a system of ODEs to describe the interactions between cytotoxic T lymphocytes and a growing B-lymphoma. The model predicted the experimentally observed oscillations in tumour growth and the parameter values used were validated using experimental data.

Key dynamics can be confirmed or expanded in a wider range of biologically relevant situations by extending these ODE and IDE models into partial differential equation models through the inclusion of spatial phenomena, *e.g.* random motility or chemotaxis, of the cells (Al-Tameemi et al., 2012; d'Onofrio and Ciancio, 2011; Kolev, 2003). In particular, following the work of Kuznetsov et al. (1994), Matzavinos et al. (2004) developed a system of four partial differential equations (PDEs) to describe the interactions between tumour-infiltrating CTLs, tumour cells, CTL-tumour complexes and chemokines. Through stability analysis techniques and numerical simulations, their model revealed the key parameter spaces required for the onset of tumour dormancy. Furthermore, the authors proved the existence of travelling wave solutions which can replicate tumour invasion patterns (Matzavinos and Chaplain, 2004).

By using computational models such as cellular automata (CA) and IB models a wider spectrum of biological phenomena can be translated into mathematical terms and described. These models can be posed on a spatial domain (e.g. a grid), and a set of rules can be given to each cell with certain probabilities to achieve a more

detailed description of cancer-immune competition (Chowdhury et al., 1991; Hu et al., 2012; Kather et al., 2017; Pappalardo et al., 2008). For example, Christophe et al. (2015) used an individual-based approach to study the interactions between cytotoxic T lymphocytes (CTLs) and a genetically evolving melanoma. Their results indicated that the initial time of interaction between the CTLs and melanoma cells determines the outcome of their competition, as highly mutated tumour cells became less susceptible to immune action.

Hybrid or combination models have been used to a great extent to study the immune response to cancer. Tumour-immune dynamics have been considered in this way using: PDE-CA combination models (Alemani et al., 2012; Mallet and de Pillis, 2006); ODE-IB combination models (Wu et al., 2018); DDE-ABM combination models (Kim and Lee, 2012) and PDE-IB combination models (Anderson and Chaplain, 1998; Bauer et al., 2007). In particular, de Pillis et al. (2006b) used a hybrid PDE-CA approach to describe tumour-immune competition. They used PDEs to describe the evolution of pro-tumour nutrients within the tumour microenvironement and described tumour cell, CTL and natural killer (NK) cell movement and interactions through the CA approach. Using this framework they explored the role of nutrients, cell-cell adhesion and immune cell capabilities on the growing tumour.

Mathematical approaches have additionally been used to describe the role of tumour antigen expression within tumour-immune interactions. Traditionally, tumour antigen expression and recognition by the immune system have been implicitly modelled by tuning the rates of T cell recruitment, T cell proliferation or tumour cell removal (Arciero et al., 2004; Balea et al., 2014; Besse et al., 2018; De Boer et al., 1985; de Pillis et al., 2009; Köse et al., 2017; Mallet and de Pillis, 2006). More recently, these processes have been explicitly captured by mathematical mod-

els formulated in terms of either ordinary differential equations (Balachandran et al., 2017; d'Onofrio and Ciancio, 2011; Łuksza et al., 2017) or integro-differential equations (Delitala et al., 2013; Delitala and Lorenzi, 2013; Kolev et al., 2013; Lorenzi et al., 2015). In Chapters 5 and 6 of this thesis, we develop individual-based models to describe the interactions between solid tumour and the immune system and in Chapter 6, we explicitly consider tumour evolution through epimutations.

3.4.3 Mathematical modelling of immunotherapies

Prediction of the success of cancer treatment protocols, especially immunotherapies, can be achieved through the use of mathematical models. Models of immunotherapy have been used to investigate the conditions of therapies which lead to tumour dormancy or tumour removal without an overactive immune response (d'Onofrio, 2005; Frascoli et al., 2014). In particular, ODE models have been used to predict the effects of immunotherapy techniques by allowing the user to vary the dose, administration and timing of a variety of treatments to find the hypothetical optimal situation, which can then be further investigated through experiments and clinical trials (Walker and Enderling, 2016). Furthermore, predator-prey like models have been used to describe dynamics of the immune and tumour cells, where the number or properties of competing immune cells change due to therapy (Arciero et al., 2004; Babbs, 2012; Bunimovich-Mendrazitsky et al., 2015; Burden et al., 2004; Cappuccio et al., 2006; Radunskaya et al., 2013; d'Onofrio and Ciancio, 2011; Frascoli et al., 2014; Hu et al., 2012; Konstorum et al., 2017; Köse et al., 2017; Kuznetsov and Knott, 2001; Nani and Freedman, 2000; Sotolongo-Costa et al., 2003). Additionally, key markers for therapies to target, such as tumour antigens, can also be discovered through ODE models (Balachandran et al., 2017; Łuksza et al., 2017). Moreover, a combination of PDE and IB models has been used, for example, to describe tumour

growth in the presence of cytotoxic and cytostatic drugs, highlighting that the local tumour cell environment plays a key role (Lorenzi et al., 2015; Lorz et al., 2015; Cho and Levy, 2017). Contrastingly, computational models have also been utilized to predict the success of immunotherapy techniques (Chowdhury et al., 1991; Mallet and de Pillis, 2006), such as PD-L1 inhibition therapies (Gong et al., 2017).

Mathematical approaches may focus on immunotherapy alone, or the combination of immunotherapy with other forms of therapy, *e.g.* chemotherapy or cytokine therapy (de Pillis et al., 2006a; Kirschner and Panetta, 1998) which generally lead to a more successful response and can block immunosuppression (Dritschel et al., 2018). For example, Joshi et al. (2009) describe adoptive cell therapy and cancer vaccine therapy against a solid tumour using an ODE model. They found that adoptive cell therapy could actually enhance tumour growth, which has been observed experimentally. However, cancer vaccines that targeted antigen presenting cells were able to reduce tumour growth and prevent tumour relapse once dormancy was established.

Model validity and interdisciplinary research

Due to the difficulty in estimating parameter values, many models consider simple systems of equations and instead identify potential parameter spaces of interest (Besse et al., 2018). More in-depth communication between experimentalists, clinicians, statisticians and mathematicians means that more in-depth models can be developed. A key trait of a mathematical model of biological phenomena is that it is biologically relevant. Several models attempt the validation of results with clinical data (Cappuccio et al., 2006; Gatenby and Gawlinski, 1996). However, many models have only estimated parameters or use nonhuman data. Therefore there is a great need for the collaboration of biologists, clinicians and mathematicians to ensure

that models are more in-depth. Interdisciplinary groups can increase the success of research into the development of new cancer therapies (Masoudi-Nejad and Wang, 2015; McGuire et al., 2013). Interdisciplinary work has become more common in cancer research where biological experiments can feed into the model, which can then predict the next step for the experiments, that can then be tested (Christophe et al., 2015; Hua et al., 2016; Walker and Enderling, 2016).

Chapter 4

A simple individual-based model describing immune cell motion

4.1 Overview

In this chapter we introduce the modelling approaches used to capture active and inactive immune cell migration in the tumour microenvironment. Here, the terms inactive and active refer to the interactions of the immune cells with tumour antigens. Therefore, an active dendritic cell has recognised and collected the antigen, whereas an active cytotoxic T lymphocyte has been presented the antigen by the dendritic cell. The work we describe in this short chapter will provide a foundation for the development of the more detailed individual-based (IB) models described in subsequent chapters.

4.2 Background

Boissonnas et al. (2007) used individual cell tracking to study the movement of cytotoxic T lymphocytes (CTLs) in the presence and absence of tumour antigen, and verified a change in the mechanisms of movement between these two situations. In the instance where tumour antigen was absent the cells migrated in a search-like pattern. On the other hand, when the tumour antigen was present the cells exhibited a restricted form of motion whereby they could only travel short distances in any direction. Therefore, these results can be used to describe the migration of CTLs which are in an inactive state or the migration of CTLs which are activated by tumour antigen. Engelhardt et al. (2012) observed that dendritic cells (DCs) alter their migration pattern in a similar manner to CTLs when exposed to tumour antigen.

In this chapter, we aim to capture these two forms of cell motion using mathematical modelling techniques. As mentioned in Section 3.3, stochastic models, such as individual-based (IB) models, are appropriate for describing complex spatial migration patterns. Therefore, we develop an IB model of cell motion based on random walk methods to describe the experimental results of Boissonnas et al. (2007). The code was developed and the simulations were run in MATLAB. The model described in this chapter and some of the results shown have been published in Macfarlane et al. (2018).

4.3 Determining the appropriate form of random walk

To determine which form of random walk is appropriate to capture the migration patterns of immune cells in the absence and presence of tumour antigen we extract the key properties of the migration patterns observed in the experimental works mentioned previously. Immune cells, when tumour antigen is absent, appear to persist in one direction for a period of time before changing direction and repeating the process. These search-like patterns have been observed in other areas of cell biology and have been mathematically described as Lévy processes (Ariel et al., 2015; Detcheverry, 2017; Miller et al., 2002; Wolf et al., 2003). We refer the reader to Section 3.3 for further information on Lévy processes and how they have previously been modelled. Following these methods, we hypothesise that a Lévy walk implemented into an individual-based model may be suitable to represent the migration patterns of inactive immune cells in the tumour microenvironment. Interestingly, recent literature, based on experimental data and fitting the data to mathematical models, suggests that T cells may move in a superdiffusive or Lévy like motion (Agliari et al., 2014; Fricke et al., 2016; Harris et al., 2012; Krummel et al., 2016; Weninger et al., 2014). Therefore, we hypothesise that a Lévy walk will capture the migration of inactivate immune cells in the tumour microenvironment.

In contrast to the immune cells when no antigen is present, from the experimental observations of Boissonnas et al. (2007), immune cells in the presence of tumour antigen appear to have a limited migration pattern. That is, the cells do not move in one direction for significant periods of time, suggesting that they change direction very frequently. Brownian motion is a standard form of diffusion and is used regularly in modelling cell motion, including that of T cells (Casal et al., 2005;

Celli et al., 2012; de Pillis et al., 2006b; Matzavinos et al., 2004). Each cell that undergoes Brownian motion moves randomly where each step is unrelated to the previous one. This generally leads to cells staying within a smaller area over time and therefore we choose this to represent the active immune cells that were shown to have restricted movement in Boissonnas et al. (2007). Therefore, we hypothesise that Brownian motion will capture the migration of activated immune cells in the tumour microenvironment.

4.4 The individual-based model

The individual-based model is designed on a 2D spatial domain, which we separate into a grid with sites of length Δ_x in the x direction, and Δ_y in the y direction. Each time-step of the simulations of the model will have length Δ_t. We will consider a number of cells, N, on the grid and allow them to move using either a Lévy walk or Brownian motion, as described above. To consider a biologically realistic situation, we additionally impose a volume exclusion limit whereby only one cell can occupy any grid-position at any one time. We set up the two forms of random walk utilising the probabilities of moving to one of the eight neighbouring grid positions, as shown in Figure 4.1a.

4.4.1 The Lévy walk mechanism

If a cell is following a Lévy walk process, the direction of movement is initially chosen randomly, with equal probability, from one of the eight possible directions. The probability of choosing a step-length s is determined by the Lévy distribution,

$$\mathrm{L}(s) \sim s^{-(\alpha+1)}, \tag{4.1}$$

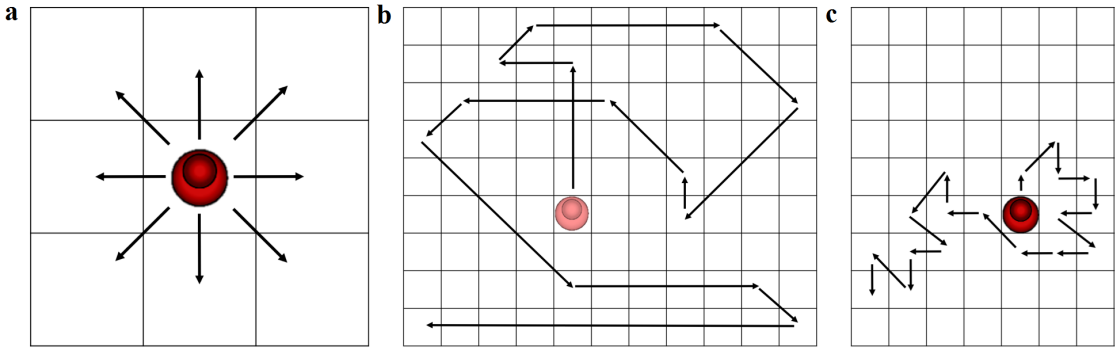

Figure 4.1: Cell neighbourhood and example immune cell trajectories using the random walk mechanisms. ***a*** *At each time-step, immune cells can move to one of the eight neighbouring grid-sites provided it is unoccupied.* ***b*** *Immune cells which move via a Lévy walk have probabilities of moving in a given direction for s time-steps which is taken from the Lévy distribution given by equation* (4.1). ***c*** *Immune cells which move via Brownian motion have an equal probability of moving to neighbouring grid-sites at each time-step.*

where s is the number of time-steps the cell will move in a given direction and α is the walk exponent (see Harris et al. (2012) for full details). If the number of steps is one, *i.e.* $s = 1$, then the process repeats at the next time-step, otherwise the cell will keep moving in the initially chosen direction until all steps have been taken. Once the step-number is completed the process begins again. The Lévy distribution for step-length results in a high probability that cells will choose a short step-length, however longer step-lengths can still be chosen. These properties ensure that cells whose motion is governed by a Lévy walk have a larger probability of moving in a given direction for longer, compared to a Brownian motion, as shown by Figure 4.1b. We make the assumption that cells cannot move to a grid-site outside the boundary of the domain, that is, we impose reflective boundary conditions. Although boundary conditions are imposed, the time-step we consider throughout simulations is small enough that cells will remain well within the boundary. Therefore, the boundary

conditions will not alter the movement trajectories of the cells.

4.4.2 The Brownian motion mechanism

When undergoing a random walk which follows Brownian motion, at each time-step each cell will have the capacity to change direction and move to any of the eight neighbouring grid positions, as shown in Figure 4.1c. That is, cells have an equal probability of moving to any neighbouring grid position at any one time, independent of previous movements, and the process repeats at the next time-step. As in the case of the Lévy walk, we impose reflective boundary conditions to ensure all cells remain within the domain, however the time-step is small enough that these do not effect cell movement. Cells can then move within the grid using either a Brownian motion or Lévy walk mechanism, which we describe below.

4.5 Model set up and results

4.5.1 Set up of simulations

We set up the 2D grid by assigning the step-lengths Δ_x and Δ_y as well as the time-step-length Δ_t. To be consistent with the average cell size of immune cells (Goya et al., 2008; Rozenberg, 2011), we choose our spatial step-lengths to be $\Delta_x = \Delta_y = 10$ μm. Note that, since we consider the diagonal neighbourhoods of cells the grid-spacing can increase if moving diagonally to $\sqrt{2}\ \Delta_{x/y}$, with these values still within the biological ranges of immune cell diameter. Furthermore, to satisfy the immune cell speed and set up given in Boissonnas et al. (2007), we consider: a time-step of $\Delta_t = 1$ min, define a 200×200 μm^2 grid and consider $N = 50$ cells within the system.

The Lévy walk mechanism: For cells moving via the Lévy walk mechanism, the probability of changing direction depends on the number of steps that the cell had taken in the current direction s. The probability of moving in any direction, D_i of the eight possible directions, $i = 1, \ldots, 8$, at any one time can be calculated as,

$$\mathrm{P}(D_i) = \left\{ \begin{array}{l} \frac{1}{8}, \quad \text{if } s = 0, \\ 1, \text{ if } s > 0 \text{ and } i \text{ is the previous direction taken}, \\ 0, \text{ if } s > 0 \text{ and } i \text{ is not previous direction taken}, \end{array} \right\} \quad \text{for } i = 1, \ldots, 8.$$

For the Lévy walk we also need to consider the exponent α of the step-length distribution given in equation (4.1). Following work by Harris et al. (2012) we consider an exponent of,

$$\alpha = 1.15.$$

Using this exponent and allowing only integer step-lengths we define a Lévy distribution. From this distribution we calculate the probability of choosing a step-length of at least length s. As we consider only integer step-lengths we obtain the probabilities of choosing a certain step-length, represented in Figure 4.2, where cells choose a step-length of $s \in \{1, \ldots, 11\}$.

The Brownian motion mechanism: For cells which undergo the Brownian motion random walk, each movement is independent of the previous movement choices. The probability of moving in any direction, D_i of the eight possible directions, $i = 1, \ldots, 8$, at any one time can be calculated as,

$$\mathrm{P}(D_i) = \frac{1}{8} \quad \text{for } i = 1, \ldots, 8.$$

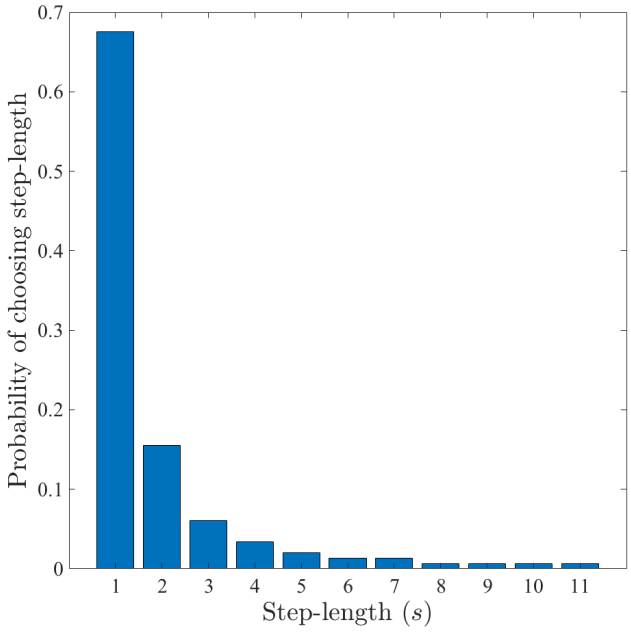

Figure 4.2: Probability of choosing step-lengths for cells undergoing a Lévy walk. *The bars represent the probability of choosing a step-length of length s for each cell undergoing a Lévy walk. These values are calculated using the Lévy distribution given in equation* (4.1) *and using the exponent* $\alpha = 1.15$.

4.5.2 Comparison of the models with experimental data of single CTL tracking

To test that using Lévy walk and Brownian motion mechanisms are appropriate for modelling immune cell motion in the absence and presence of tumour antigen, we attempt to qualitatively replicate the experimental observations of Boissonnas et al. (2007). In this experimental work they considered cytotoxic T lymphocyte (CTL) motion over time in the presence or absence of a tumour antigen. The experimental results indicated that if tumour antigen is present the CTLs cover a more restricted area moving at a speed of around 5μm min^{-1}, whereas in the absence of antigen CTLs move in a search type pattern exploring a wider portion of space over the same time interval, moving at a faster speed of around 10μm min^{-1}. To reproduce, *in silico*, the experimental setting used in Boissonnas et al. (2007), we considered 50 cells with their starting positions aligned and tracked each individual cell's trajectory over time in the case where cell movement was modelled by the two afore mentioned random walks. Initially, we consider the case where there is no tumour antigen present and wish to compare our model to the experimental observations, displayed in Figure 4.3a. As mentioned previously, we hypothesised that a Lévy walk would be an appropriate method of describing the search-like pattern of the CTLs. Therefore, we ran simulations, for a time consistent with the time-frame of the experimental data, allowing 50 cells to undergo a Lévy walk. Furthermore, to align with the experimental data we allowed each cell to move at a speed of 10μm min^{-1}. Each cell was tracked over time and the resulting movements are displayed in Figure 4.3c. A good qualitative match is observed between Figure 4.3a and Figure 4.3c, where cells can move a significant distance from the origin and appear to be able to persist in one direction for a period of time before changing direction. We then turn our attention

to the case where tumour antigen is present and again wish to compare our model to the experimental observations, displayed in Figure 4.3b. In this situation, we hypothesised that Brownian motion would be an appropriate method of describing the restricted motion of the CTLs. To investigate this we ran simulations, for a time consistent with the time-frame of the experimental data, allowing 50 cells to move via Brownian motion. Again, to align with the experimental data we allowed each cell to move at a speed of 5μm min^{-1}. Each cell was tracked over time and the resulting movements are displayed in Figure 4.3d. When comparing Figure 4.3b and Figure 4.3d we can conclude that Brownian motion is an appropriate modelling method here, as we capture the restricted motion of the cells where they change direction frequently. To confirm that these qualitative matches between the experimental data and computational results are not dependent on the speed at which cells travel, we also consider a faster version of Brownian motion and a slower version of the Lévy walk. We consider cells moving via Brownian motion at a cell speed of 10μm min^{-1}, displaying the results in Figure 4.3e and compare these to the results in Figure 4.3a. Here, we observe that the faster Brownian motion does not capture the persistance of the cells when there is no tumour antigen present. Similarly, we consider cells moving via a Lévy walk at a cell speed of 5μm min^{-1}, displaying the results in Figure 4.3f and compare these to the results in Figure 4.3b. Here, we demonstrate that the slower Lévy walk does not capture the restricted motion of cells when tumour antigen is present.

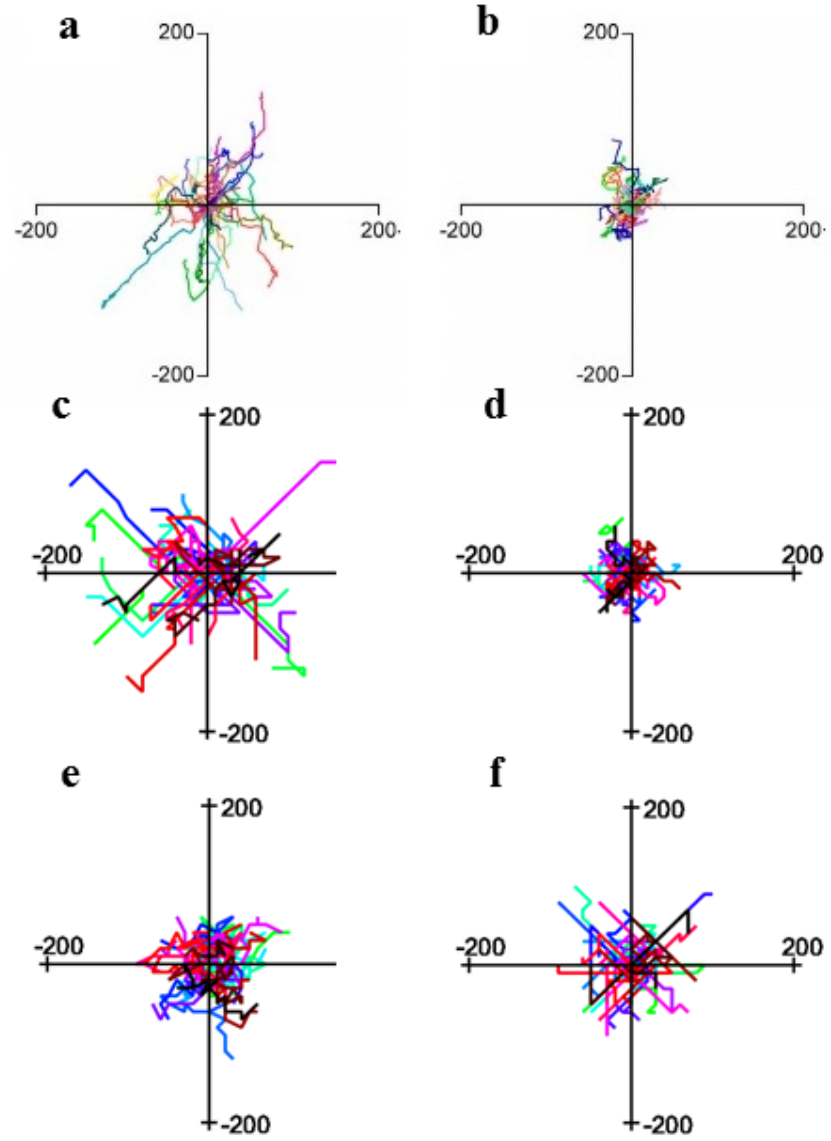

Figure 4.3: Comparison of the models with experimental data of single CTL tracking. *Each figure displays the overlay of* 50 *cell tracks with aligned starting positions.* ***a*** *Experimental observations from Boissonnas et al. (2007) of CTLs when there is no tumour antigen.* ***b*** *Experimental observations from Boissonnas et al. (2007) of CTLs in the presence of tumour antigen.* ***c*** *Cells undergoing a Lévy walk with a speed of* $10\mu m\ min^{-1}$. ***d*** *Cells moving via Brownian motion with a a speed of* $5\mu m\ min^{-1}$. ***e*** *Cells moving via Brownian motion with a speed of* $10\mu m\ min^{-1}$. ***f*** *Cells undergoing a Lévy walk with a speed of* $5\mu m\ min^{-1}$.

Figure 2B: Image 1, Image 3, used with permission, from (Boissonnas et al., 2007)
 Journal of Experimental Medicine. 204(2):345-356. doi: 10.1084/jem.20061890

4.5.3 Comparison of the key properties of Brownian motion and Lévy walk mechanisms

To allow for further understanding of the differences between using Brownian motion and Lévy walk mechanisms we investigate and compare some of the key properties of each random walk.

The cover time of a random walk is defined to be the time taken for a random walker to cover all points in the grid. Mathematical analysis and comparison of the cover time of random walks has been described previously (Chupeau et al., 2015; Koren et al., 2007; Yokoi et al., 1990), highlighting the dependence of the cover time on the first passage time (Condamin et al., 2007; Tejedor et al., 2009). Through these works, it can be suggested that a Lévy walk should be more efficient, *i.e.* have a faster cover time, than Brownian motion. We verify this by considering the cover time of both mechanisms within our individual-based model. We placed one cell on the grid defined previously and allowed it to perform either a Lévy or Brownian random walk. The cell continued until all grid positions have been covered. We did this for both the Lévy and Brownian mechanisms with two cell speeds, *i.e.* 5μm min^{-1} and 10μm min^{-1}, and a range of values for the Lévy exponent α. The resulting cover times are shown in Figure 4.4. We ran each simulation ten times and average the results to obtain a deeper understanding of the cover time of each walk process. We first compare the case where α=1.15 in the Lévy walk mechanisms and Brownian motion, *i.e.* the red and black results in Figure 4.4. Our results suggest that independent of cell speed, the Lévy walk mechanism is generally more efficient than the process of Brownian motion. By considering the standard deviations of these results, we find that in general the Lévy walk mechanism appears to have more consistent cover times. The Brownian motion mechanism, on the other hand,

has a larger standard deviation suggesting that there is greater variability in the cover time of this method. These results indicate that the Lévy walk response is more consistent in terms of reproducibility. We can also compare the cover time of the Lévy walk with increasing values of α. From the results displayed in Figure 4.4 we observe a general increase in cover time with the increase of α for both cell speeds investigated. When comparing the two cell speeds we observe an decrease in the cover time for all cases when we increase the cell speed from 5μm min^{-1} to 10μm min^{-1}. However, the decrease in cover time appears to be more prominent in the Brownian motion case compared to the Lévy walk cases. Furthermore, for several cases the standard deviation between runs is smaller for the larger cell speed indicating that the a faster cell speed leads to more consistent results.

The outcomes of our model suggest that following a Lévy walk allows cells to spread further in the domain. To investigate this further, we consider the maximum distance that any cell travels from its starting position. We allowed cells to move via the two distinct random walk processes and then calculated their distance from the origin, *i.e.* their starting position, at each time-step. We tested both the Lévy walk with exponent α=1.15 and the Brownian motion for the two cell speeds. Each parameter setting was tested ten times with the average results being displayed in Figure 4.5. The simulation results suggest that the Lévy walk allows cells to move further from the origin than Brownian motion. Generally, the result indicate that the distance travelled is also more varied when using the Lévy walk, as can be seen from the standard deviation lines in Figure 4.5.

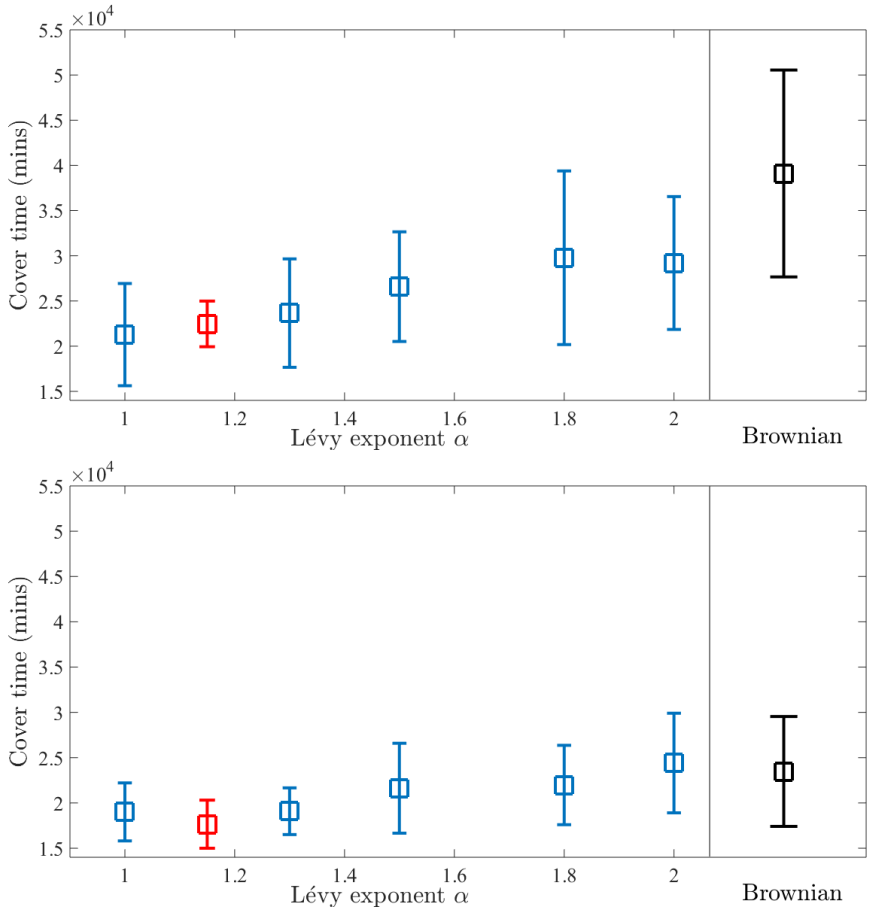

Figure 4.4: Comparison of the cover time of each walk mechanism. *The cover time is calculated as the time taken to visit all* 1681 *positions of the grid. The squares represent the average cover time for each chosen cell motion and the lines represent the standard deviation over ten runs of the simulations. The top panel displays the results for the case where cells move at the speed* $5\mu m\ min^{-1}$ *and the lower panel displays the results for the case where cells move at the speed* $10\mu m\ min^{-1}$*. Results are displayed for Brownian motion (black) and a Lévy walk with increasing values of the exponent* α *(blue) with the results for* α*=1.15 highlighted in red.*

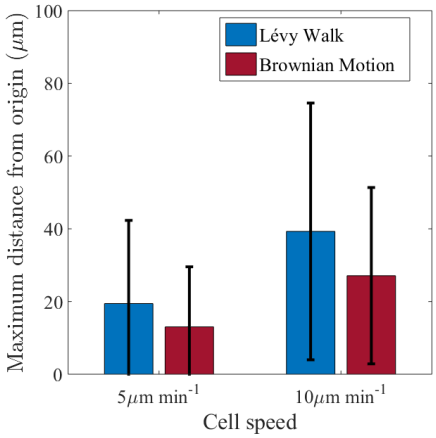

Figure 4.5: Comparison of the maximum distance from the origin of cells using each walk mechanism. *Bars represent the maximum distance travelled of the Lévy walk (blue) and Brownian motion (red) for two different cell speeds. The error bars represent the standard deviation between ten runs of the simulations.*

4.6 Concluding remarks and discussion

In this chapter we have developed a discrete individual-based model of immune cell motion which takes into account the difference of motion in regard to the presence of tumour antigen. Our simulation results demonstrate that the strategies we adopted to modelling cell motion make it possible to qualitatively reproduce trajectories of cytotoxic T lymphocytes (CTLs) observed in experimental data (Boissonnas et al., 2007). In particular, the Lévy walk provides a good representation of CTLs' motion when the antigen is not present, whilst Brownian motion captures the movement of CTLs in the presence of a tumour antigen. Due to the similar cell motions observed in dendritic cells by Engelhardt et al. (2012), we assume that dendritic cells will respond to tumour antigen in the same way.

Furthermore, systematic comparisons can be made between the two random walk methodologies. We consider the cover time of both processes and demonstrate that, generally, the Lévy walk process is more efficient than the Brownian motion process.

This is supported by previous mathematical analysis of both walk mechanisms (Chupeau et al., 2015; Koren et al., 2007; Yokoi et al., 1990). Additionally, our results suggest that the smaller the walk exponent α the faster the cover time. Furthermore, exploration into the maximum distance that cells can travel from their original position allows us to confirm that the Lévy walk allows cells to spread further into the domain compared to Brownian motion.

Overall, our results suggest that it would be appropriate to model the movement of inactive immune cells using a Lévy walk, whereas the movement of active immune cells can be modelled using Brownian motion. Through comparing the results of the two different cell speeds, we can observe that the resulting dynamics of cells will be similar when using faster or slower cell speeds. Therefore, for simplicity, we can allow both inactive and active immune cells to have the same speed. In the following chapter, we develop an individual-based model of tumour-immune competition and utilise the random walk methods described in this chapter to describe immune cell motion. We do this by introducing a solid tumour into the system and, in turn, considering the interactions between the immune cells and the cancer cells.

Chapter 5

An individual-based modelling approach to describe tumour-immune interactions

5.1 Overview

In this chapter, we will develop an individual-based (IB) model to describe tumour-immune competition. We do this by utilising the IB approach described in Chapter 4 to model the movement of the immune cells. Furthermore, we include a solid tumour, made up of tightly packed cancer cells, and consider the interactions between the tumour cells and the immune cells in the surrounding microenvironment. Once the model is set up, we tune certain parameters to investigate their role in the removal of solid tumours by the immune system. The computational simulation results of the model highlight which mechanisms control the outcome of tumour-immune competition indicating that they may be potential targets in the development of new immunotherapies. The model described in this chapter and several of the results

shown have been published in Macfarlane et al. (2018).

5.2 Model development

We consider the interactions, in an *in vitro* situation, between three cell types: cancer cells, dendritic cells (DCs) and cytotoxic T lymphocytes (CTLs) through individual-based modelling techniques. The total numbers of these cells will be denoted by N_T, N_D and N_C, respectively.

As in Chapter 4, the IB model is posed on a 2D spatial grid of spacing Δ_x in the x direction and Δ_y in the y direction. To incorporate the biophysical constraints upon the cells, we make the assumption that only one cell of any type is allowed on each grid position at any time-step of duration Δ_t.

5.2.1 Tumour cell population growth and migration

Tumour cell division: Initially, we consider a tumour consisting of tightly packed cancer cells with a circular geometry. The solid tumour can expand over time through cell division. Specifically, each cancer cell can divide at the rate λ, forming two progeny cells. One progeny cell will occupy the parent cell's grid position and the other shall be placed at an unoccupied neighbouring position - see Figure 5.1a. This method ensures that only cancer cells which have free grid positions in their neighbourhood can divide (*i.e.* cancer cells in the centre of the solid tumour will not divide).

Tumour cell death: It can be assumed that the rate of natural tumour cell death will be much lower compared to the rate of tumour cell division, therefore we omit tumour cell death from the model.

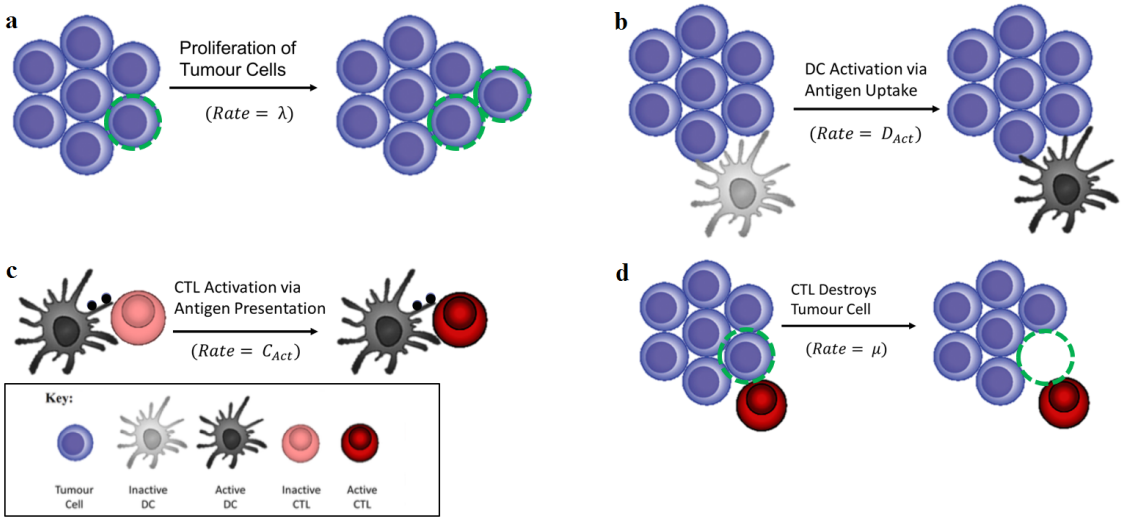

Figure 5.1: A schematic overview of the biological and immunological mechanisms that are considered in the individual-based model. *Three cell types: cancer cells, dendritic cells (DCs) and cytotoxic T lymphocytes (CTLs) and the inactive/active states of both immune cells are included in the model (key subpanel).* ***a*** *Division of each tumour cell can occur at the rate λ, provided a neighbouring grid position is unoccupied.* ***b*** *Through contact with tumour cells, DCs can become activated at the rate D_{Act}.* ***c*** *At the rate C_{Act}, CTLs can become activated through interactions with activated DCs.* ***d*** *Once activated, CTLs can remove tumour cells at the rate μ, through cell-cell interactions.*

Tumour cell migration: We do not consider migration of the tumour cells as we assume that the tumour is in the early stages of development and, therefore, has not yet initiated the invasion and metastasis processes (for more detail we direct the reader to Section 2.3). This means that spreading of the tumour throughout the domain is controlled by cell division only.

5.2.2 Immune cell migration and activation

Movement of inactive immune cells: At the start of the simulations, we assume that only inactive immune cells are present and we assume that they are randomly distributed throughout the domain. Both the inactive DCs and inactive CTLs will migrate within the domain following a Lévy random walk mechanism that was developed in Chapter 4.

Activation of dendritic cells: While moving within the domain, each inactive DC can interact with a tumour cell if they are positioned on neighbouring grid-sites. At the rate D_{Act}, we allow the DC to become activated by the tumour cell - see Figure 5.1b. For most simulations, we assume that once each DC has become activated it will remain activated over the time-frame considered. However, we will also consider an exhaustion limit in some simulations, where each DC can only activate a certain number of CTLs. Once it has reached the exhaustion limit it will become an exhausted DC, *i.e.* it will move around like an active DC but will be unable to interact with CTLs.

Activation of cytotoxic T lymphocytes: Inactive CTLs can become activated via cell-cell interactions with activated DCs. If an active DC and an inactive CTL are situated on neighbouring grid positions then they can interact and the CTLs

can become activated at the rate C_{Act} - see Figure 5.1c. We assume, in the model, that each DC can then go on to activate an infinite number of CTLs, although an exhaustion process is considered later in the chapter. As with the DCs, for most simulations we assume that once each CTL has become activated it will remain activated over the time-frame considered. However, we will also consider an exhaustion limit in some simulations, where each CTL can only interact with a certain number of tumour cells. Once it has reached the exhaustion limit it will become an exhausted CTL, *i.e.* it will move around like an active CTL but will be unable to interact with tumour cells.

Movement of activated immune cells: Upon activation, the immune cells will alter their form of cell migration from a Lévy walk to the Brownian motion mechanism developed in Chapter 4.

Immune cell number and proliferation: We use reflective boundary conditions to ensure that all cells remain within the domain, to replicate an *in vitro* situation, *i.e.* there will be no additional cells entering the domain and no cells leaving the domain. We additionally omit the effects of cell division and cell death on both immune cell populations for simplicity. Therefore, their respective cell numbers will remain constant over the time-frame considered. Furthermore, as mentioned in Chapter 2, there can be mechanisms where the tumour cells can damage and remove immune cells directly, however we will not consider these mechanisms in this work.

5.2.3 Tumour cell removal by CTLs

Once activated, each CTL has the capability to interact with and remove tumour cells. If an active CTL and a tumour cell occupy neighbouring grid positions, the

Table 5.1: *The average diameters of human cell types considered in the IB model*

Cell Type	Average Diameter	Reference
Cytotoxic T lymphocyte	9-16 μm	(Rozenberg, 2011)
Dendritic cell	$\sim 7\mu$m	(Goya et al., 2008)
Melanoma cell	~ 12.5 μm	(Christophe et al., 2015)

CTL can instantly remove the tumour cell from the system at the rate μ - see Figure 5.1d. We then allow each CTL to continue to interact with an infinite number of other tumour cells in the system, that is, no exhaustion or deactivation process occurs. Note that we will briefly discuss the effect of an exhaustion process later in this chapter.

5.3 Individual-based model set up and results

5.3.1 Model parameterisation and numerical set up

Using biologically relevant values, from published data where possible, we parametrise the IB model developed in Section 5.2.

Set up of the 2D grid: To determine an appropriate domain for the model, we consider the average size of our three cell types where we choose the cancer cells to be melanoma cells - see Table 5.1. To allow for simplicity, we take an average and set the length of each grid position to be 10 μm in both the x and y directions. This translates to setting,

$$\Delta_x = 10 \ \mu\text{m} \quad \text{and} \quad \Delta_y = 10 \ \mu\text{m}. \tag{5.1}$$

As in the previous chapter, since we consider the diagonal neighbourhoods of cells the grid-spacing can increase if moving diagonally to $\sqrt{2}\ \Delta_{x/y}$, with these values still within the biological ranges of immune cell diameter. Additionally, we define our domain in such a way that we obtain a two-dimensional 100×100 position grid, representing a 1 mm^2 *in vitro* sample of tissue.

Setting the time-step of simulations: Each time-step is of length Δ_t, the value of which we can assign by considering the speed of moving immune cells. Referring to the biological data used to model immune cell motion in Chapter 4, the average speed of CTLs has been found to be approximately $10 \pm 5\mu\text{m min}^{-1}$ (Boissonnas et al., 2007). For simplicity, we assume an average cell speed of $10\mu\text{m min}^{-1}$ for both inactive and active immune cells and choose a time-step of length,

$$\Delta_t = 1 \text{ min}, \tag{5.2}$$

i.e. we allow each cell to move one grid-step per time-step.

Division of tumour cells: Christophe et al. (2015) calculated the average doubling time of a melanoma cell to be 1000 mins which translates to a cell division rate of,

$$\lambda = 0.001 \text{ min}^{-1}, \tag{5.3}$$

which we choose in our numerical simulations of our IB model.

Movement of inactive immune cells: Harris et al. (2012) studied the migration of CTLs in the brains of infected mice in response to the pathogen *Toxoplasma gondii* and found that they followed a Lévy walk with exponent of 1.15. Therefore, as in

Chapter 4, we choose the Lévy exponent

$$\alpha = 1.15. \tag{5.4}$$

Activation of dendritic cells: We choose the activation rate of dendritic cells to be the same as that found by Bianca et al. (2012), that is

$$D_{Act} = 0.07 \text{ cells min}^{-1}. \tag{5.5}$$

Activation of cytotoxic T lymphocytes: From the experimental work of Engelhardt et al. (2012), it can be calculated that it takes on average around 562 secs for a single DC to activate a CTL through antigen presentation. This corresponds to an activation rate of

$$C_{Act} \approx 0.12 \text{ cells min}^{-1}, \tag{5.6}$$

which we choose in our numerical simulations of our IB model.

Tumour cell removal by CTLs: In addition to the cell division rate, the rate at which active CTLs can remove melanoma cells was described in the experimental work of Christophe et al. (2015) and was found to be

$$\mu = 0.038 \text{ cells min}^{-1}. \tag{5.7}$$

The full list of parameter values is displayed in Table 5.2, and unless stated otherwise these are the values used in numerical simulations of the IB model. The code was developed and the simulations were run in MATLAB. Furthermore, all simulation results were averaged over three separate runs with the same parameter settings to ensure reliability of results. Examples of the spatial distributions of

Table 5.2: *Model parameters and related values used in computational simulations.*

Symbol	Description	Value/ Units	References
Δ_t	time-step of simulations	1 min	(Boissonnas et al., 2007)
$\Delta_{x(y)}$	grid spacing in the x (y) direction	10 μm	Calculated
N_T	total number of tumour cells	initial values: 400 or 1200 cells	(Christophe et al., 2015)
N_C	total number of CTLs	400 cells	(Christophe et al., 2015)
N_D	total number of DCs	400 cells	Estimated
μ	rate at which a CTL kills a tumour cell	0.03 cells min^{-1}	(Christophe et al., 2015)
λ	tumour cell division rate	0.001 min^{-1}	(Christophe et al., 2015)
D_{Act}	DC activation rate	0.07 cells min^{-1}	(Bianca et al., 2012)
C_{Act}	CTL activation rate	$\approx$ 0.12 cells min^{-1}	(Engelhardt et al., 2012)
α	Lévy walk exponent	1.15	(Harris et al., 2012)

the cells over the simulation time are provided in Appendix A, Figure A.1 and Figure A.2.

5.3.2 Increasing the number of DCs can cause overcrowding and lead to longer tumour removal times

As mentioned in Section 2.6, a potential aim of adoptive cell therapies is to increase the number of activated DCs or CTLs within the tumour microenvironment. To investigate this further, using our IB model, we can consider the effect that increasing either the number of DCs and/or CTLs has on the immune response to a solid tumour. We ran each simulation over a 72 hr time-frame, in line with the work of Christophe et al. (2015), or until all tumour cells were removed from the system. Each simulation was carried out with the parameter values displayed in Table 5.2 and we considered a range of 40 values for the total number of DCs, N_D, and/or the total number of CTLs, N_C, within the system. We consider a range of cell numbers, from 60 cells to 2400 cells, of each cell type and we consider three situations: either only the number of CTLs is varied, only the number of DCs is varied or both immune cell numbers are varied. The resulting dynamics are described in Figure 5.2. The left panels display heat maps showing the evolution of the tumour cell number over

time for each given value of N_C and/or N_D and the right panels display the resulting tumour cell number over time for four chosen values of N_C and/or N_D (*i.e.* values of 60, 420, 1200 and 2400 cells). When we increase the number of CTLs, N_C, in the system the results shown in Figure 5.2a,b suggest a corresponding decrease in the time it takes to remove the tumour from the system. However, upon further inspection the tumour removal time does not decrease as strongly for increasing N_C when the value is sufficiently large, *e.g.* the results when $N_C = 1200$ and $N_C = 2400$ are similar. Varying the number of DCs within the system, through the parameter N_D, does not appear to be correlated to the time it takes for the immune system to remove a tumour, as seen in the results displayed in Figure 5.2c,d. Particularly, we note that in some cases a larger value of N_D can result in a longer tumour removal time, *e.g.* the time taken to remove the tumour when $N_D = 1200$ is longer than the tumour removal time when $N_D = 420$, as displayed in Figure 5.2d. Interestingly, when we increase both N_C and N_D, the results displayed in Figure 5.2e,f, suggest a correlation between increasing cell number and a decreasing tumour removal time, as was observed in the case where only N_C was varied. To ensure that the results obtained were not unique to the case of a relatively small tumour we also consider a larger tumour, where initially $N_T = 1200$, and observe similar resulting dynamics, as shown in Appendix A, Figure A.3. One key observation of the results displayed in Figure 5.2 is the emergence of situations where a larger number of CTLs, DCs or both cell types can lead to a longer tumour removal time. These observed dynamics could be explained by an overcrowding effect whereby a larger number of cells within the system leads to limited immune access to the tumour site. We consider this in more detail by calculating the average distance of CTLs from the centre of the tumour for the three situations investigated previously: *i.e.* varying N_C only, N_D only or both N_C and N_D. We compare the average distance of CTLs from the centre

of the tumour for two larger values of N_C and/or N_D where the resulting tumour cell number over time for each value is displayed in Figure 5.3. When considering the number of CTLs only, the results shown in Figure 5.3a suggest that when $N_C = 2400$ the CTLs cannot travel as close to the centre of the tumour compared to when $N_C = 1200$. Similarly, when we vary both N_C and N_D the activated CTLs appear to be limited in their capacity to migrate closer to the tumour centre as shown by the results in Figure 5.3c. Interestingly, if only N_D is varied the larger number of DCs present, again, prevents the activated CTLs from travelling towards the centre of the tumour, as the results shown by Figure 5.3b suggest. In particular, when $N_D = 2400$ it appears that the CTLs are not only prevented from travelling towards the centre of the tumour but appear to be pushed even further from the tumour centre over time.

5.3.3 The ratio between the removal rate of tumour cells by CTLs and the tumour cell division rate is a crucial parameter in tumour removal

The rate at which a CTL can successfully remove tumour cells has previously been highlighted as a key parameter which controls the outcome of tumour-immune competition (Matzavinos et al., 2004). To investigate this further we examine the effect of varying the parameter μ. Additionally, we consider the effects of varying the tumour cell division rate λ. As in the previous subsection, each simulation was run over a 72 hr period or until all of the tumour cells were removed from the system. Each simulation was carried out with the parameter values shown in Table 5.2 and we considered a range of 40 values of μ and/or λ. The values of these parameters were scaled ranging from a half to twenty times the original values, which are given

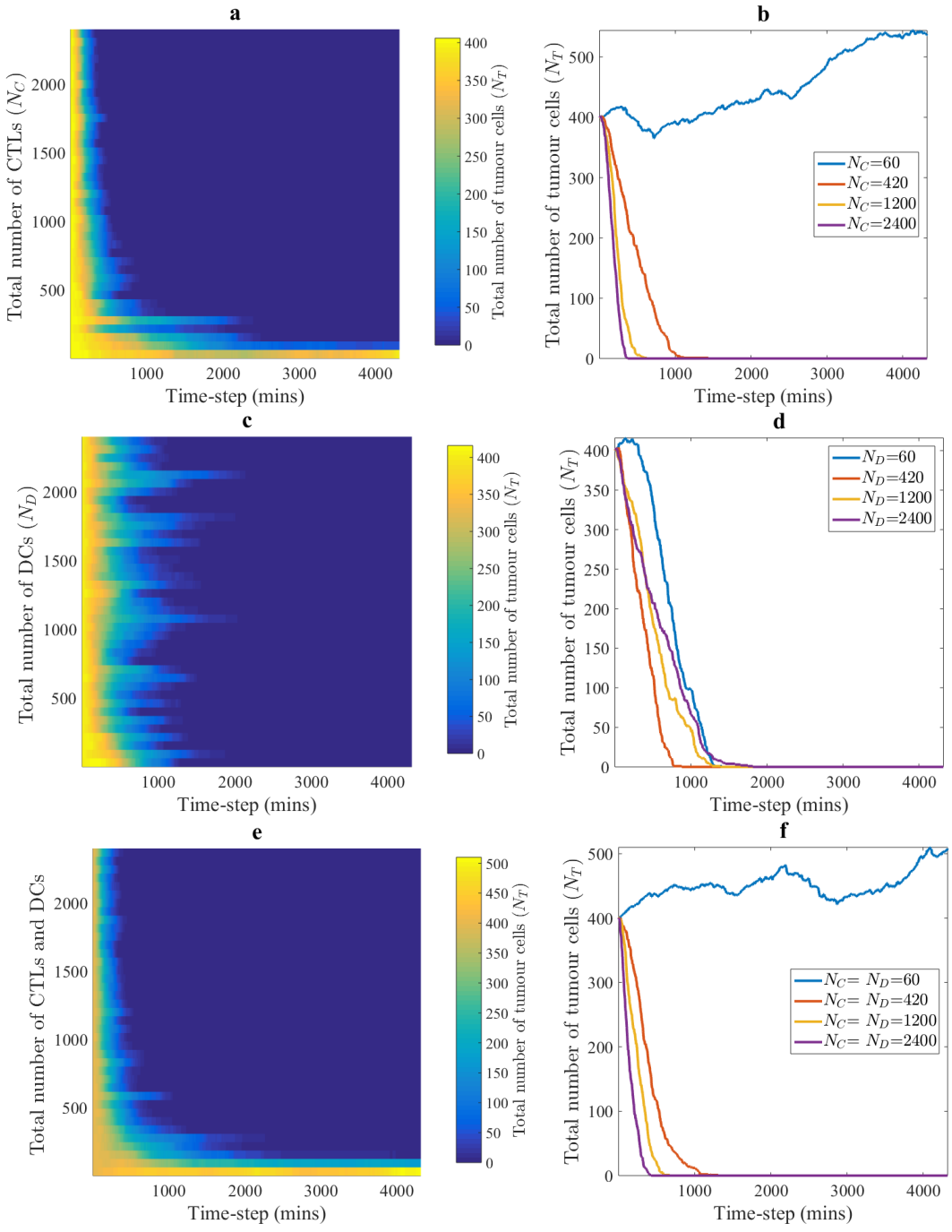

Figure 5.2: Increasing the number of DCs can lead to longer tumour removal times. *The heat maps show the evolution of the tumour cell number over time for each given value of N_C and/or N_D (left panels). We select four simulation results for cell numbers, of* 60, 420, 1200 *and* 2400 *cells, and compare the tumour cell number over time for each parameter setting (right panels). In each case, we begin the simulations with* 400 *tumour cells and test for varying values of:* ***a,b*** *N_C only,* ***c,d*** *N_D only and* ***e,f*** *N_C and N_D. All values displayed are an average over three simulation runs.*

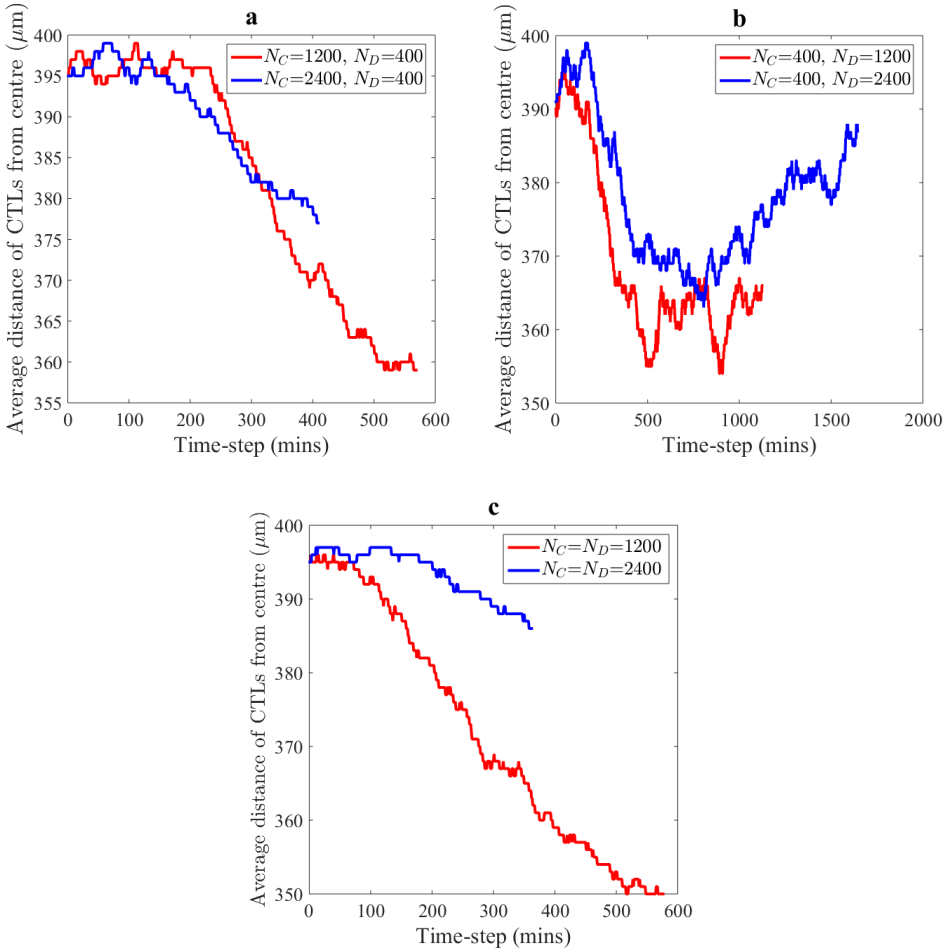

Figure 5.3: Increasing the number of DCs can cause overcrowding. *Plots displaying the average distance of the CTLs from the centre of the domain (*i.e. *the initial centre of the tumour). We test for varying values of:* **a** N_C *only,* **b** N_D *only and* **c** N_C *and* N_D*. In each case we compare the results of simulations for two values of the varied parameter(s), choosing values of* 1200 *cells (red line) or* 2400 *cells (blue line). All values displayed are an average over three simulation runs.*

in Table 5.2. The resulting dynamics are described in Figure 5.4. The left panels display heat maps to show the evolution of the tumour cell number over time for each given value of μ and/or λ. In the right panels of Figure 5.4, we display the results of using values of a half, one, ten and twenty times the original parameter values and compare the tumour cell number over time for each parameter setting. Through increasing μ only a decrease in tumour removal time is observed in the results shown in Figure 5.4a,b. However, when multiplying our original value of μ by ten or twenty there is no significant difference in the resulting tumour removal time. As expected when we only increase λ, as the results shown in Figure 5.4c,d, we observe an increase in tumour removal time and eventually we encounter situations where the tumour grows too large and cannot be removed in the time-frame considered. However, by increasing both λ and μ we observe a general decrease in tumour removal time, although slightly slower than the cases where only μ is altered, as shown in Figure 5.4e,f. Once again, to ensure that the results obtained were not specific the case of a relatively small tumour we also consider a larger tumour, where initially $N_T = 1200$, and observe similar resulting dynamics, as shown in Appendix A, Figure A.4..

5.3.4 Increasing the activation rates of DCs and CTLs has little effect on tumour removal

Through the biological experiments of immune cells within the tumour microenvironment, the role of immune cell activation through antigen presentation has been highlighted (Boissonnas et al., 2007). Therefore, we consider the effect of altering the activation rate of both CTLs and DCs, C_{Act} and D_{Act}, respectively. As in the previous subsections, each simulation was run over a 72 hr period or until all of the

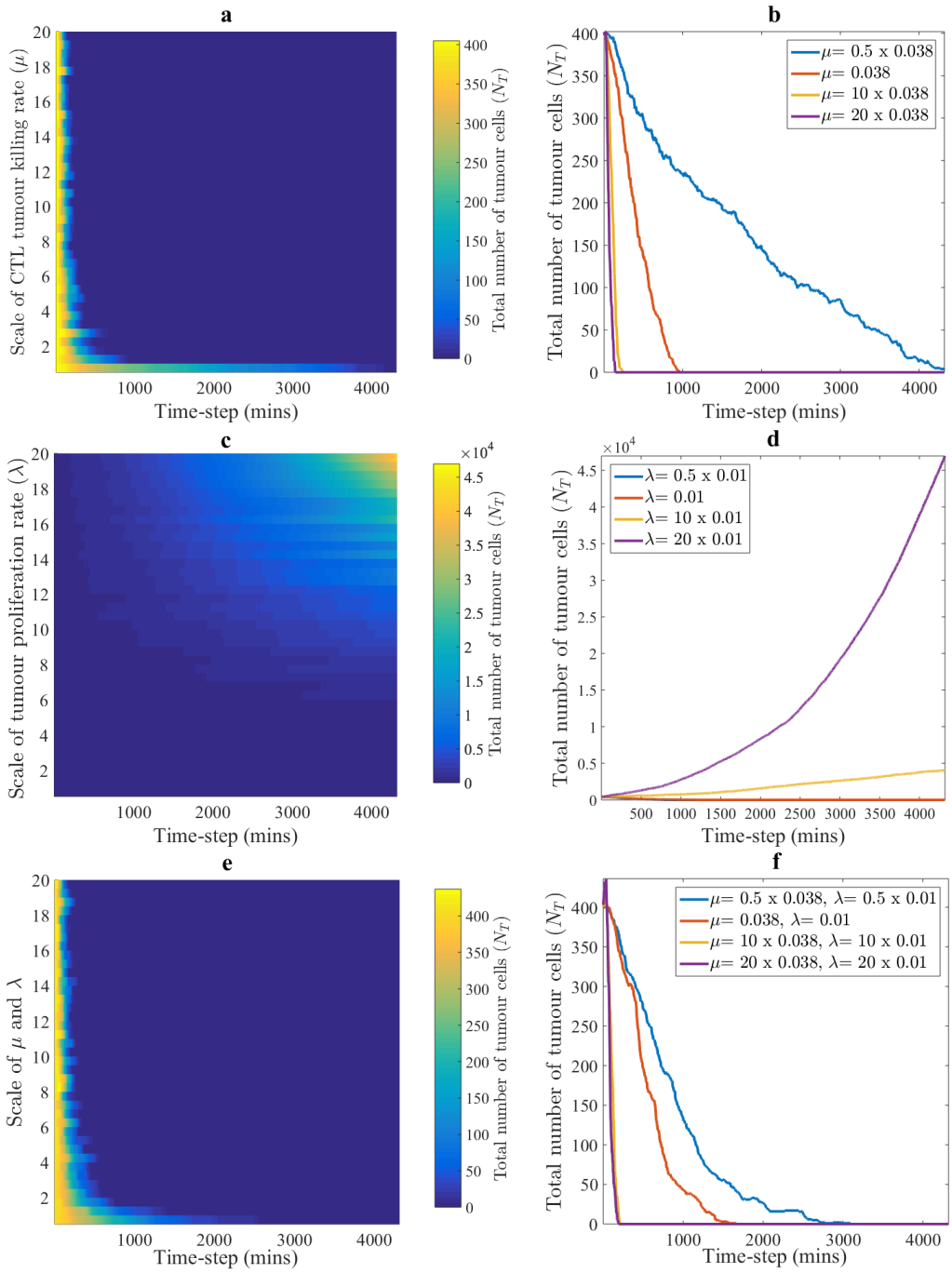

Figure 5.4: The ratio between the removal rate of tumour cells by CTLs and the tumour cell division rate is a crucial parameter in tumour removal. *The heat maps show the evolution of the tumour cell number over time for each given value of μ and/or λ (left panels). We select four values of μ and/or λ and compare the tumour cell number over time for each parameter setting (right panels). In each case, we begin the simulations with 400 tumour cells and test for varying values of:* ***a,b*** *μ only,* ***c,d*** *λ only and* ***e,f*** *μ and λ. All values displayed are an average over three simulation runs.*

tumour cells were removed from the system. Each simulation was carried out with the parameter values shown in Table 5.2 and we considered a range of 40 values of C_{Act} and/or D_{Act}. To compare results we considered two initial tumour sizes: a smaller tumour made up of 400 cells at the beginning of simulations (results shown in Figure 5.5) and a larger tumour made up of 1200 tumour cells at the beginning of simulations (results shown in Figure 5.6). The values of D_{Act} and/or C_{Act} were scaled ranging from a half to twenty times the original parameter values and the resulting dynamics are described in Figure 5.5 and Figure 5.6. The left panels display heat maps to show the evolution of the tumour cell number over time for each given value of C_{Act} and/or D_{Act}. In the right panels of Figure 5.5 and Figure 5.6, we select results of simulations that used a half, one, ten and twenty times the original values of D_{Act} and/or C_{Act}, and compare the tumour cell number over time for each parameter setting. In both the initially larger and initially smaller tumour situations there appears to be no clear correlation between altering either C_{Act} and/or D_{Act} and tumour removal time, which can be inferred by the fluctuating results displayed by the heat maps. Interestingly, when we considered the initially larger tumour we can obtain results whereby higher activations rates lead to a slower tumour removal time, *e.g.* the results shown in the right panels of Figure 5.6. This was not observed in the case of a initially smaller tumour, *e.g.* the results shown in the right panels of Figure 5.5.

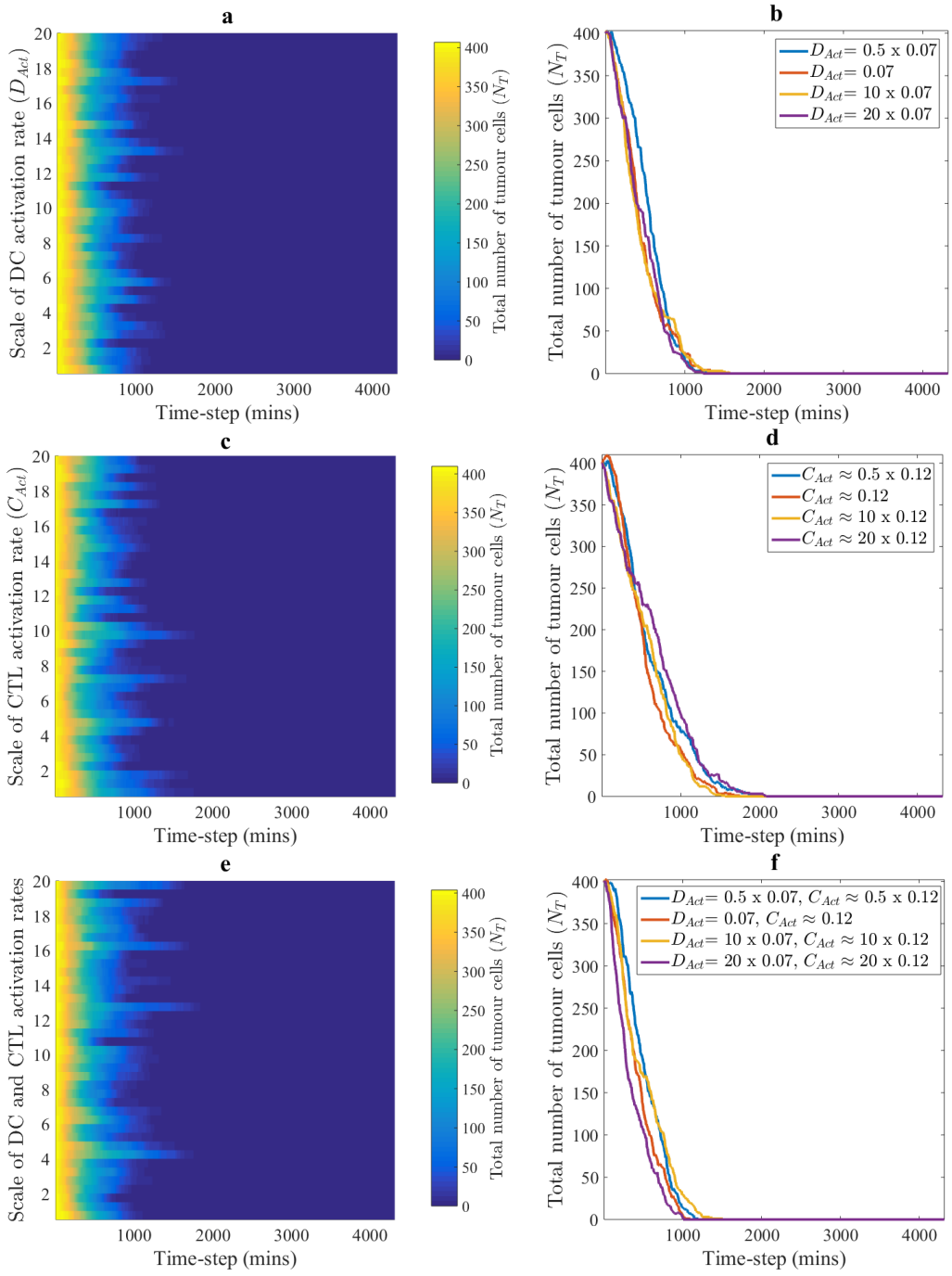

Figure 5.5: Increasing the activation rates of DCs and CTLs has little effect on the removal of an initially smaller tumour. *The heat maps show the evolution of the tumour cell number over time for each given value of C_{Act} and/or D_{Act} (left panels). We select four values of C_{Act} and/or D_{Act} and compare the tumour cell number over time for each parameter setting (right panels). In each case, we begin the simulations with 400 tumour cells and test for varying values of:* ***a,b*** *D_{Act} only,* ***c,d*** *C_{Act} only and* ***e,f*** *D_{Act} and C_{Act}. All values displayed are an average over three simulation runs.*

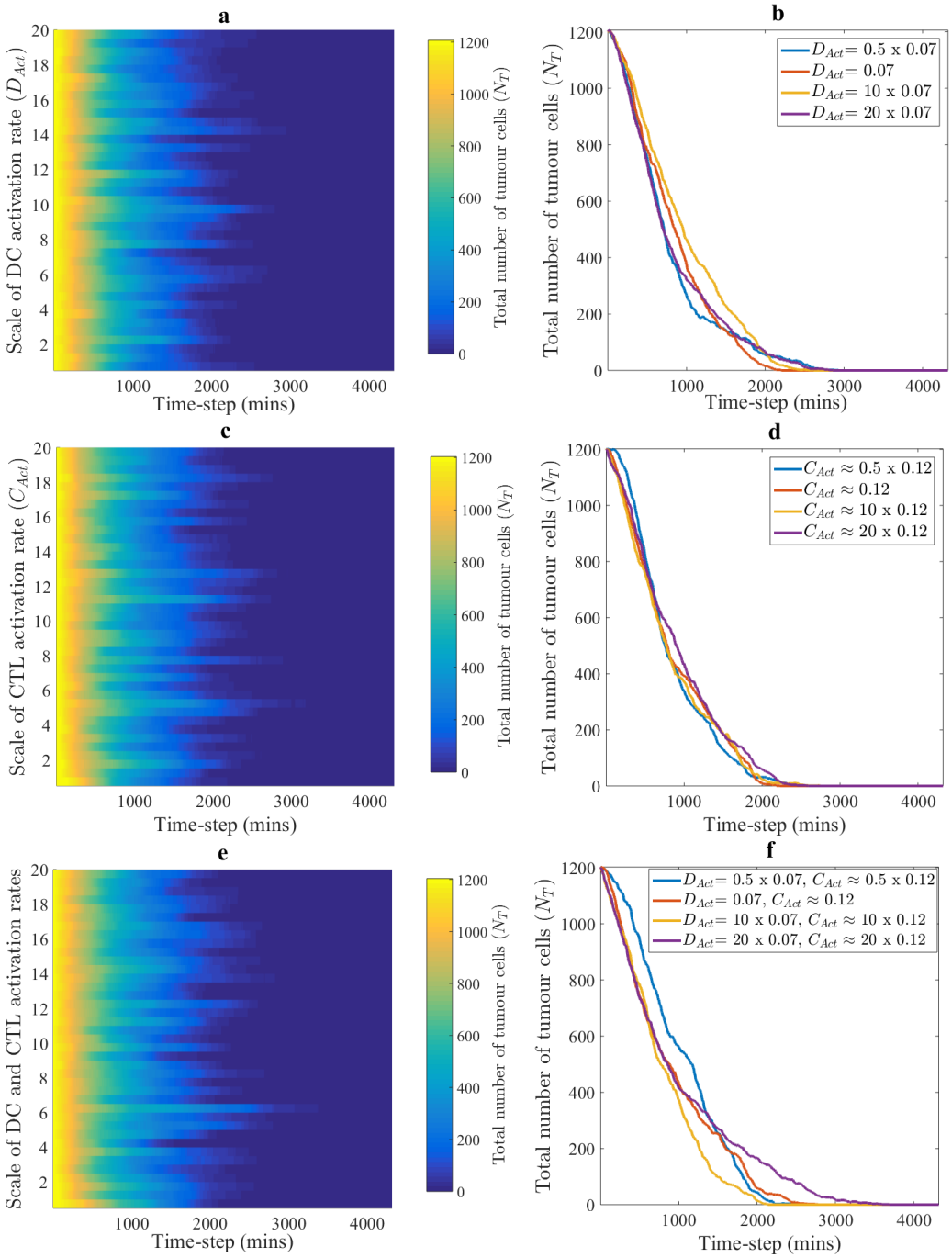

Figure 5.6: Increasing the activation rates of DCs and CTLs has little effect on the removal of an initially larger tumour. *The heat maps show the evolution of the tumour cell number over time for each given value of C_{Act} and/or D_{Act} (left panels). We select four values of C_{Act} and/or D_{Act} and compare the tumour cell number over time for each parameter setting (right panels). In each case, we begin the simulations with* 1200 *tumour cells and test for varying values of:* ***a,b*** *D_{Act} only,* ***c,d*** *C_{Act} only and* ***e,f*** *D_{Act} and C_{Act}. All values displayed are an average over three simulation runs.*

5.3.5 For large exhaustion limits, immune cell exhaustion does not impact the outcomes of tumour immune competition

It has been suggested that immune cells can be limited in their activity through exhaustion, whereby they can only interact with a certain number of cells (Christophe et al., 2015). Hence, we investigated the role of immune cell exhaustion on the outcomes of tumour-immune competition by limiting the number of CTLs that a single DC can activate and limiting the number of tumour cells that a single CTL can remove from the system. As in the previous subsections, each simulation was run over a 72 hr period or until all of the tumour cells were removed from the system. Furthermore, each simulation was carried out with the parameter values shown in Table 5.2 for a range of values for the limiting cell number that causes exhaustion. Values of this limit were chosen to range from 1 cell to an infinite number of cells, with suitable intermediate values investigated. The resulting evolutions of the tumour cell number over time are shown in Figure 5.7 where each line represents the tumour cell density over time for the tested parameter setting. In the case where each immune cell can only interact with one cell, we observe that the tumour cell number steadily increases over time. For limits of either two or three cells we observe a slight decrease in tumour mass, before the tumour cell number increases again. For a limit of four cells we observe a steady decrease in the tumour cell number with very few cells remaining at the end of simulations. For all higher exhaustion limit values we observe that the tumour can be removed and for larger values (*i.e.* over twenty cells) the tumour removal times are very similar.

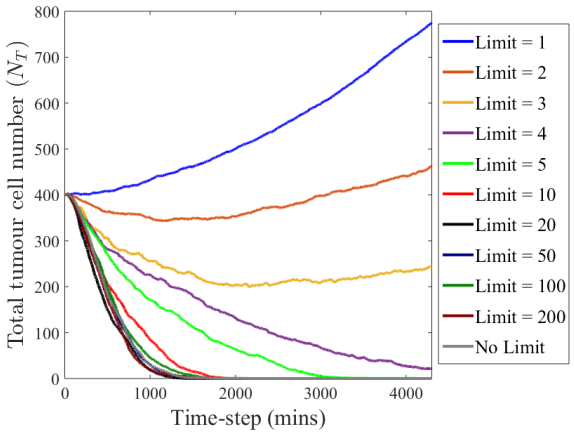

Figure 5.7: For large exhaustion limits, immune cell exhaustion does not impact the outcomes of tumour immune competition. *Line plots showing the evolution of the number of tumour cells over time for eleven different limits of immune cell exhaustion. The limit shown in the legend indicates how many cells both single DCs and single CTLs can interact with over the time-frame considered. All values displayed are the average over three simulation runs.*

5.3.6 Using a switch in immune cell motion decreases tumour elimination time

In the model, immune cells switch their form of motion from a Lévy walk to Brownian motion upon activation. However, another modelling approach is to simply use Brownian motion for both inactive and active immune cells. To investigate the impact of the inclusion of the switch in cell motion we run simulations whereby both inactive and active immune cells undergo Brownian motion and compare the results to those from previous sections here immune cells switched from Lévy to Brownian motion. As in the previous subsections, each simulation was run over a 72 hr period or until all of the tumour cells were removed from the system. Furthermore, each simulation was carried out with the parameter values shown in Table 5.2. We compare the tumour elimination time and numbers of active/inactive immune cells with the case where the cells switched motion in Figure 5.8. The bars display the

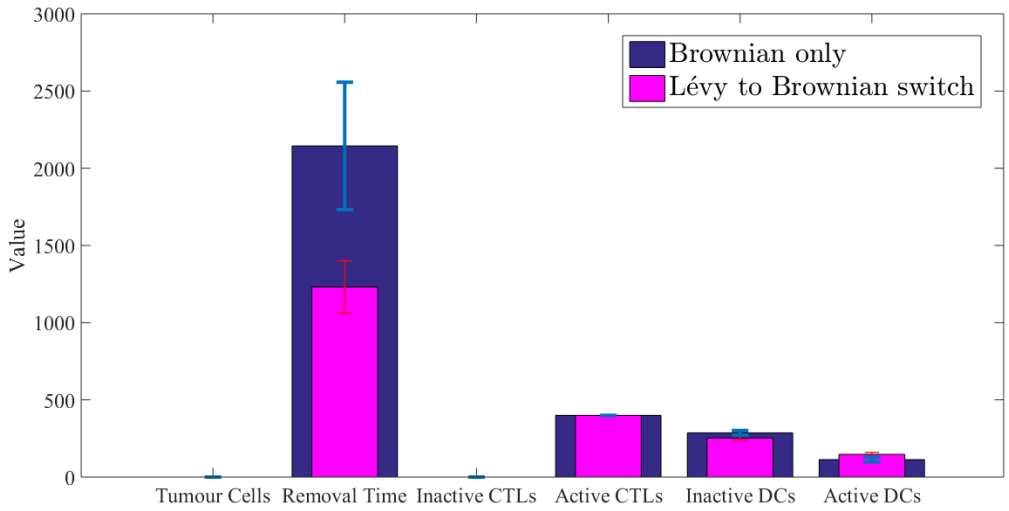

Figure 5.8: Using a switch in immune cell motion decreases tumour elimination time. *We compare the case where both inactive and active immune cells undergo Brownian motion (blue) and the case where the immune cells switch from a Lévy walk to Brownian motion upon activation (pink). We compare the number of tumour cells at the end of simulation, the time taken to remove the tumour and the numbers of inactive/active immune cells within the system. The bars display the mean value of ten runs of the simulation and the error lines represent the standard deviation between these ten runs.*

mean value of ten runs of the simulation and the error lines represent the standard deviation between these ten runs. We observe that the tumour elimination time for the case with no switch (Brownian only) is larger than that when the cells switch from a Lévy walk to Brownian motion upon activation. In the case of Brownian motion the number of active and inactive immune cells at the end of simulations is similar to the results of the case where cell switch from a Lévy walk to Brownian motion upon activation.

5.4 Concluding remarks and discussion

In this chapter we have developed a stochastic individual-based (IB) spatial model of tumour-immune competition focussing on cell-cell interactions between cancer cells, dendritic cells and cytotoxic T lymphocytes.

The results of numerical simulations of this IB model recapitulate the findings of experimental work which highlighted that a (limited) beneficial effect on the immune response to cancer can be induced through enhancing the number of CTLs in the tumour microenvironment (Spranger, 2016). Furthermore, in agreement with the experimental results presented in Li et al. (2010) and Ye et al. (2011) – where the authors showed that cellular overcrowding can hamper immune action – our computational results indicate that higher numbers of DCs can lead to overcrowding and prevent activated CTLs from reaching the tumour resulting in reduced success of tumour removal. This may be useful in explaining instances of unsuccessful dendritic cell therapy (Ahmed et al., 2014; Butterfield, 2013; Garg et al., 2017; Lim et al., 2007) and suggests that increasing CTL numbers may be a better objective for immunotherapy rather than increasing DC numbers.

As expected, when we increase the division rate of the tumour cells we observe

that tumour growth could no longer be controlled by the immune system and could eventually lead to situations of exponential tumour growth. However, if the capability of CTLs to remove tumour cells is also enhanced, in agreement with previous theoretical works (d'Onofrio and Ciancio, 2011; Frascoli et al., 2014; Matzavinos et al., 2004), our model predicts that tumour eradication can be re-established. Such results illustrate how the ratio between the tumour proliferation rate and the immune cell's tumour kill rate (*i.e.* the ratio between λ and μ) is a crucial determinant of the outcome of anti-tumour immune action.

The outcomes of this initial model demonstrate that, in general, increasing the activation rates of CTLs and DCs has very little effect on removal of the tumour, in the parameter settings we have considered . Taken together, our results testify to the idea that choosing the activation rates of CTLs and DCs as designated targets in adoptive cell therapy, or other forms of immunotherapy, may not enhance the efficacy of the immune response against solid tumours.

Through investigation of the immune cell exhaustion process, our model indicates that the exhaustion limit of immune cells does not greatly impact the tumour-immune competition, unless the immune cells are limited to interacting with less than five cells. Experimentally, it has been shown that T cells can have an exhaustion limit of around 5 cells (Christophe et al., 2015) and there is evidence that this limit is closer to 10 cells (Halle et al., 2016), both of which our model suggests would still result in the same dynamics as the case where there was no exhaustion limit. Therefore, this mechanism can be easily omitted from our model to allow for simplicity and to focus on more influential processes and parameter settings.

We compare the case where all immune cells undergo Brownian motion, to our model where immune cells switch from a Lévy walk mechanism to Brownian motion upon activation by tumour antigen. Our results suggest that including this switch

in cell motion does not alter the resulting dynamics of the system, but does result in a faster tumour removal time, for the parameter setting considered. This further supports the results of Chapter 4 where the Lèvy walk mechanism was found to be more efficient than the Brownian motion walk mechanism.

In the individual-based model described in this chapter we have considered a homogeneous tumour, where all tumour cells are of the same phenotype. However, a tumour can be heterogeneous in relation to the antigens which each tumour cell expresses. This individual-based model will be further developed in Chapter 6 to incorporate such tumour antigens and their effect on the immune response.

Chapter 6

An individual-based model to describe the role of tumour heterogeneity in tumour-immune competition

6.1 Overview

In the previous chapter, we developed an individual-based (IB) model of tumour-immune competition to describe the interactions between dendritic cells (DCs), cytotoxic T lymphocytes (CTLs) and tumour cells. In the model, we considered a homogeneous tumour, *i.e.* all tumour cells exhibited the same antigenic profile. However, the antigenic composition of solid tumours can be heterogeneous. Therefore, each cell within the tumour mass may have an antigen profile characterised by different expression levels of tumour antigens which may vary over time through epimutations or mutations. In light of these considerations, in this chapter we extend

the IB model described in Chapter 5 further to explicitly capture tumour antigen expression and recognition by the immune system. In this extended model, each cancer cell is characterised by an antigen profile which can change over time due to either epimutations or mutations. The immune response towards the cancer cells is initiated by the DCs that recognise the tumour antigens and present them to the CTLs. Consequently, CTLs become activated against the tumour cells which express such antigens and can subsequently remove them from the system. The model described in this chapter and several of the results shown have been submitted for publication (Macfarlane et al., 2019).

6.2 The mathematical model

The model developed in this chapter is based upon the individual-based model described in Chapter 5. Therefore, we again consider three cell types: tumour cells, dendritic cells (DCs) and cytotoxic T lymphocytes (CTLs) and use an individual-based approach to describe the interactions between these three cell types. Furthermore, the model is again posed on a 2D spatial grid of spacing Δ_x in the x direction and Δ_y in the y direction, with the constraint that only one cell of any type is allowed at each grid-site at any time-step of duration Δ_t.

As in the previous chapter, initially, inactive immune cells are randomly distributed on the spatial grid, while the cancer cells are tightly packed in a circular configuration positioned at the centre of the grid, to reproduce the geometry of a solid tumour. We again assume that, at the start of simulations, there are no activated immune cells. Throughout the simulations, we allow the tumour to grow through cell division. In agreement with the previous model, a cancer cell divides at the rate λ into two progeny cells of which one occupies the position of the parent

cell while the other is positioned at an unoccupied neighbouring grid-site. This ensures that only cancer cells with free grid-sites in their neighbourhood can divide, that is, cells with no free neighbouring grid sites will not proliferate. In line with the previous models we have described, inactive immune cells update their position according to a Lévy walk and can become activated via interactions with other cells which initiates a change in motion, *i.e.* activated immune cells follow a Brownian walk. Furthermore, DCs are activated at the rate D_{Act} upon contact with tumour cells, and CTLs become activated at the rate C_{Act} upon contact with active DCs. Once again, we let active CTLs remove tumour cells, upon contact, at the rate μ. For simplicity, we again omit the effects of natural death of tumour cells and the proliferation of both DCs and CTLs, *i.e.* the total numbers of DCs and CTLs are constant over time. Chapter 5 contains a detailed description of these modelling strategies.

In this chapter, we develop each of these modelling strategies further to include: the antigen profiles of cancer cells and their possible variation, the immune recognition of tumour antigens by DCs, and the targeted activation of CTLs against specific tumour antigens. We incorporate antigen expression into our model by letting each tumour cell express eleven different antigens, to represent the eleven MAGE-A antigens that, as mentioned in Section 2.3, have a key role in tumour development (Coulie et al., 2014). The eleven antigens are reported in Table 6.2 and we label them by an index $i = 1, \ldots, 11$. In the model, we assume there is no correlation between the expression of the eleven MAGE-A antigens (Roch et al., 2010), therefore each antigen is expressed independently of the others. The modelling strategies used to take into account such additional layers of biological complexity are described in detail in the following subsections, and are also schematically illustrated in Figure 6.1 and Figure 6.2.

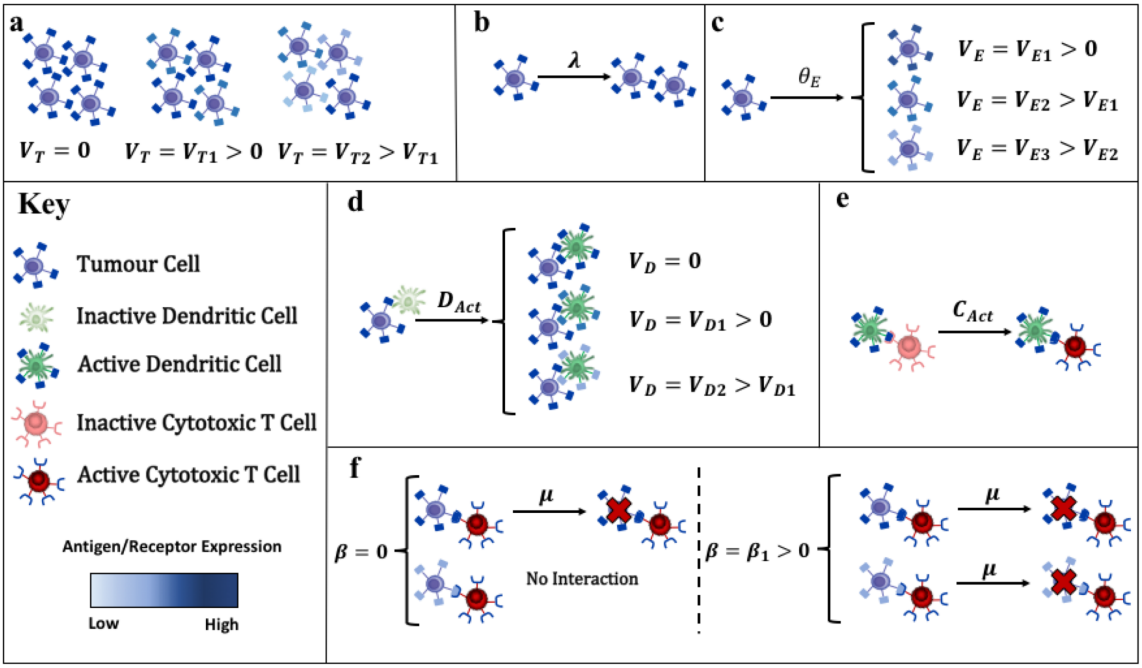

Figure 6.1: ***Schematic representation of the mechanisms and processes included in the individual-based model. Key*** *We consider three cell types in the model: tumour cells, DCs and CTLs, along with their corresponding antigen and receptor profiles.* ***a*** *Initially the tumour is composed of tumour cells characterised by different antigenic profiles. The standard deviation of the initial tumour antigen profiles from the experimental profile is determined by the parameter V_T.* ***b*** *Tumour cells divide at the rate λ.* ***c*** *Tumour cells may undergo epimutations with probability θ_E. The standard deviation of the epimutation altered tumour antigen profiles from the original profile is determined by the parameter V_E.* ***d*** *DCs become activated upon contact with tumour cells at the rate D_{Act}. The standard deviation of the antigen profiles recognised by DCs from the tumour antigen profiles is determined by the parameter V_D.* ***e*** *Upon contact, active DCs present the antigen profile they have recognised to inactive CTLs. This leads to the targeted activation of CTLs against specific tumour antigens at the rate C_{Act}.* ***f*** *Activated CTLs remove tumour cells, upon contact, at the rate μ, on the condition that the tumour cells express a sufficient amount of the antigens corresponding to the CTL receptors. The binding affinity of the CTLs is measured by the parameter β.*

6.2.1 Mathematical modelling of antigen expression

We denote by $N_T(t)$ the number of tumour cells in the system at time $t = h\,\Delta_t$, with $h \in \mathbb{N}_0$, and we label each cell by an index $n = 1, \ldots, N_T(t)$. There can be high variability in MAGE-A antigen expression between patients with the same type of cancer (Hartmann et al., 2016; Müller-Richter et al., 2009; Urosevic et al., 2005) and even within cancer cell samples from the same patient (Hartmann et al., 2016; Müller-Richter et al., 2009; Urosevic et al., 2005). Therefore, at each time instant t, we characterise the antigen profile of the n^{th} tumour cell by means of a vector

$$\mathbf{A}_{Tn}(t) = (A_{Tn}^{(1)}(t), \ldots, A_{Tn}^{(11)}(t)),$$

with $A_{Tn}^{(i)}(t)$ representing the expression level of antigen i. As schematically illustrated in Figure 6.1, for each tumour cell n we define the initial expression of the i^{th} antigen as

$$A_{Tn}^{(i)}(0) = (M_i + V_T\ R_i)_+, \quad i = 1, \ldots, 11. \tag{6.1}$$

In equation (6.1), the parameter M_i denotes a mean expression level of antigen i taken from published experimental data, the values of which are reported in Table 6.2. The value of R_i is sampled from a standard normal distribution centred at zero. We take the positive part of equation (6.1) to ensure nonnegativity of the antigen expression level. As R_i is taken from a standard normal distribution, the parameter V_T can be described as the standard deviation of the initial antigen profile from the experimental value M_i (Kenney and Keeping, 1962). Therefore the parameter V_T determines how close the value of $A_{Tn}^{(i)}(0)$ will be to the value of M_i - see the scheme in Figure 6.1a.

6.2.2 Modelling variations in antigen expression

At each time-step, we let the tumour cells divide at the rate λ, as shown in the schemes in Figure 6.1b, and allow their antigen profile to vary either through epimutations or through mutations. We assume that epimutations can occur at any time during the lifespan of a cell - see the schemes in Figure 6.1c and Figure 6.2a. On the other hand, mutations take place during cell division and may cause the antigen profile of one progeny cell to be different from that of the parent cell - see the scheme in Figure 6.2b. We allow epimutations and mutations to occur with probabilities θ_E and θ_M, respectively.

Epimutations: A variation in the level of expression of the i^{th} antigen of the n^{th} tumour cell at the time instant t due to an epimutation is modelled according to the following equation

$$A_{Tn}^{(i)}(t + \Delta_t) = (A_{Tn}^{(i)}(t) + V_E \; R_i)_+, \quad i = 1, \ldots, 11. \tag{6.2}$$

In equation (6.2), the value of R_i is sampled from a normal distribution centred at zero. We take the positive part of equation (6.2) to ensure nonnegativity of the antigen expression level. Following on from the definition of the parameter V_T, since R_i is taken from a standard normal distribution, the parameter V_E can be described as the standard deviation of the updated antigen profile from the previous expression profile (Kenney and Keeping, 1962). Therefore, V_E determines how close the value of $A_{Tn}^{(i)}(t + \Delta_t)$ will be to the value of $A_{Tn}^{(i)}(t)$.

Mutations: Upon division at the time instant t, the n^{th} tumour cell is replaced by two cells, one labelled by the index n and the other one labelled by the index

$N_T(t)+1$. If mutations do not occur, the progeny cells inherit the antigen profile of the parent cell, *i.e.* $A^{(i)}_{Tn}(t+\Delta_t) = A^{(i)}_{Tn}(t)$ and $A^{(i)}_{T\,N_T(t)+1}(t+\Delta_t) = A^{(i)}_{Tn}(t)$. Conversely, if a mutation occurs, the antigen profile of the progeny cells will be given by the following equations

$$A^{(i)}_{Tn}(t+\Delta_t) = A^{(i)}_{Tn}(t), \quad i = 1,\ldots,11 \tag{6.3}$$

and

$$A^{(i)}_{T\,N_T(t)+1}(t+\Delta_t) = (A^{(i)}_{Tn}(t) + V_M\ R_i)_+, \quad i = 1,\ldots,11. \tag{6.4}$$

Equations (6.3) and (6.4) rely on notation analogous to that of equation (6.2) and therefore V_M can be described as the standard deviation of the progeny antigen profiles from the parent antigen profiles (Kenney and Keeping, 1962). Therefore, the value of V_M determines how close the value of $A^{(i)}_{T\ N_T(t)+1}(t+\Delta_t)$ will be to the value of $A^{(i)}_{Tn}(t)$.

Clearly, in the absence of changes in antigen expression, *i.e.* if $\theta_E = 0$ and $\theta_M = 0$, the antigen profiles of the tumour cells will remain constant over time, that is, $\mathbf{A}_{Tn}(t) = \mathbf{A}_{Tn}(0)$ for all $t > 0$ and $n = 1,\ldots,N_T$.

6.2.3 Activation of immune cells

Activation of DCs: We denote by N_D the number of DCs, which we assume to be constant, and we label each DC by an index $k = 1,\ldots,N_D$. Activation of each DCs occurs, at the rate D_{Act}, through contact with a tumour cell. There is biological evidence supporting heterogeneity within the antigen presentation process where a less prevalent antigen may be recognised presented by DCs (Boes et al., 2002; Fehres et al., 2014; Ljunggren et al., 1990). Additionally, it is known that the MAGE-A

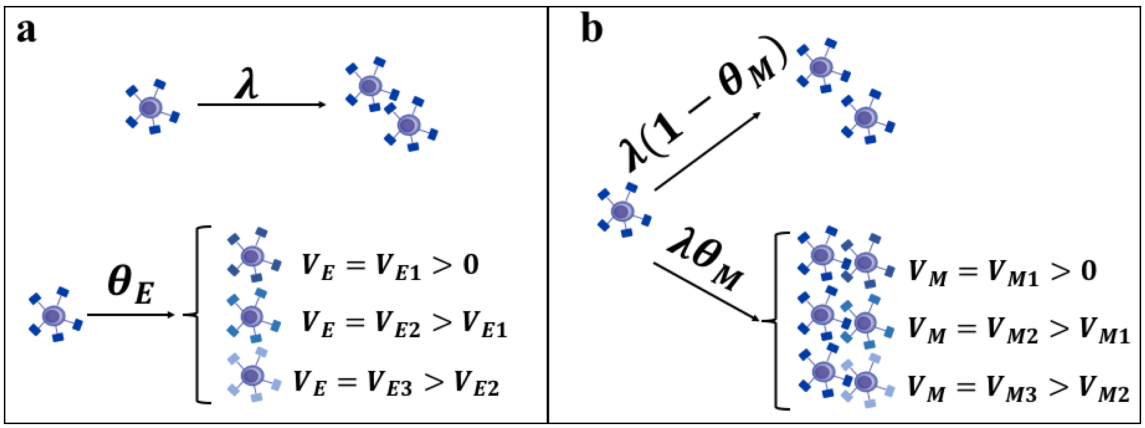

Figure 6.2: ***Schematic comparison of the modelling strategies used to describe changes in antigen expression induced by epimutations and mutations within tumour cells.*** ***a*** *Antigenic variations due to epimutations can occur, with probability θ_E, at any time during the life of a tumour cell. The standard deviation of the new antigen profile from the original one is determined by the parameter V_E.* ***b*** *Mutations can take place, with probability θ_M, only during cell division, which occurs at the rate λ. Due to mutations, one progeny cell may exhibit an antigen profile different from that of the parent cell. The standard deviation between the parent and progeny cell antigen profiles is determined by the parameter V_M.*

genes have similar homology (Roch et al., 2010; Zajac et al., 2017) and therefore there is a potential that they could be mis-recognised as each other (Graff-Dubois et al., 2002; Linette et al., 2013; Raman et al., 2016; Schueler-Furman et al., 1998; Tong et al., 2004). Therefore, we incorporate variability into the DC activation process whereby the DCs may recognise different expression levels of the tumour antigen from this actually present. At any time instant t, the k^{th} DC is characterised by a recognised antigen profile

$$\mathbf{A}_{Dk}(t) = (A_{Dk}^{(1)}(t), \ldots, A_{Dk}^{(11)}(t)).$$

We let all DCs be initially inactive and thus assume

$$A_{Dk}^{(i)}(0) = 0, \quad i = 1, \ldots, 11,$$

for all $k = 1, \ldots, N_D$. As schematically described by Figure 6.1d, we consider the case where there may be potential variation in the antigen recognition process. To capture this idea, upon activation through contact with the n^{th} tumour cell at the time instant t, we assign the recognised antigen profile of the k^{th} DC using the following equation

$$A_{Dk}^{(i)}(t + \Delta_t) = (A_{Tn}^{(i)}(t) + V_D \ R_i)_+, \quad i = 1, \ldots, 11. \tag{6.5}$$

In equation (6.5), the value of R_i is sampled from a normal distribution centred at zero. We take the positive part of equation (6.5) to ensure nonnegativity of the antigen expression level. We can describe V_D as the standard deviation of the antigen profile recognised by each DC from the actual tumour antigen profile (Kenney and Keeping, 1962). Therefore, V_D determines how close the value of $A_{Dk}^{(i)}(t + \Delta_t)$ will

be to the value of $A_{Tn}^{(i)}(t)$. We note that biologically, V_D captures the potential of the immune system to target an antigen which is not the highest expressed by the tumour cell. Therefore, introducing V_D allows the dendritic cells to have variation in which antigens they present to the CTLs and thus determines the diversity of the T cell receptor expression within the CTL population. The results we have discussed previously in Chapter 5, indicate that realistic exhaustion limits of cells would not change the outcome of tumour immune competition, compared to no limit of exhaustion. Therefore, once activated, the DCs remain activated against their recognised tumour antigen profile.

Activation of CTLs: We denote by N_C the number of CTLs, which we assume to be constant, and we label each CTL by an index $m = 1, \ldots, N_C$. As schematically described by Figure 6.1e, activation of CTLs occurs, at the rate C_{Act}, through contact with activated DCs. At any time instant t, each CTL m has a receptor profile

$$\mathbf{A}_{Cm}(t) = (A_{Cm}^{(1)}(t), \ldots, A_{Cm}^{(11)}(t)).$$

We let all CTLs be initially inactive and thus assume

$$A_{Cm}^{(i)}(0) = 0, \quad i = 1, \ldots, 11,$$

for all $m = 1, \ldots, N_C$. While DCs can recognise multiple types of antigens, CTLs can produce copies of one antigen receptor only (Brenner et al., 2008; Coico and Sunshine, 2015). This means that each CTL can only be activated against one of the eleven MAGE-A antigens. To capture this fact, upon activation through contact with the k^{th} DC at the time instant t, we let the m^{th} CTL become activated against the most prevalent antigen within the tumour antigen profile recognised by the k^{th}

DC, *i.e.* we assign the receptor profile of the m^{th} CTL using the following equation

$$A_{Cm}^{(i)}(t) = \begin{cases} 1 \text{ for } i = \hat{i}, \\ 0 \text{ for } i \neq \hat{i}, \end{cases} \qquad \text{with } \hat{i} = \arg\max_j A_{Dk}^{(j)}(t), \tag{6.6}$$

where the index $\hat{i}$ specifies the target antigen of the activated CTL. Note that, if $|\arg\max_j A_{Dk}^{(j)}(t)| > 1$, then we arbitrarily choose $\hat{i} = \min \arg\max_j A_{Dk}^{(j)}(t)$. Again, the results we have discussed previously in Chapter 5, indicate that realistic exhaustion limits of cells would not change the outcome of tumour immune competition, compared to no limit of exhaustion. Therefore, once activated, a CTL remains activated against the same tumour antigen.

6.2.4 Removal of tumour cells by activated CTLs

Upon contact, each activated CTL can induce death of the tumour cells which express a sufficiently high level of the CTL's target antigen (Coulie et al., 2014; Stone et al., 2009), which we assume to be given by the mean antigen expression levels reported in Table 6.2. In particular, as schematically described by Figure 6.1f, when the m^{th} CTL interacts with the n^{th} tumour cell at time t, we compare the receptor profile $\mathbf{A}_{Cm}(t)$ with the antigen profile $\mathbf{A}_{Tn}(t)$ and let the tumour cell be removed from the system at the rate μ provided that

$$A_{Tn}^{(i)}(t) \geq (M_i - \beta) \text{ for } i \text{ such that } A_{Cm}^{(i)}(t) = 1. \tag{6.7}$$

In equation (6.7), the parameter β describes the binding affinity of the CTLs, which determines the range of tumour cells that each CTL can interact with. If β is larger, then the CTL can recognise tumour cells with a lower level of expression of

Table 6.1: *Model parameters and related values used in computational simulations. Note, standard deviation has been abbreviated to StD.*

Symbol	Description	Value(s)	Reference
Δ_t	time-step	1 min	(Boissonnas et al., 2007)
$\Delta_{x,y}$	grid spacing in the x or y direction	10 μm	(Macfarlane et al., 2018)
$N_T(0)$	initial number of tumour cells	400 cells	(Christophe et al., 2015)
N_C	total number of CTLs	400 cells	(Christophe et al., 2015)
N_D	total number of DCs	400 cells	(Macfarlane et al., 2018)
n	Index identifier of each tumour cell	$n = 1, \ldots, N_T$	-
k	Index identifier of each DC	$k = 1, \ldots, N_D$	-
m	Index identifier of each CTL	$m = 1, \ldots, N_C$	-
$\mathbf{M}$	Antigen profile from experimental data	see Table 6.2	(Hartmann et al., 2016)
$\mathbf{A}_{Tn}(t)$	Antigen profile of tumour cell n at time t	values ≥ 0	-
$\mathbf{A}_{Dk}(t)$	Recognised antigen profile of DC k at time	values ≥ 0	-
$\mathbf{A}_{Cm}(t)$	Antigen receptor profile of CTL m at time	values of 0 or 1	-
λ	tumour cell division rate	0.001 min^{-1}	(Christophe et al., 2015)
θ_E^*	Average probability of epimutations	0.23	(De Smet et al., 1996)
μ	removal rate of tumour cells by CTLs	0.03 cells min^{-1}	(Christophe et al., 2015)
D_{Act}	DC activation rate	0.07 cells min^{-1}	(Bianca et al., 2012)
C_{Act}	CTL activation rate	≈ 0.12 cells min^{-1}	(Engelhardt et al., 2012)
α	Lévy walk exponent	1.15	(Harris et al., 2012)
β	T cell binding affinity	$0 \rightarrow 0.2$	(Schmid et al., 2010)
V_T	StD of the initial tumour antigen profiles from experimental profile $\mathbf{M}$	$0 \rightarrow 1$	-
V_D	StD of the antigen profiles recognised by DCs from the tumour antigen profiles	$0 \rightarrow 1$	-
$V_{E/M}$	StD of the tumour antigen profiles after epimutations/mutations	same as V_T	-

the antigen that they target. Independent of the outcome of the interaction, the CTL can interact with further tumour cells following the same process.

6.3 Computational simulations and results

6.3.1 Model parametrisation and simulation set up

In line with the IB model developed in Chapter 5, we use 100 grid points both in the x and in the y direction, which correspond to a 2D spatial domain of size 1 mm^2. The code was developed and the simulations were run in MATLAB, for an appropriate number of time-steps, with one time-step chosen to be $\Delta_t = 1$ min, to allow for the resulting dynamics of the system to be investigated. Chapter 5 contains a detailed description of the parametrisation of the original model, and we describe here the way in which the additional components of the model are calibrated using the parameter values reported in Table 6.1.

Initial tumour antigen expression levels: Hartmann et al. (2016) investigated the levels of expression of the eleven MAGE-A antigens in oral squamous cell cancers of 38 patients. The mean antigen expression levels were taken to be values between 0-12 arbitrary units as an immune-reactivity score, which are normalised and reported in Table 6.2. In our model the initial expression level of each antigen for each tumour cell is defined by using equation (6.1) along with the values of M_i from Table 6.2. To determine the value of $(V_T\ R_i)$ in equation (6.1) we consider the properties of R_i, which is a random value taken from a standard normal distribution. A standard normal distribution with mean 0 and standard deviation 1, has a 95% confidence interval of ± 1.96 (Kenney and Keeping, 1962). Therefore, for 95% of values, we expect -1.96 $\leq R_i \leq$1.96 with the majority of the values being close to the mean value, zero. We then use the parameter V_T to control the minimum and maximum value of $(V_T\ R_i)$, i.e when V_T=1 then $(V_T\ R_i) \in \{-1.96, 1.96\}$, for most values. However, if V_T is lower, *e.g.* V_T=0.1, then the values of $(V_T\ R_i)$ will also be lower, *e.g.* $(V_T\ R_i) \in \{-0.196, 0.196\}$. To consider a wide range of biological situations, in regards to the initial heterogeneity between tumour antigen profiles, we use a range of values, between 0 and 1, for the parameter V_T. As the experimental data in Table 6.2 is unitless, we also consider V_T to be unitless.

Probabilities of epimutations and mutations: De Smet et al. (1996) found that cancer cell lines expressing the MAGE-A1 antigen were 23% more likely to undergo demethylation events than tumour cell lines that did not express this antigen. Such values are supported by other studies that consider the likelihood of DNA demethylation in various cancers (Chalitchagorn et al., 2004; Ehrlich, 2002). We make the assumption that this holds true for the other ten MAGE-A antigens,

Table 6.2: *Average levels of expression of the MAGE-A antigens in human oral squamous cell cancer cell lines. The experimental values were taken from (Hartmann et al., 2016) and then normalised by dividing by 12.*

Antigen (i)	Mean Expression, M_i
MAGE-A1 (1)	0.10
MAGE-A2 (2)	0.25
MAGE-A3 (3)	0.41
MAGE-A4 (4)	0.24
MAGE-A5 (5)	0.36
MAGE-A6 (6)	0.35
MAGE-A8 (7)	0.17
MAGE-A9 (8)	0.16
MAGE-A10 (9)	0.38
MAGE-A11 (10)	0.06
MAGE-A12 (11)	0.32

and let the average probability of epimutations in our model be

$$\theta_E^* = 0.23.$$

In the model we consider the effect of increase or decreasing the probability of epimutations or mutations by setting θ_E and θ_M, respectively, as multiples of θ_E^*. The parameters V_E and V_M control how much the antigen expression of a tumour cell can change through epimutations or how much the antigen expression of a daughter tumour cell can change through mutations - see equations (6.2) and (6.3). The values of V_M and V_E are chosen to match the values of V_T, that is we assume that the antigenic profiles of cells will only be able to evolve according to the levels of heterogeneity in the antigen expression levels between initial antigen profiles. As the experimental data in Table 6.2 is unitless, we also consider V_E and V_M to be unitless.

Antigen recognition process: In line with the choice of values for the parameter V_T, to consider a wide range of biological situations, in regards to the antigen recognition process, we use a range of values, between 0 and 1, for the parameter V_D - see equation (6.5). As the experimental data in Table 6.2 is unitless, we also consider V_D to be unitless.

T cell binding affinity: The binding affinity of a T cell is related to the association rate, that is the inverse of the dissociation rate K_D. In general this value is between 0.005 μM^{-1} and 1 μM^{-1} for all natural T cells (Davis et al., 1998; Slansky and Jordan, 2010). Furthermore, the MAGE-A T cell receptors association rates have been found to be even larger than this range, *e.g.* for MAGE-A3 the values are between 0.018 μM^{-1} and 5.917 μM^{-1} (Tan et al., 2015). However, Schmid et al. (2010) have shown that an association rate of 0.2 μM^{-1} or higher did not improve the binding affinity and therefore higher binding affinities may have a limited effect. We take M_i to be the minimal binding and allow the likelihood of binding to increase depending on β. In line with the experimental evidence, we investigate a range of unitless values between 0 and 0.2 for the parameter, β, that models the T cell receptor binding affinity - see equation (6.7).

6.3.2 Variability between the initial tumour antigen profiles determines the effectiveness of the immune response

To investigate how the immune response is affected by variability in the initial tumour antigen profiles, we test for three increasing values of the parameter V_T, *i.e.* $V_T = 0.001$, $V_T = 0.01$ and $V_T = 0.1$. We choose $\beta = 0.01$ and we let the tumour cell antigen profiles remain constant over time, *i.e.* we choose $\theta_E = \theta_M = 0$. For each value of V_T considered, we also explore the effect of increasing the value of

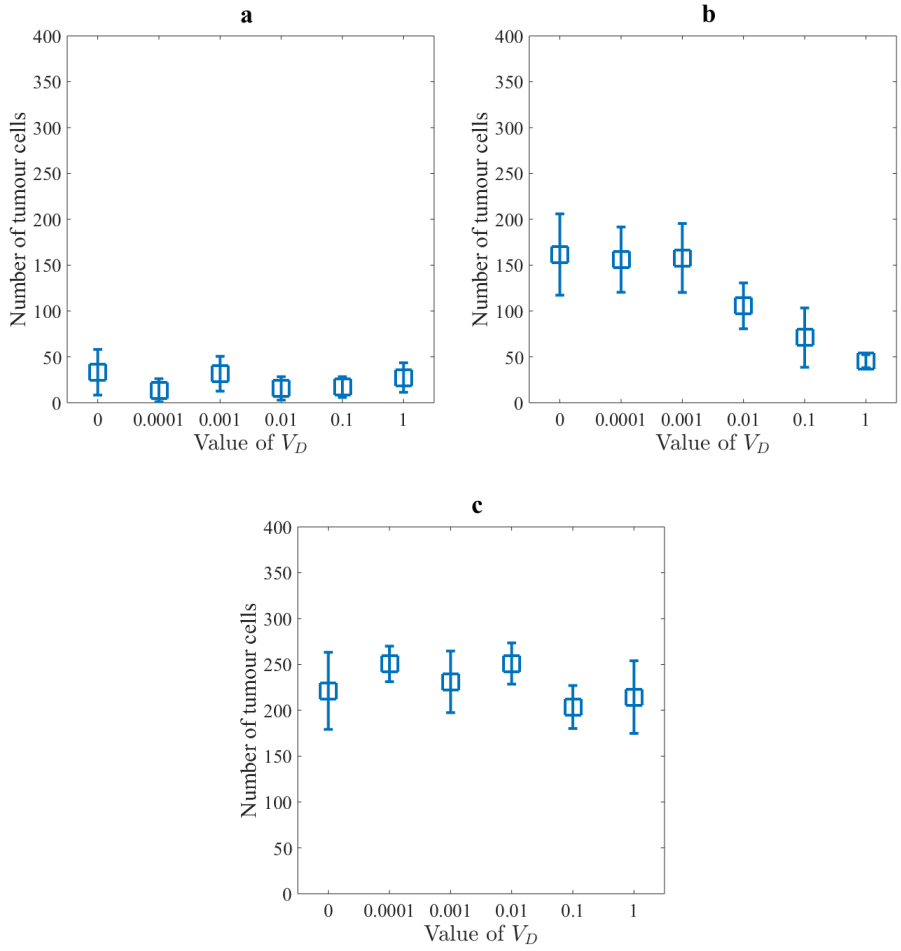

Figure 6.3: ***Variability between the initial tumour antigen profiles determines the effectiveness of the immune response.*** *Plots displaying the number of tumour cells remaining after 1000 time-steps for increasing values of the parameter V_T:* ***a*** $V_T = 0.001$, ***b*** $V_T = 0.01$ *and* ***c*** $V_T = 0.1$. *For each value of V_T a range of values of the parameter V_D are tested. The tumour cell numbers presented have been obtained as the average over 5 simulations and the error bars display the related standard deviation. Here, $\beta = 0.01$, $\theta_E = \theta_M = 0$, and all the other parameter values are reported in Table 6.1.*

the parameter V_D. In all cases, we carried out simulations for 1000 time-steps. As shown by Figure 6.3a, when there is a small difference between the initial tumour cell antigen profiles, very few tumour cells remain in the system after 1000 time-steps for all considered values of V_D. Conversely, the results presented in Figure 6.3c show that if we allow V_T to be relatively large, there is a significant number of remaining tumour cells after 1000 time-steps for all values of V_D. Moreover, as shown by Figure 6.3b, for an intermediate level of initial antigen variability, there appears to be a correlation between the number of tumour cells remaining after 1000 time-steps and the parameter V_D. In particular, larger values of the parameter V_D correspond to smaller numbers of the remaining tumour cells after 1000 time-steps. These results suggest that for tumours characterised by intermediate levels of V_T, higher levels of variability between the antigen profile recognised by DCs and the actual antigen profile of tumour cells may result in a more effective immune response. This is further illustrated by the computational results presented in the next subsection.

6.3.3 Increasing variability between the antigen profile recognised by DCs and the actual antigen profile of tumour cells results in immune escape, chronic dormancy or immune clearance of the tumour

The results discussed in the previous subsection illustrate how different cell dynamics can be observed for increasing values of the parameter V_D. We test this further by using the parameter setting of Figure 6.3b, *i.e.* $V_T = 0.01$, $\theta_E = 0$ and $\beta = 0.01$, and comparing the dynamics obtained for three different values of V_D, *i.e.* $V_D = 0.001$, $V_D = 0.05$ and $V_D = 0.1$. In Figure 6.4, we compare the average antigen profile of the tumour cells at the end of simulations with the average antigen profile recognised

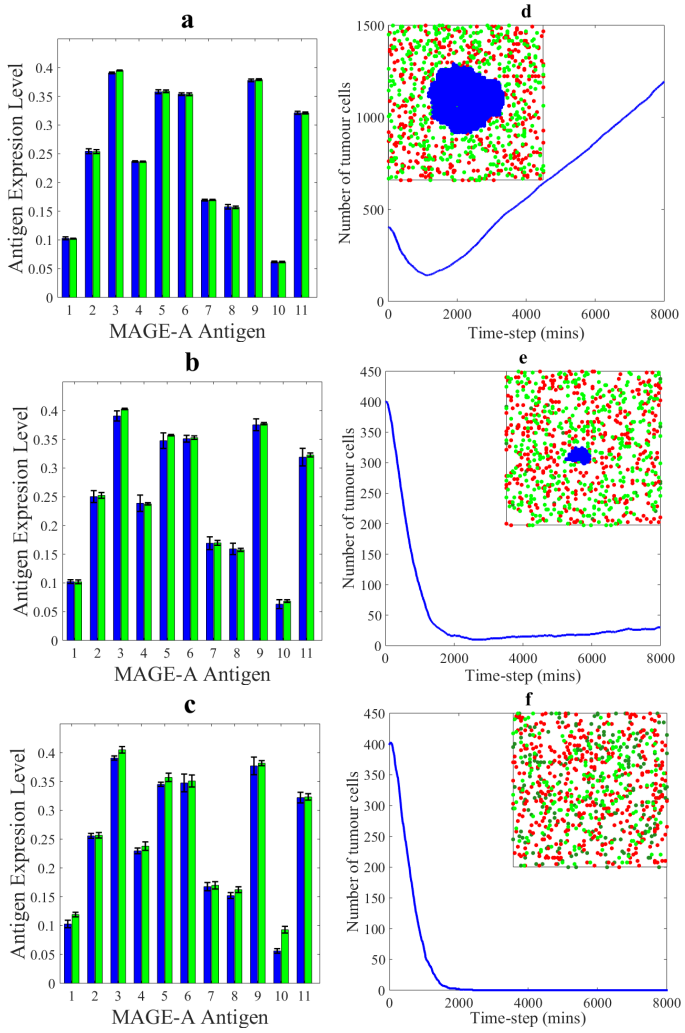

Figure 6.4: ***Increasing V_D can result in immune escape or chronic dormancy or immune clearance of the tumour.*** *Plots in panels* ***a-c*** *display the average antigen profile of tumour cells (blue) and the average antigen profile recognised by the DCs (green) at the end of simulations. The black lines describe the standard deviation between 5 runs of the simulation. Plots in panels* ***d-f*** *display the time evolution of the tumour cell number with an example of the observed cell spatial distributions at the final time-step shown in the insets. Values are taken to be the average over five simulation runs. Tumour cells are blue, DCs are green, CTLs are red and inactive immune cells are darker green and red, respectively. Three values for the parameter V_D are tested:* ***a,d*** *$V_D = 0.001$,* ***b,e*** *$V_D = 0.05$ and* ***c,f*** *$V_D = 0.1$. Here, $V_T = 0.01$, $\beta = 0.01$, $\theta_E = \theta_M = 0$, and all the other parameter values are reported in Table 6.1.*

by the DCs, and we show the corresponding time evolution of the number of tumour cells. The insets also display the spatial cell distributions observed at the end of simulations to allow for a clearer understanding of the resulting dynamics. We observe that V_D is a bifurcation parameter whereby three distinct situations result from choosing increasing values of V_D. In particular, Figures 6.4a,d refer to the case where the value of V_D is relatively low, *i.e.* $V_D = 0.001$, and show that there is a small difference between the average antigen profile of the tumour cells and the average recognised antigen profile at the end of simulations. Moreover, after an initial decrease, the tumour cell number increases steadily over time resulting in a relatively large final number of tumour cells. Furthermore, Figures 6.4b,e refer to the case where an intermediate value of V_D is considered, *i.e.* $V_D = 0.05$, and show that there is a larger difference between the average antigen profile of the tumour cells and the average recognised antigen profile at the end of simulations. Moreover, after a steep decrease, the tumour cell number remains at a low, almost constant, level for the remainder of the simulation time interval. Finally, Figures 6.4c,f refer to the case where the value of V_D is relatively large, *i.e.* $V_D = 0.1$, and show that the difference between the average antigen profile of the tumour cells and the average recognised antigen profile at the end of simulations is even larger than in the previous cases. Moreover, the number of tumour cells decreases steadily over time and eventually the tumour is completely removed.

6.3.4 Increasing the T cell receptor binding affinity can benefit the immune system response to cancer

To explore the effect of altering the T cell receptor binding affinity, we test for three increasing values of the parameter β, *i.e.* $\beta = 0$, $\beta = 0.0001$ and $\beta = 0.001$. We

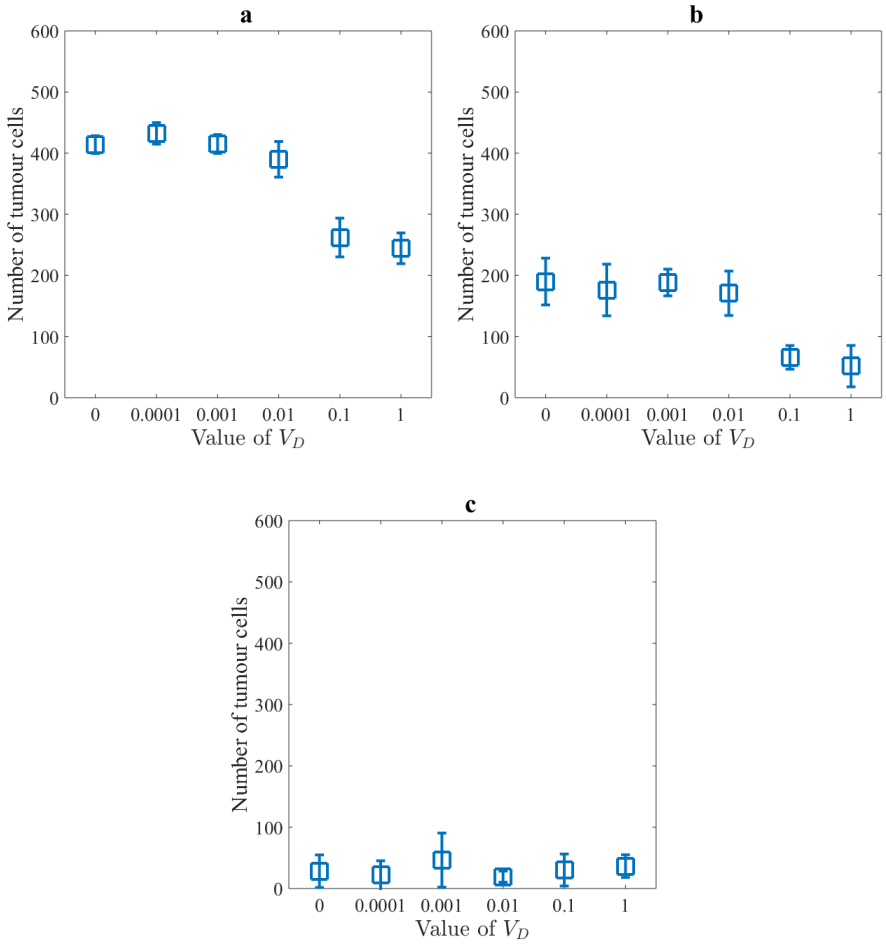

Figure 6.5: ***Increasing the T cell receptor binding affinity can benefit the immune system response to cancer.*** *Plots displaying the number of tumour cells remaining after* 1000 *time-steps for increasing values of the parameter* β*:* ***a*** $\beta = 0$*,* ***b*** $\beta = 0.0001$ *and* ***c*** $\beta = 0.001$*. For each value of* β *a range of values of the parameter* V_D *are tested. The tumour cell numbers presented have been obtained as the average over* 5 *simulations and the error bars display the related standard deviation. Here,* $V_T = 0.0001$*,* $\theta_E = \theta_M = 0$*, and all the other parameter values are reported in Table 6.1.*

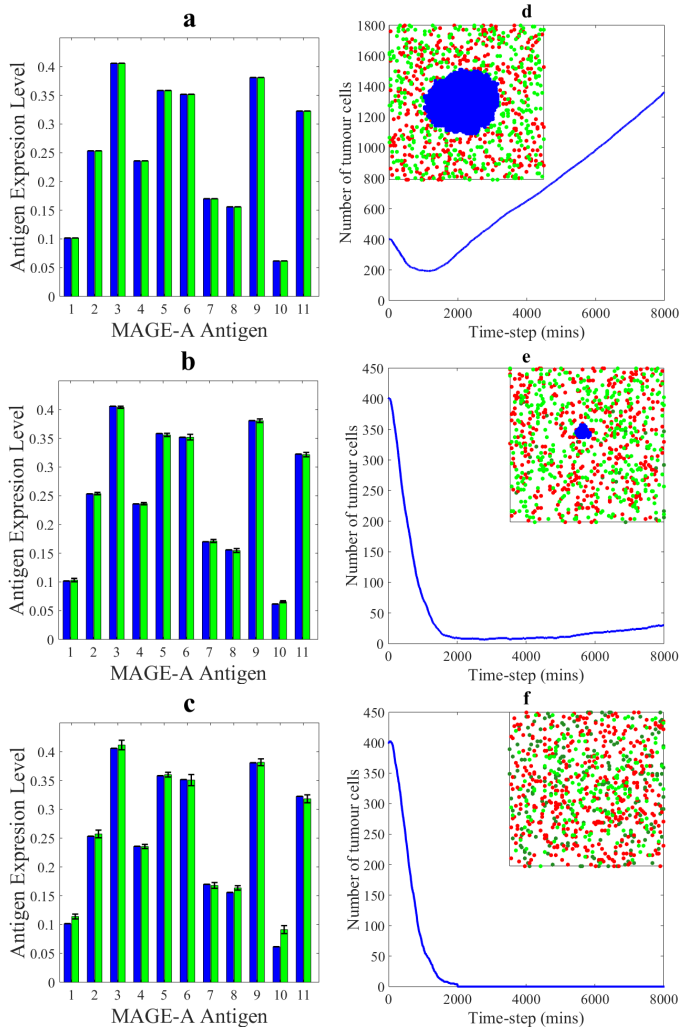

Figure 6.6: ***Increasing the T cell receptor binding affinity can benefit the immune system response to cancer.*** *Plots in panels* ***a-c*** *display the average antigen profile of tumour cells (blue) and the average antigen profile recognised by the DCs (green) at the end of simulations. The black lines describe the standard deviation between 5 runs of the simulation. Plots in panels* ***d-f*** *display the time evolution of the tumour cell number with an example of the observed cell spatial distributions at the final time-step shown in the insets. Values are taken to be the average over five simulation runs. Tumour cells are blue, DCs are green, CTLs are red and inactive immune cells are darker green and red, respectively. Three values for the parameter* V_D *are tested:* ***a,d*** $V_D = 0.001$, ***b,e*** $V_D = 0.05$ *and* ***c,f*** $V_D = 0.1$. *Here,* $V_T = 0.0001$, $\beta = 0.0001$, $\theta_E = \theta_M = 0$, *and all the other parameter values are reported in Table 6.1.*

choose $V_T = 0.0001$ and we let the tumour cell antigen profiles remain constant over time, *i.e.* we choose $\theta_E = \theta_M = 0$. For each value of β considered, we also explore the effect of increasing the value of the parameter V_D. In all cases, we carried out simulations for 1000 time-steps. As shown by Figure 6.5a, for $\beta = 0$, a considerable number of tumour cells remain inside the system at the end of simulations for all values of V_D. Conversely, the results presented in Figure 6.5c show that when β is sufficiently high, very few tumour cells remain in the system after 1000 time-steps for all values of V_D. Moreover, as shown by Figure 6.5b, for intermediate values of β, there appears to be a correlation between the number of tumour cells remaining after 1000 time-steps and the parameter V_D. In particular, larger values of the parameter V_D correspond to smaller numbers of the remaining tumour cells after 1000 time-steps. These results suggest that the T cell receptor binding affinity plays a key role in the immune response to tumour cells. In the same way as Figure 6.4, Figure 6.6 shows that, under the parameter choice of the computational simulations related to Figure 6.5b, increasing the value of the parameter V_D leads to immune escape or chronic dormancy or immune clearance of the tumour.

6.3.5 Increasing the probability of epimutations can lead to variations in the immune response to tumour cells

So far we have considered only the situation where the antigen profile of each tumour cell remains constant over time, *i.e.* the probability at which epimutations and mutations, leading to antigenic variations, occur are $\theta_E = 0$ and $\theta_M = 0$. To investigate the effect of epimutations on the success of the immune response against tumour cells, we consider the parameter setting that we have used in the computational simulations shown either in Figures 6.4a,d or in Figures 6.6c,f but now we

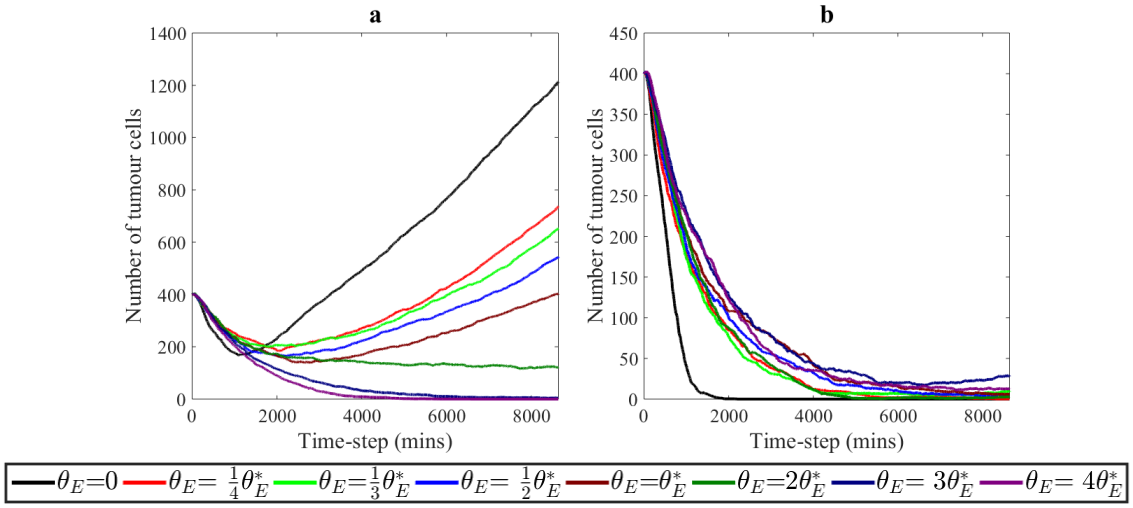

Figure 6.7: ***Increasing the probability of epimutations can lead to variations in the immune response to tumour cells.*** *Panels* **a** *and* **b** *display the time evolution of the tumour cell number for increasing values of* θ_E *(cf. the legend below the panels). For the numerical results reported in panel* **a** *we use the parameter setting of the simulations whose results are displayed in Figures 6.4a,d and* $V_E = 0.01$*, while for the numerical results reported in panel* **b** *we use the parameter setting of the simulations whose results are displayed in Figures 6.6c,f and* $V_E = 0.0001$*. Values are taken to be the average over five simulation runs.*

allow the antigen profiles of tumour cells to change through epimutations, *i.e.* we choose $\theta_E > 0$. We consider eight specific values of θ_E defined as fractions or multiples of the average probability of epimutations θ_E^*, given in Table 6.1. In all cases, we carried out simulations for 8640 time-steps and we report on tumour cell numbers obtained as the average over 5 simulations. Figure 6.7a displays the time evolution of the tumour cell number for the parameter setting of Figures 6.4a,d. These results show that increasing values of θ_E correspond to decreasing numbers of tumour cells inside the system at the end of simulations. In summary, by increasing the probability of epimutations the dynamics of tumour cells change from immune escape, through to chronic dormancy to immune clearance. On the other hand, Figure 6.7b displays the time evolution of the tumour cell number for the parameter setting of Figures 6.6c,f. These results show that for sufficiently small values of θ_E there are no tumour cells left inside the system at the end of simulations, whereas for larger values of θ_E a small number of tumour cells persist at the final time-step. Generally, by increasing the probability of epimutations the dynamics of tumour cells change from immune clearance to chronic dormancy. The range we consider, $0 \leq \theta_E \leq 0.92$, is above the range of De Smet et al. (1996), where the largest value was 0.45 and lowest 0.12. However values up to $2\theta_E^*$ are within the biological range and as from our results we expect larger θ_E to exhibit the same dynamics as $2\theta_E^*$. Therefore, the results we observe would be viable in a biological setting.

6.3.6 Mutations have a weaker impact on the immune response to tumour cells compared to epimutations

We now compare the impact of mutations and epimutations on the immune response to tumour cells. Following what we have done in the subsection above, we consider

the parameter setting used in the computational simulations shown either in Figures 6.4a,d or in Figures 6.6c,f but now we allow the antigen profiles of tumour cells to change through mutations, *i.e.* we choose $\theta_M > 0$. We consider eight specific values of θ_M defined as fractions or multiples of the average probability of epimutations θ_E^*, given in Table 6.1. In all cases, we carried out simulations for 8640 time-steps and we report on tumour cell numbers obtained as the average over 5 simulations. Figure 6.8a displays the time evolution of the tumour cell number for the parameter setting of Figures 6.4a,d and shows that immune escape occurs for all values of θ_M considered. On the other hand, Figure 6.8b displays the time evolution of the tumour cell number for the parameter setting of Figures 6.6c,f and shows that immune clearance occurs for all values of θ_M considered. Comparing these results with those displayed in Figure 6.7a and Figure 6.7b, respectively, we reach the conclusion that mutations have a weaker impact on the immune response to tumour cells compared to epimutations.

6.4 Concluding remarks and discussion

Spatial interactions between cancer and immune cells, as well as the recognition of tumour antigens by cells of the immune system, play a key role in the immune response against solid tumours. The existing mathematical models generally focus only on one of these key aspects. We have presented, in this chapter, a spatially explicit stochastic individual-based model that incorporates the adaptive processes driving tumour antigen recognition. Our model takes explicitly into account the dynamical heterogeneity of tumour antigen expression, and effectively captures the way in which this affects the immune response against the tumour.

Our computational simulation results show that the standard deviation of the

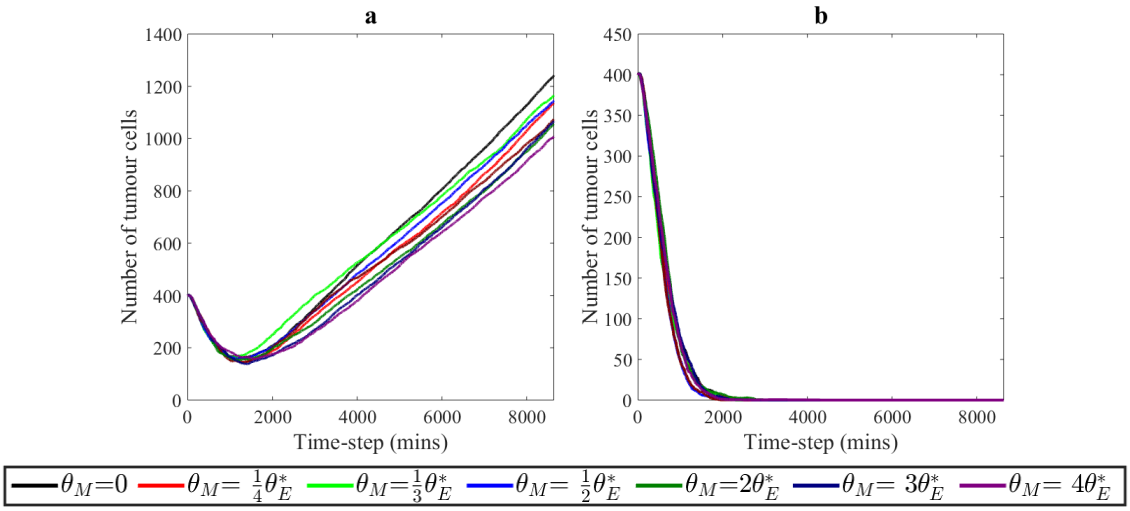

Figure 6.8: ***Mutations have a weaker impact on the immune response to tumour cells compared to epimutations.*** *panels* ***a*** *and* ***b*** *display the time evolution of the tumour cell number for increasing values of* θ_M *(cf. the legend below the panels). For the numerical results reported in panel* ***a*** *we use the parameter setting of the simulations whose results are displayed in Figures 6.4a,d and* $V_M = 0.01$*, while for the numerical results reported in Panel* ***b*** *we use the parameter setting of the simulations whose results are displayed in Figures 6.6c,f and* $V_M = 0.0001$*. Values are taken to be the average over five simulation runs.*

initial antigen expression profiles of cancer cells within the tumour, *i.e.* the parameter V_T, has a crucial impact upon the outcome of the immune response. In the situation of an almost homogeneous tumour, *i.e.* where all tumour cells have a similar antigen profile, immune clearance occurs. Conversely, when the antigenic composition between cancer cells is highly heterogeneous the tumour may be able to escape the immune system response and continue growing. Interestingly, for moderate levels of initial antigenic heterogeneity our results demonstrate that the fate of the tumour is determined by the specificity of the cellular immune response.

The computational outcomes of our model indicate that the parameter controlling the specificity of the antigen recognition process of the dendritic cells, *i.e.* the parameter V_D, ultimately dictates which receptors are produced by the cytotoxic T lymphocytes. A larger value of this parameter brings about a more diverse receptor repertoire of the CTLs, and in turn results in a better immune response. This suggests that it is advantageous for the T cell population to be multi-specific, whereby several different antigen receptors are simultaneously expressed by the CTL population. In this respect, the outcomes of our model recapitulate the conclusions of experimental papers showing the success of a more diverse T cell repertoire in response to cancer (Carreno et al., 2015; Gerdemann et al., 2011; Ott et al., 2017; Sahin et al., 2017; Schumacher and Hacohen, 2016; Sharma and Allison, 2015).

Moreover, our computational results support the idea that varying the specificity of the immune response can result in three distinct scenarios, from immune escape, through to chronic dormancy to immune clearance of the tumour. The importance of tumour dormancy controlled by the immune system, *i.e.* immunological dormancy, has been highlighted by previous experimental and theoretical work (Kuznetsov et al., 1994; Lorenzi et al., 2015; Matzavinos et al., 2004; Wu et al., 2018). In particular, immunological dormancy can explain situations where there is an extended

period of time before the occurrence of tumour relapse (Aguirre-Ghiso, 2007; Gomis and Gawrzak, 2017; Manjili, 2018; Teng et al., 2008; Wang and Lin, 2013; Yeh and Ramaswamy, 2015). In this regard, our model suggests the existence of a possible relationship between the specificity of the immune response and the emergence of prolonged immunological dormancy. Furthermore, in recent years, new experimental techniques have been developed which allow for the specificty of T cell receptors to be altered (Smith et al., 2014). One particular approach is to use gene editing, *in vitro*, to modify which antigen the T cell receptors will respond to (Albers et al., 2019). These approaches would allow for greater control over which tumour antigens the T cells target.

We have also explored the way in which altering the binding affinity of the CTLs, *i.e.* the parameter β, to their corresponding tumour antigen may change the immune response to the tumour. Our results indicate that a stronger binding affinity leads to a more effective immune response, as the CTLs have a wider range of tumour cells that they can interact with. Previously, Gerdemann et al. (2011) found experimentally that a strong T cell binding affinity to tumour antigens played a key role in the overall immune response to the disease. Integrating the outcomes of our model and such experimental findings suggests that enhancing the binding affinity of T cells, *e.g.* through the modification of the receptors that the T cells of a patient can produce, could be a potential target of adoptive T cell therapy.

Furthermore, the results from our computational simulations suggest that changes in the antigenic expression of tumour cells due to epimutations can be either beneficial or detrimental to the immune response to a solid tumour. In more detail, we have found that in some cases increasing the frequency of epimutations could transform situations of immune escape into tumour dormancy and eventually tumour removal. These findings are interesting in light of cancer therapy as they suggest

that the efficacy of the immune response against solid tumours could be enhanced by increasing the frequency of epimutations. In regards to this, the loss of DNA methylation was the first epimutation to be identified in cancer cells (Feinberg and Tycko, 2004) and several experimental and clinical works found that the expression of MAGE antigens could be increased through demethylation (Chinnasamy et al., 2011; Gerdemann et al., 2011; Graff-Dubois et al., 2002; Wischnewski et al., 2006). Taken together, the outcomes of our model suggest that by combining a T cell therapy targeting multiple MAGE genes – *e.g.* using approaches similar to those of Gerdemann et al. (2011) – and increasing the probability of epimutations through demethylating agents, *e.g.* using methods similar to those of Chinnasamy et al. (2011) and Wischnewski et al. (2006), a stronger immune response could be induced. However, in other cases, we have observed that increasing the frequency of epimutations can turn instances of tumour removal into scenarios whereby a small number of tumour cells persisted over time. These contrasting results were also suggested previously through experimental research, where epimutations could be either beneficial or detrimental to tumour development (Chen and Mellman, 2017; Yarchoan et al., 2017).

We have additionally studied the effect of changes in the antigenic expression of tumour cells caused by mutations. In all parameter settings we have considered, increasing the frequency of mutations did not change the resulting dynamics of the tumour-immune response. This suggests that mutations have a weaker effect on tumour-immune competition than antigenic variations caused by epimutations. This finding is coherent with experimental observations indicating that epimutations generally occur more frequently than mutations in tumour development (Feinberg, 2004; Peltomäki, 2012). Hence our results demonstrate the importance of understanding the underlying causes of antigenic variations in tumour cells when

considering tumour-immune competition.

In a variety of contexts the benefit of relating stochastic individual-based models to deterministic continuum models has been highlighted (Champagnat et al., 2006; Chisholm et al., 2016, 2015; Deroulers et al., 2009; Painter and Hillen, 2015; Penington et al., 2011; Stevens, 2000). Combining such modelling approaches makes it possible to integrate computational simulations with analytical results, thus enabling a more extensive exploration of the model parameter space. However, our individual-based model described in this chapter (and those described in Chapter 4 and Chapter 5) includes various complex mechanisms. These mechanisms, such as the Lévy walk mechanisms and antigenic expression modelling, will be challenging to capture using continuum methods. With the aim of achieving a continuum form of the discrete individual-based models presented, we initially consider a simpler biological scenario. In the following chapter we present a stochastic individual-based model describing motion and proliferation of cell populations and derive the continuum version of this model to allow for mathematical analysis.

Chapter 7

Deriving continuum models from individual-based models

7.1 Overview

In general, individual-based (IB) models are useful for observing emergent dynamics from these interactions they can be computationally time consuming and do not allow for analysis to be completed on the model. Considering the continuum counterpart of our stochastic discrete IB models would allow for mathematical analysis. In the previous chapters we have developed IB models to describe tumour immune competition including the antigen recognition process and evolution of the tumour through changes in antigenic expression. In these models we also describe the change in cell motion of cytotoxic T cells (CTLs) and dendritic cells (DCs) due to the presence of tumour antigen. Due to the complexity approaches used in the previous chapters to model the antigen recognition process and the movement of immune cells, the derivation of a continuum version of these models would be potentially challenging. The derivation of a continuum description of Lévy walk mechanisms

has been studied (Fedotov, 2016; Fedotov and Korabel, 2017; Gan et al., 2015; Golovin et al., 2008; Hanert, 2012; Stage et al., 2016), however the methods used are complex and may not be applicable to interacting populations. Therefore, to gain an understanding of the process of deriving a continuum limit from individual-based models, in this chapter, we consider a simpler biological situation to investigate whether deriving continuum models from the IB schemes can still result in the same numerical results and provide opportunities for the study of interesting mathematical properties. The work described in this chapter has been published in Chaplain et al. (2019).

7.2 Motivation

For a population of cells whose growth rate depends on the local pressure (Brú et al., 2003; Byrne and Preziosi, 2003; Drasdo and Hoehme, 2012; Ranft et al., 2010), a prototypical example of such models was proposed by Byrne and Drasdo (2009), that is,

$$\partial_t \rho - \mu \operatorname{div}(\rho \nabla p) = G(p)\rho. \tag{7.1}$$

This is a conservation equation for the cell density function $\rho(t, x) \geq 0$ at position $x \in \mathbb{R}^d$, with $d = 1, 2, 3$ in the biologically relevant cases, and time $t \in \mathbb{R}^+$. In this case, the function p stands for the cell pressure and the term G is the net growth rate of the cell density. In analogy with the classical Darcy law for fluids, the parameter $\mu > 0$ is the cell mobility coefficient, which is defined as the quotient between the permeability of the porous medium in which the cells are embedded (*e.g.* the extracellular matrix) and the cellular viscosity.

The pressure-driven movement, which is modelled by the second term on the left-hand side of equation (7.1), dictates that cells tend to move towards regions of

lower local pressure where they feel less compressed. That is, we assume cells exert pressure on each other through physical interactions, and therefore when there are a large number of cells then the pressure will be greater through compression of space. The definition of this term builds on the seminal paper of Greenspan (1976) and subsequent work of Byrne and Chaplain (1997).

Pressure-limited growth, *i.e.* cell division and cell death, of the cell population is determined by the term on the right-hand side of equation (7.1). From a mathematical perspective, the effect of this pressure-limited growth can be captured by assuming that $G(p)$ is a smooth function which satisfies,

$$\frac{\partial G}{\partial p} < 0, \quad G(P) = 0. \tag{7.2}$$

In the assumptions given by equation (7.2), the parameter $P > 0$ stands for the pressure at which cell death exactly compensates cell division. The term homeostatic pressure has been coined to indicate such a critical pressure (Basan et al., 2009).

In order to close equation (7.1) the pressure p must be defined. Several works consider a barotropic relation $p \equiv \Pi(\rho)$. Typically, the function $\Pi(\rho)$ is identically zero for $\rho \leq \rho^*$ and is monotonically increasing for $\rho > \rho^*$, with $0 < \rho^* < \Pi^{-1}(P)$ being the density below which cells do not exert any force upon one another (Tang et al., 2014). For instance, it is common to assume Π is a smooth function of ρ that satisfies the following assumptions

$$\Pi(0) = 0, \quad \frac{\partial \Pi}{\partial \rho} > 0 \ \text{ for } \ \rho > 0. \tag{7.3}$$

In the attempt to reduce the biological problem to its essentials while ensuring analytical tractability of the mathematical model, Perthame et al. (2014b) have

proposed the following definition of $\Pi(\rho)$, which satisfies the assumptions given by equation (7.3):

$$\Pi(\rho) = K_\gamma \, \rho^\gamma \quad \text{with} \quad \gamma > 1 \quad \text{and} \quad K_\gamma > 0. \tag{7.4}$$

In the definition given by equation (7.4), the parameter γ provides a measure of the stiffness of the barotropic relation and K_γ is a scale factor. Interestingly, the limit $\gamma \to \infty$ corresponds to the case where cells behave like an incompressible fluid. In this asymptotic regime, it has been proven that models of the form of equation (7.1) converge to free-boundary problems of Hele-Shaw type (Kim and Požár, 2018; Kim et al., 2016; Mellet et al., 2017; Perthame et al., 2014a).

The model given by equation (7.1) can be generalised to the case of multiple cell populations with different biophysical properties, *i.e.* different mobilities and growth rates, as follows

$$\partial_t \rho_h - \mu_h \operatorname{div}(\rho_h \nabla p) = G_h(p)\rho_h, \quad h = 1, \ldots, M. \tag{7.5}$$

The system of coupled equations (7.5) contains notation, and relies on assumptions, analogous to those underlying equation (7.1). In particular, the coefficient $\mu_h > 0$ measures the mobility of cells in the h^{th} population and the pressure p is given by a barotropic relation $p \equiv \Pi(\rho)$, where ρ stands for the total cell density, *i.e.*

$$\rho(t, x) = \sum_{h=1}^{M} \rho_h(t, x). \tag{7.6}$$

The function Π satisfies the conditions given by equation (7.3) and the net growth rate $G_h(p)$ can be assumed to be a smooth function of the cell pressure that satisfies the assumptions given by equation (7.2) for all $h = 1, \ldots, M$.

For example, building on the computational results presented by Drasdo and

Hoehme (2012), Lorenzi et al. (2017) considered the following system of equations,

$$\begin{cases} \partial_t \rho_1 - \mu_1 \operatorname{div}(\rho_1 \nabla p) = G(p)\rho_1, \\ \partial_t \rho_2 - \mu_2 \operatorname{div}(\rho_2 \nabla p) = 0, \end{cases} \tag{7.7}$$

complemented with the barotropic relation given by equation (7.4). The system of equations (7.7) describes the interaction dynamics between a population of proliferating cells, *i.e.* population 1, and a population of nonproliferating cells, *i.e.* population 2, with different mobilities.

As detailed in Section 3.3.1, the derivation of continuum models from stochastic IB models can allow for a more robust description of biological phenomena. However, with the exception of the qualitative comparisons of growth dynamics carried out by Byrne and Drasdo (2009) and Fozard et al. (2010), and the study of long-time behaviour by Motsch and Peurichard (2018) for the case of one single cell population, little prior work has investigated the relation between single-cell-based models and continuum models in the form of equation (7.1) and the system of equations (7.7).

In this chapter, we develop a simple stochastic individual-based model for the dynamics of growing cell populations. Our model is based on a branching random walk that takes into account the effects of pressure-driven cell movement and pressure-dependent cell proliferation. We show that equation (7.1) and the system of equations (7.5) can be formally derived from the branching random walk that underlies our discrete model. Furthermore, we carry out a systematic quantitative comparison between the individual-based model and its continuum counterparts, both in the case of one single cell population and in the case of multiple cell populations with different biophysical properties. Specifically, we construct travelling-wave solutions both for equation (7.1) and for the system of equations (7.7). Finally, we

present numerical solutions that illustrate the results of the travelling-wave analysis, and compare such numerical solutions with the results of computational simulations of the individual-based model. Comparison of the models indicates that simple IB models can lead to the emergence of complex spatial patterns of population growth observed in continuum models.

7.3 An individual-based model for growing cell populations

To allow for multiple biological situations to be considered we examine a multicellular system made up of M cell populations, where we index each population with $h = 1, \ldots, M$. Each cell within the system is modelled as an agent which occupies a lattice position on the real line $\mathbb{R}$. Although in this chapter we will focus on a one dimensional situation, there is little additional difficulty extending these ideas to higher dimensions. Each cell can undergo pressure-driven movement and pressure-limited growth according to a set of simple rules that result in a discrete-time branching random walk.

To set up our individual-based (IB) model we begin by discretising the time variable $t \in \mathbb{R}^+$ as $t_k = k\tau$ with $k \in \mathbb{N}_0$. We additionally discretise the space variable $x \in \mathbb{R}$ as $x_i = i\chi$ with $i \in \mathbb{Z}$ where $0 < \tau, \chi \ll 1$. From these discretisations we obtain a time-step of length τ and grid spaces of length χ .

At any chosen time-step k, we denote the number of cells in population $h = 1, \ldots, M$ at the lattice position i to be denoted as $n_{hi}^k \in \mathbb{N}_0$, and from this can

calculate the total cell density as,

$$\rho_h(t_k, x_i) = \rho_{hi}^k = n_{hi}^k \, \chi^{-1} \quad \text{and} \quad \rho(t_k, x_i) = \rho_i^k = \sum_{h=1}^{M} \rho_h(t_k, x_i). \tag{7.8}$$

Additionally, at each lattice site i and time-step k we calculate the cell pressure $p(t_k, x_i) = p_i^k$, which is defined through a barotropic relation $p_i^k \equiv \Pi(\rho_i^k)$. We assume that Π is a function of the total cell density that satisfies the conditions given by equation (7.3). At each time-step, we allow every cell to undergo pressure-limited growth and pressure-driven movement according to a set of algorithmic rules, which are shown schematically in Figure 7.1. Note that, unlike the individual-based models we have developed in the previous chapters, we allow multiple cells to inhabit each grid position where the total number is limited by the pressure.

Pressure-limited population growth: At each time-step each cell may divide, die or remain quiescent with probabilities which depend on the local pressure. If a cell divides, two daughter cells are formed and replace the parent cell on the original lattice position of the parent cell. Furthermore, any cells that undergo cell death are removed from the system. In particular, we incorporate pressure-limited cell growth into our model by assuming that at the k^{th} time-step a focal cell of population h on the lattice site i can divide with probability

$$\tau \, G_h(p_i^k)_+ \quad \text{where} \quad G_h(p_i^k)_+ = \max\{0, G_h(p_i^k)\} \tag{7.9}$$

or die with probability

$$\tau \, G_h(p_i^k)_- \quad \text{where} \quad G_h(p_i^k)_- = -\min\{0, G_h(p_i^k)\} \tag{7.10}$$

or remain quiescent with probability

$$1 - \left(\tau\, G_h(p_i^k)_+ + \tau\, G_h(p_i^k)_-\right) = 1 - \tau|G_h(p_i^k)|. \tag{7.11}$$

Here, we let the rate G_h be a function of the local pressure that satisfies the assumptions given by equation (7.2) for all values of h. Moreover, the length of each time-step τ is chosen to be sufficiently small to ensure that the quantities given by equations (7.9)-(7.11) are all between 0 and 1. The assumptions that we consider on the growth function G_h, given by equation (7.2), are such that if $p_i^k > P$ then each cell within the population h at the position i can only die or remain quiescent at the k^{th} time-step. This can be summarised by the conditions,

$$p_i^k \leq \overline{p} \;\text{ for all }\; (k,i) \in \mathbb{N}_0 \times \mathbb{Z}, \;\text{ with }\; \overline{p} = \max\Big\{ \max_{i\in\mathbb{Z}} p_i^0, P \Big\}. \tag{7.12}$$

Pressure-driven cell movement: We model pressure-driven cell movement, *i.e.* the tendency of cells to move down pressure gradients, as a biased random walk. We consider that the probabilities of movement depend on the difference between the pressure at the site occupied by a cell and the pressure at the neighbouring sites. In particular, for a cell of population h on the lattice site i at the time-step k, we define the probability of moving to the lattice site $i-1$, *i.e.* the probability of moving left, as

$$J_h^L(p_i^k - p_{i-1}^k) = \nu_h \frac{(p_i^k - p_{i-1}^k)_+}{2\,\overline{p}}, \tag{7.13}$$

where $(p_i^k - p_{i-1}^k)_+ = \max\{0, (p_i^k - p_{i-1}^k)\}$. Similarly, we model the probability of moving to the lattice site $i+1$, *i.e.* the probability of moving right, as

$$J_h^R(p_i^k - p_{i+1}^k) = \nu_h \frac{(p_i^k - p_{i+1}^k)_+}{2\,\overline{p}}, \tag{7.14}$$

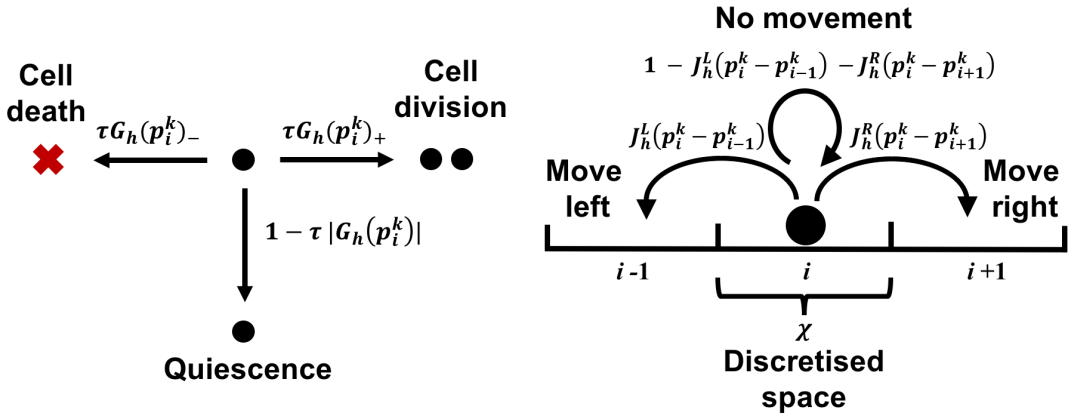

Figure 7.1: Schematic representation of the simple algorithmic rules governing cell dynamics in our stochastic individual-based model. *Pressure-limited cell growth is modelled by letting the probabilities of a cell dividing, dying and remaining quiescent be dependent on the local pressure (left panel). Pressure-driven cell movement is modelled by letting the movement probabilities depend on the difference between the pressure at the site occupied by a cell and the pressure at the neighbouring sites (right panel).*

where $(p_i^k - p_{i+1}^k)_+ = \max\{0, (p_i^k - p_{i+1}^k)\}$. Therefore we can calculate the probability of remaining stationary on the lattice site i as

$$1 - J_h^L(p_i^k - p_{i-1}^k) - J_h^R(p_i^k - p_{i+1}^k). \tag{7.15}$$

In the above equations, the coefficient $0 < \nu_h \leq 1$ is directly proportional to the mobility of cells in population h and the parameter $\overline{p}$ is defined in equation (7.12). We note that, the definitions given by equations (7.13)-(7.15) are such that the cells will move down pressure gradients, *i.e.* they will favour positions with lower pressure values. Moreover, the assumptions given by equation (7.12) guarantee that the quantities given by equations (7.13)-(7.15) are all between 0 and 1.

7.4 Formal derivation of continuum models

In this section, we show how continuum models of growing cell populations of the form of equation (7.1) and of the system of equations (7.5) and (7.7) can be derived as formal limits of the branching random walk that underlies our individual-based model.

For a multicellular system whose dynamics are governed by the algorithmic rules for cell movement and cell proliferation, that are presented in Section 7.3, the principle of mass balance gives

$$\begin{aligned}
\rho_{hi}^{k+1} &= \nu_h \frac{(p_{i-1}^k - p_i^k)_+}{2\,\overline{p}} \left[2\tau G_h(p_{i-1}^k)_+ + \left(1 - \tau|G_h(p_{i-1}^k)|\right)\right] \rho_{h\,i-1}^k \\
&\quad + \nu_h \frac{(p_{i+1}^k - p_i^k)_+}{2\,\overline{p}} \left[2\tau G_h(p_{i+1}^k)_+ + \left(1 - \tau|G_h(p_{i+1}^k)|\right)\right] \rho_{h\,i+1}^k \\
&\quad + \left[1 - \nu_h \frac{(p_i^k - p_{i-1}^k)_+}{2\,\overline{p}} - \nu_h \frac{(p_i^k - p_{i+1}^k)_+}{2\,\overline{p}}\right] \\
&\qquad\qquad \times \left[2\tau G_h(p_i^k)_+ + \left(1 - \tau|G_h(p_i^k)|\right)\right] \rho_{hi}^k,
\end{aligned}$$

and after a little algebra we find

$$\begin{aligned}
\rho_{hi}^{k+1} &= \nu_h \frac{(p_{i-1}^k - p_i^k)_+}{2\,\overline{p}} \left(\tau G_h(p_{i-1}^k) + 1\right) \rho_{h\,i-1}^k \\
&\quad + \nu_h \frac{(p_{i+1}^k - p_i^k)_+}{2\,\overline{p}} \left(\tau G_h(p_{i+1}^k) + 1\right) \rho_{h\,i+1}^k \\
&\quad + \left[1 - \nu_h \frac{(p_i^k - p_{i-1}^k)_+}{2\,\overline{p}} - \nu_h \frac{(p_i^k - p_{i+1}^k)_+}{2\,\overline{p}}\right] \left(\tau G_h(p_i^k) + 1\right) \rho_{hi}^k.
\end{aligned}$$

The above equation simplifies to

$$\begin{aligned}
\rho_{hi}^{k+1} - \rho_{hi}^{k} &= \tau G_h(p_i^k)\rho_{hi}^k \\
&\quad + \frac{\nu_h}{2\,\overline{p}}\left[\rho_{h\,i-1}^k (p_{i-1}^k - p_i^k)_+ + \rho_{h\,i+1}^k (p_{i+1}^k - p_i^k)_+\right] \\
&\quad - \frac{\nu_h}{2\,\overline{p}}\left[\rho_{hi}^k (p_i^k - p_{i-1}^k)_+ + \rho_{hi}^k (p_i^k - p_{i+1}^k)_+\right] \\
&\quad + \frac{\nu_h \tau}{2\,\overline{p}}\left[\rho_{h\,i-1}^k G_h(p_{i-1}^k)(p_{i-1}^k - p_i^k)_+ + \rho_{h\,i+1}^k G_h(p_{i+1}^k)(p_{i+1}^k - p_i^k)_+\right] \\
&\quad - \frac{\nu_h \tau}{2\,\overline{p}}\left[\rho_{hi}^k G_h(p_i^k)(p_i^k - p_{i-1}^k)_+ + \rho_{hi}^k G_h(p_i^k)(p_i^k - p_{i+1}^k)_+\right]. \qquad (7.16)
\end{aligned}$$

Using the fact that the following relations hold for τ and χ sufficiently small

$$t_k \approx t, \quad t_{k+1} \approx t + \tau, \quad x_i \approx x, \quad x_{i\pm1} \approx x \pm \chi,$$

$$\rho_{hi}^k \approx \rho_h(t,x), \quad \rho_{hi}^{k+1} \approx \rho_h(t+\tau,x), \quad \rho_{h\,i\pm1}^k \approx \rho_h(t, x \pm \chi),$$

$$p_i^k \approx p(t,x), \quad p_{i\pm1}^k \approx p(t, x \pm \chi),$$

we rewrite equation (7.16) in the following approximate form:

$$\begin{aligned}
\rho_h(t+\tau,x)-\rho_h(t,x) \;\approx\;& \tau G_h(p)\rho_h(t,x)\\
&+\frac{\nu_h}{2\,\overline{p}}\left[\rho_h(t,x-\chi)(p(t,x-\chi)-p(t,x))_+\right]\\
&+\frac{\nu_h}{2\,\overline{p}}\left[\rho_h(t,x+\chi)(p(t,x+\chi)-p(t,x))_+\right]\\
&-\frac{\nu_h}{2\,\overline{p}}\left[\rho_h(t,x)(p(t,x)-p(t,x-\chi))_+\right]\\
&-\frac{\nu_h}{2\,\overline{p}}\left[\rho_h(t,x)(p(t,x)-p(t,x+\chi))_+\right]\\
&+\frac{\nu_h\tau}{2\,\overline{p}}\left[\rho_h(t,x-\chi)G_h(p(t,x-\chi))(p(t,x-\chi)-p(t,x))_+\right]\\
&+\frac{\nu_h\tau}{2\,\overline{p}}\left[\rho_h(t,x+\chi)G_h(p(t,x+\chi))(p(t,x+\chi)-p(t,x))_+\right]\\
&-\frac{\nu_h\tau}{2\,\overline{p}}\left[\rho_h(t,x)G_h(p(t,x))(p(t,x)-p(t,x-\chi))_+\right]\\
&-\frac{\nu_h\tau}{2\,\overline{p}}\left[\rho_h(t,x)G_h(p(t,x))(p(t,x)-p(t,x+\chi))_+\right]. \quad (7.17)
\end{aligned}$$

Throughout the remainder of this section we will assume

$$\rho_h \in C^2(\mathbb{R}^+ \times \mathbb{R}), \quad h = 1, \ldots, M. \tag{7.18}$$

Since the function $\rho_h(t,x)$ is twice continuously differentiable for all values of h, we can approximate the terms $\rho_h(t+\tau,x)$, $\rho_h(t,x-\chi)$ and $\rho_h(t,x+\chi)$ in equation (7.17) by their second order Taylor expansions about the point (t,x). Under the assumption given by equation (7.18), since $p \equiv \Pi(\rho)$ with Π being a smooth function of ρ, the pressure $p(t,x)$ is twice continuously differentiable w.r.t the variable x as well. Therefore, we can also approximate the terms $p(t,x-\chi)$ and $p(t,x+\chi)$ in equation (7.17) by their second order Taylor expansions about the point (t,x). After a

little algebra, we find that

$$\begin{aligned}
\tau\,\partial_t\rho_h(t,x)+\frac{\tau^2}{2}\partial^2_{tt}\rho_h(t,x) &\approx \tau G_h(p(t,x))\rho_h(t,x)+\frac{\nu_h\chi^2}{2\,\overline{p}}\rho_h(t,x)\partial^2_{xx}p(t,x)\\
&\quad+\frac{\nu_h\chi^2}{2\,\overline{p}}\left[(\partial_x p(t,x))_+-(-\partial_x p(t,x))_+\right]\partial_x\rho_h(t,x)\\
&\quad+\frac{\nu_h\tau}{2\,\overline{p}}\rho_h(t,x)G_h(p(t,x-\chi))\,(-\chi\partial_x p(t,x))_+\\
&\quad+\frac{\nu_h\tau}{2\,\overline{p}}\rho_h(t,x)G_h(p(t,x+\chi))\,(\chi\partial_x p(t,x))_+\\
&\quad-\frac{\nu_h\tau}{2\,\overline{p}}\rho_h(t,x)G_h(p(t,x))\,(\chi\partial_x p(t,x))_+\\
&\quad-\frac{\nu_h\tau}{2\,\overline{p}}\rho_h(t,x)G_h(p(t,x))\,(-\chi\partial_x p(t,x))_+\,,
\end{aligned}$$

which implies

$$\begin{aligned}
\tau\,\partial_t\rho_h(t,x)+\frac{\tau^2}{2}\partial^2_{tt}\rho_h(t,x) &\approx \tau G_h(p(t,x))\rho_h(t,x)\\
&\quad+\frac{\nu_h\chi^2}{2\,\overline{p}}\left(\rho_h(t,x)\partial^2_{xx}p(t,x)+\partial_x\rho_h(t,x)\partial_x p(t,x)\right)\\
&\quad+\frac{\nu_h\tau\chi}{2\,\overline{p}}\,F(t,x),
\end{aligned}\tag{7.19}$$

with

$$\begin{aligned}
F(t,x) &= \left[G_h(p(t,x-\chi))\,(-\partial_x p(t,x))_+ + G_h(p(t,x+\chi))\,(\partial_x p(t,x))_+\right]\rho_h(t,x)\\
&\quad-\left[(\partial_x p(t,x))_+ + (-\partial_x p(t,x))_+\right]G_h(p(t,x))\rho_h(t,x).
\end{aligned}$$

Dividing both sides of the resulting equation by τ we obtain

$$\begin{aligned}
\partial_t\rho_h(t,x)+\frac{\tau}{2}\partial^2_{tt}\rho_h(t,x) &\approx G_h(p(t,x))\rho_h(t,x)\\
&\quad+\frac{\nu_h\chi^2}{2\,\overline{p}\tau}\left(\rho_h(t,x)\partial^2_{xx}p(t,x)+\partial_x\rho_h(t,x)\partial_x p(t,x)\right)\\
&\quad+\frac{\nu_h\chi}{2\,\overline{p}}\,F(t,x).
\end{aligned}\tag{7.20}$$

Letting both $\tau \to 0$ and $\chi \to 0$ in equation (7.20) in such a way that

$$\frac{\nu_h \chi^2}{2\,\overline{p}\,\tau} \to \mu_h \quad \text{as} \quad \tau \to 0 \quad \text{and} \quad \chi \to 0, \quad \text{for} \quad h = 1, \ldots, M \tag{7.21}$$

we formally obtain the following system of coupled conservation equations

$$\partial_t \rho_h = G_h(p)\rho_h + \mu \left(\rho_h \, \partial^2_{xx} p_h + \partial_x \rho_h \, \partial_x p_h \right), \quad h = 1, \ldots, M,$$

which can be rewritten as the system of equations (7.5), that is,

$$\partial_t \rho_h - \mu_h \, \partial_x \left(\rho_h \, \partial_x p \right) = G_h(p)\rho_h, \quad h = 1, \ldots, M. \tag{7.22}$$

Remark 1. *We note that condition* (7.21) *is a natural counterpart of the usual parabolic scaling of Brownian motion. Hence, our formal derivation does not impose any additional assumptions than those commonly employed for the asymptotic investigation of random walks.*

In the case of one single cell population, letting $M = 1$ and dropping the index h we formally obtain equation (7.1). Moreover, we formally obtain the system of equations (7.7) by choosing $M = 2$, labelling the two populations by $h = 1$ and $h = 2$, and setting $G_1 \equiv G$ and $G_2 \equiv 0$.

7.5 Comparison between individual-based and continuum models

In this section, we aim to quantitatively compare the outcomes of the IB model and the derived continuum models, for both a single population case and the case where

we have two cell populations. Firstly, we look for travelling wave solutions of the continuum models given by equation (7.1) and the system of equations (7.7) - see Section 7.5.1. Following this, we construct numerical solutions of the model equations, which support our findings from the travelling-wave analysis, and compare these results to numerical simulations of our IB model - see Section 7.5.2.

7.5.1 Travelling-wave analysis of the continuum models

We first consider the continuum model given by equation (7.1) and we look for one-dimensional travelling-wave solutions of the form

$$\rho(t,x) = \rho(z) \quad \text{with} \quad z = x - ct \quad \text{and} \quad c > 0,$$

that satisfy the following asymptotic conditions

$$\rho(z) \xrightarrow[z\to-\infty]{} \Pi^{-1}(P) \quad \text{and} \quad \rho(z) \xrightarrow[z\to\infty]{} 0. \tag{7.23}$$

Therefore, we study the existence of pairs (ρ, c) that satisfy the problem defined by the differential equation

$$-c\,\rho' - \mu\,(\rho\,p')' = G(p)\,\rho, \tag{7.24}$$

complemented with the asymptotic conditions given by equation (7.23). Our main results are summarised by the following theorem.

Theorem 1. *Under the assumptions given by equations* (7.2) *and* (7.3)*, there exists* $c > 0$ *such that the travelling-wave problem defined by equation* (7.24) *complemented with the asymptotic conditions given by equation* (7.23) *admits a nonnegative and nonincreasing solution* ρ*.*

Proof. We divide the proof of Theorem 1 into two steps. First we prove that for $c > 0$ fixed equation (7.24) complemented with the asymptotic conditions given by equation (7.23) admits a nonnegative and nonincreasing solution ρ (Step 1). Then we show that there exists a unique value of the wave speed c that satisfies the travelling-wave problem (Step 2).

Step 1. Multiplying both sides of equation (7.24) by $\dfrac{\partial p}{\partial \rho}$ we obtain the following boundary-value problem for p:

$$-p' \, (c + \mu \, p') - \mu \, p'' \, \rho \, \frac{\partial p}{\partial \rho} = G \, (p) \, \rho \frac{\partial p}{\partial \rho}, \tag{7.25}$$

$$p(z) \xrightarrow[z \to -\infty]{} P \quad \text{and} \quad p(z) \xrightarrow[z \to \infty]{} 0. \tag{7.26}$$

Let z^* be a critical point of p in $\mathbb{R}$. Using the differential equation (7.25) we see that

$$p''(z^*) = -\frac{1}{\mu} G \, (p(z^*))$$

and, under assumptions (7.2) and conditions (7.26), using the strong maximum principle we conclude that $p < P$ in $\mathbb{R}$ and that p cannot have a local minimum in $\mathbb{R}$, *i.e.*

$$p'(z) < 0 \ \text{ for all } \ z \in \mathbb{R}. \tag{7.27}$$

Hence the solution p of the differential equation (7.25) subject to conditions (7.26) is a nonnegative and nonincreasing function that satisfies

$$0 < p(z) < P \ \text{ for all } \ z \in \mathbb{R}. \tag{7.28}$$

Since $p \equiv \Pi(\rho)$ and Π is a smooth monotonically increasing function of ρ, we can then conclude that the cell density ρ is a nonnegative and nonincreasing function as

well.

Step 2. We prove that p is a monotonically decreasing function of the parameter c. This guarantees that given the cell density ρ the wave speed c can be uniquely identified through a monotonicity argument. Differentiating equation (7.24) w.r.t. z yields

$$-c\,(\rho')' - \mu\,\left[(p')''\,\rho + p''\,\rho' + (p')'\rho' + p'(\rho')'\right] = \frac{\partial G}{\partial p}\,p'\,\rho + G\,(p)\;\rho', \tag{7.29}$$

while differentiating equation (7.24) w.r.t. c gives

$$\begin{aligned} -c\left(\frac{\partial \rho}{\partial c}\right)' - \mu\,\left[\left(\frac{\partial p}{\partial c}\right)''\rho + p''\frac{\partial \rho}{\partial c} + \left(\frac{\partial p}{\partial c}\right)'\rho' + p'\left(\frac{\partial \rho}{\partial c}\right)'\right] \\ = \frac{\partial G}{\partial p}\,\frac{\partial p}{\partial c}\,\rho + G\,(p)\,\frac{\partial \rho}{\partial c} + \rho'. \end{aligned} \tag{7.30}$$

Using the fact that $p' = \dfrac{\partial p}{\partial \rho}\,\rho'$, we rewrite equations (7.50) and (7.51), respectively, as

$$-c\,(\rho')' - \mu\,\left[(p')''\,\rho + p''\rho' + (p')'\rho' + \frac{\partial p}{\partial \rho}\,\rho'\,(\rho')'\right] = \frac{\partial G}{\partial p}\,p'\,\rho + G\,(p)\;\rho' \tag{7.31}$$

and

$$\begin{aligned} -c\left(\frac{\partial \rho}{\partial c}\right)' - \mu\,\left[\left(\frac{\partial p}{\partial c}\right)''\rho + p''\frac{\partial \rho}{\partial c} + \left(\frac{\partial p}{\partial c}\right)'\rho' + \frac{\partial p}{\partial \rho}\,\rho'\,\left(\frac{\partial \rho}{\partial c}\right)'\right] \\ = \frac{\partial G}{\partial p}\,\frac{\partial p}{\partial c}\,\rho + G\,(p)\,\frac{\partial \rho}{\partial c} + \rho'. \end{aligned} \tag{7.32}$$

Since $\dfrac{\partial p}{\partial \rho} > 0$, we have

$$\rho' = p'\,\left(\frac{\partial p}{\partial \rho}\right)^{-1} \text{ and } \frac{\partial \rho}{\partial c} = \frac{\partial p}{\partial c}\,\left(\frac{\partial p}{\partial \rho}\right)^{-1}.$$

Hence, introducing the following definitions

$$k_0 = \left(\frac{\partial p}{\partial \rho}\right)^{-1}, \qquad k_1 = \rho, \qquad k_2 = p'' \left(\frac{\partial p}{\partial \rho}\right)^{-1}, \qquad k_3 = \rho',$$
$$k_4 = \rho' \frac{\partial p}{\partial \rho}, \qquad k_5 = \frac{\partial G}{\partial p}\,\rho + G\,(p) \left(\frac{\partial p}{\partial \rho}\right)^{-1},$$

along with the notations $f = p'$ and $g = \dfrac{\partial p}{\partial c}$, we rewrite equations (7.52) and (7.53), respectively, as

$$-c\,(k_0\,f)' - \mu\,\left[k_1\,f'' + k_2\,f + k_3\,f' + k_4\,(k_0\,f)'\right] = k_5\,f, \tag{7.33}$$

and

$$-c\,(k_0\,g)' - \mu\,\left[k_1\,g'' + k_2\,g + k_3\,g' + k_4\,(k_0\,g)'\right] = k_5\,g + \rho'. \tag{7.34}$$

Since

$$\rho'(z) \xrightarrow[z\to-\infty]{} 0, \quad p(z) \xrightarrow[z\to-\infty]{} P, \quad G(p(z)) \xrightarrow[z\to-\infty]{} 0,$$

Equation (7.24) gives

$$p''(z) \xrightarrow[z\to-\infty]{} 0.$$

Therefore, we impose the following asymptotic conditions

$$f(z) \xrightarrow[z\to-\infty]{} 0, \quad f'(z) \xrightarrow[z\to-\infty]{} 0. \tag{7.35}$$

Moreover, we have that

$$g(z) \xrightarrow[z\to-\infty]{} 0, \quad g'(z) \xrightarrow[z\to-\infty]{} 0. \tag{7.36}$$

Noting that $\rho' < 0$, we conclude that if g solves the problem defined by equa-

tion (7.56) complemented with the asymptotic conditions given by equation (7.57) and f solves the problem defined by equation (7.54) complemented with the asymptotic conditions given by equation (7.55), then $g < f$. This result together with the fact that $f = p' < 0$ demonstrates that $g = \dfrac{\partial p}{\partial c} < 0$, which concludes the proof of Theorem 1. □

We now turn to the travelling-wave analysis of the system of equations (7.7). We consider one-dimensional travelling-wave solutions of the form

$$\rho_1(t,x) = \rho_1(z) \quad \text{and} \quad \rho_2(t,x) = \rho_2(z), \quad \text{with} \quad z = x - ct \quad \text{and} \quad c > 0,$$

that satisfy the following conditions

$$\rho_1(z) \begin{cases} > 0, & \text{for } z < 0, \\ = 0, & \text{for } z \geq 0, \end{cases} \qquad \rho_2(z) \begin{cases} = 0, & \text{for } z < 0, \\ > 0, & \text{for } z \in [0, \ell), \\ = 0, & \text{for } z \geq \ell, \end{cases} \tag{7.37}$$

for some $\ell > 0$, along with the asymptotic condition

$$\rho_1(z) \xrightarrow[z \to -\infty]{} \Pi^{-1}(P). \tag{7.38}$$

Hence, we study the existence of triples (ρ_1, ρ_2, c) along with $\ell > 0$ that satisfy the problem defined by the following system of differential equations

$$\begin{cases} -c\,\rho_1' - \mu_1\,(\rho_1\,p')' = G(p)\rho_1, \\ -c\,\rho_2' - \mu_2\,(\rho_2\,p')' = 0, \end{cases} \tag{7.39}$$

complemented with the conditions given by equations (7.37) and (7.38). Notice that

the principle of mass conservation gives

$$\int_0^\ell \rho_2(z)\,\mathrm{d}z = N_2, \tag{7.40}$$

for some $N_2 > 0$ that represents the number of cells in population 2. Our main results are summarised by the following theorem.

Theorem 2. *Under the assumptions given by equations* (7.2) *and* (7.3)*, for any* $N_2 > 0$ *given, there exists* $c > 0$ *and* $\ell > 0$ *such that the system of equations* (7.39) *complemented with the conditions given by equations* (7.37) *and* (7.38) *admits a component-wise nonnegative solution* (ρ_1, ρ_2) *with* ρ_1 *nonincreasing, and* ρ_2 *nonincreasing and satisfying the condition given by equation* (7.40)*. Moreover, the pressure* p *has a "kink" at* $z = 0$ *with*

$$\operatorname{sgn}(p'(0^+) - p'(0^-)) = \operatorname{sgn}(\mu_2 - \mu_1). \tag{7.41}$$

Proof. Building upon the method of proof presented by Lorenzi et al. (2017) for the case of the barotropic relation given by equation (7.4), we prove Theorem 2 in five steps. We fix the parameter $c > 0$ and first prove that, for $N_2 > 0$ given, the problem under study admits a component-wise nonnegative solution (ρ_1, ρ_2) with ρ_2 nonincreasing and with the value of ℓ being determined by the condition given by equation (7.40) (Step 1), and with ρ_1 nonincreasing (Step 2). Then we prove that the pressure p is continuous on $(-\infty, \ell)$ (Step 3) and the jump condition given by equation (7.41) holds (Step 4). Finally, we show that there exists a unique value of the wave speed c that satisfies the travelling-wave problem (Step 5).

Step 1. Integrating the second equation in equation (7.39) between a generic point $z \in [0, \ell]$ and ∞, and using the fact that both $p'(z) \to 0$ and $\rho_2(z) \to 0$ as $z \to \infty$,

we find

$$p'(z) = -\frac{c}{\mu_2} < 0 \ \text{ for all } \ z \in [0, \ell]. \tag{7.42}$$

Integrating equation (7.42) between a generic point $z \in [0, \ell)$ and ℓ, and using the fact that $p(\ell) = 0$, gives

$$p(z) = \frac{c}{\mu_2} (\ell - z) \ \text{ for } \ z \in [0, \ell], \tag{7.43}$$

which implies that

$$p(0) = \frac{c\,\ell}{\mu_2}. \tag{7.44}$$

Since $\rho_1 \equiv 0$ on $[0, \ell]$, under the assumptions given by equation (7.3), we have that p is a monotonically decreasing function of ρ_2 in $[0, \ell]$. Hence, the results given by equations (7.42) and (7.43) allow us to conclude that ρ_2 is decreasing in $(0, \ell)$. Moreover, for $N_2 > 0$ given, since the value of $\rho_2(z)$ is uniquely determined for all $z \in [0, \ell]$, the value of ℓ is uniquely fixed by the integral identity given by equation (7.40).

Step 2. Since $\rho_2 \equiv 0$ on $(-\infty, 0)$ and, therefore, $\rho_1 \equiv \rho$ on $(-\infty, 0)$, multiplying both sides of the differential equation $(7.39)_1$ by $\dfrac{\mathrm{d}p}{\mathrm{d}\rho}$ we obtain the following boundary-value problem for p

$$-p' \ (c + \mu_1 \, p') - \mu_1 \, p'' \, \rho \, \frac{\mathrm{d}p}{\mathrm{d}\rho} = G \, (p) \, \rho \frac{\mathrm{d}p}{\mathrm{d}\rho}, \tag{7.45}$$

$$p(z) \xrightarrow[z \to -\infty]{} P \quad \text{and} \quad p(0) = \frac{c\,\ell}{\mu_2}. \tag{7.46}$$

Hence, using a method similar to that used in *Step 1* of the proof of Theorem 1 one can prove that ρ_1 is decreasing in $(-\infty, 0)$.

Step 3. The results proved in *Step 1* and *Step 2* guarantee that p is nonincreasing

and continuous in $(-\infty, 0)$ and in $(0, \ell)$. To show that p is continuous in $z = 0$, we add the two equations in equations (7.39) to obtain

$$-c\,(\rho_1 + \rho_2)' - [(\mu_1\rho_1 + \mu_2\rho_2)\; p']' = G(p)\rho_1. \tag{7.47}$$

Multiplying both sides of the above equation by p and using the fact that

$$p\;[(\mu_1\rho_1 + \mu_2\rho_2)\; p']' = [p\;(\mu_1\rho_1 + \mu_2\rho_2)\; p']' - (\mu_1\rho_1 + \mu_2\rho_2)\;(p')^2,$$

we achieve

$$(\mu_1\rho_1 + \mu_2\rho_2)\;(p')^2 = G(p)\rho_1 + c\,p\,(\rho_1 + \rho_2)' + [p\;(\mu_1\rho_1 + \mu_2\rho_2)\; p']'.$$

Integrating both sides of the latter equation between a generic point $z^* < 0$ and ℓ, and estimating the right-hand side from above by using the fact that $-\infty < (\rho_1 + \rho_2)'(z) \leq 0$ for all $z \in [z^*, \ell)$, $p(\ell) = 0$ and $\rho_2(z^*) = 0$, yields

$$\int_{z^*}^{\ell} (\mu_1\rho_1 + \mu_2\rho_2)\;(p')^2\,\mathrm{d}z \leq \int_{z^*}^{\ell} G(p)\rho_1\,\mathrm{d}z - \mu_1\,\rho_1(z^*)\,p(z^*)\,p'(z^*) < \infty.$$

Using the above integral inequality we find that $p' \in L^2_{loc}(\mathbb{R})$. This result together with the fact that $p \in L^\infty(\mathbb{R})$ allow us to conclude that p is continuous in $z = 0$. Since $p \equiv \Pi(\rho)$ and Π is a smooth monotonically increasing function of ρ, we have that the total cell density ρ is continuous in $z = 0$ as well.

Step 4. Integrating equation (7.47) between a generic point $z < \ell$ and ℓ and using the fact that $\rho_1(\ell) = \rho_2(\ell) = 0$ yields

$$c\,(\rho_1(z) + \rho_2(z)) + (\mu_1\rho_1(z) + \mu_2\rho_2(z))\; p'(z) = \int_z^{\ell} G(p)\rho_1\,\mathrm{d}z'.$$

Letting $z \to 0^-$ and using the fact that $\rho_1(0^-) = \rho(0^-)$ and $\rho_1 \equiv 0$ on $[0, \ell]$ we find that

$$c\,\rho(0^-) + \mu_1\,\rho(0^-)\,p'(0^-) = 0. \tag{7.48}$$

Similarly, letting $z \to 0^+$ and using the fact that $\rho_2(0^+) = \rho(0^+)$ and $\rho_1 \equiv 0$ on $[0, \ell]$ gives

$$c\,\rho(0^+) + \mu_2\,\rho(0^+)\,p'(0^+) = 0. \tag{7.49}$$

Since $\rho(z)$ is continuous in $z = 0$, combining equations (7.48) and (7.49) we obtain

$$\mu_1\,p'(0^-) = \mu_2\,p'(0^+) \quad \Longrightarrow \quad p'(0^-) = \frac{\mu_2}{\mu_1}\,p'(0^+).$$

This result along with the expression (7.42) for $p'(0^+)$ gives

$$p'(0^-) = -\frac{c}{\mu_1} \quad \text{and} \quad p'(0^+) - p'(0^-) = \frac{c}{\mu_1\,\mu_2}\,(\mu_2 - \mu_1)\,.$$

From the above equation, noting that $p'(0^+) < 0$, we deduce the condition given by equation (7.41).

Step 5. We prove that p is a monotonically decreasing function of the parameter c on $(-\infty, 0)$. This ensures that given the cell density ρ_1 the wave speed c can be uniquely identified through a monotonicity argument. Recalling that $\rho_2 \equiv 0$ on $(-\infty, 0)$ and, therefore, $\rho_1 \equiv \rho$ on $(-\infty, 0)$, differentiating equation $(7.39)_1$ with respect to z we find

$$-c\,(\rho')' - \mu_1\left[(p')''\,\rho + p''\,\rho' + (p')'\rho' + p'(\rho')'\right] = \frac{\mathrm{d}G}{\mathrm{d}p}\,p'\,\rho + G\,(p)\;\rho' \tag{7.50}$$

with

$$p'(z) \xrightarrow[z \to -\infty]{} 0 \quad \text{and} \quad p'(0) = -\frac{c}{\mu_1}.$$

On the other hand, differentiating equation $(7.39)_1$ with respect to c gives

$$\begin{aligned} -c\left(\frac{\partial\rho}{\partial c}\right)' - \mu_1\left[\left(\frac{\partial p}{\partial c}\right)''\rho + p''\frac{\partial\rho}{\partial c} + \left(\frac{\partial p}{\partial c}\right)'\rho' + p'\left(\frac{\partial\rho}{\partial c}\right)'\right] \\ = \frac{\mathrm{d}G}{\mathrm{d}p}\frac{\partial p}{\partial c}\rho + G(p)\frac{\partial\rho}{\partial c} + \rho' \end{aligned} \tag{7.51}$$

with

$$\frac{\partial p}{\partial c}(z) \xrightarrow[z\to-\infty]{} 0 \quad \text{and} \quad \left(\frac{\partial p}{\partial c}\right)'(0) = -\frac{1}{\mu_1}.$$

Using the fact that $p' = \dfrac{\mathrm{d}p}{\mathrm{d}\rho}\rho'$, we rewrite the differential equations (7.50) and (7.51), respectively, as

$$-c\,(\rho')' - \mu\left[(p')''\rho + p''\rho' + (p')'\rho' + \frac{\mathrm{d}p}{\mathrm{d}\rho}\rho'(\rho')'\right] = \frac{\mathrm{d}G}{\mathrm{d}p}p'\rho + G(p)\,\rho' \tag{7.52}$$

and

$$\begin{aligned} -c\left(\frac{\partial\rho}{\partial c}\right)' - \mu\left[\left(\frac{\partial p}{\partial c}\right)''\rho + p''\frac{\partial\rho}{\partial c} + \left(\frac{\partial p}{\partial c}\right)'\rho' + \frac{\partial p}{\partial\rho}\rho'\left(\frac{\partial\rho}{\partial c}\right)'\right] \\ = \frac{\mathrm{d}G}{\mathrm{d}p}\frac{\partial p}{\partial c}\rho + G(p)\frac{\partial\rho}{\partial c} + \rho'. \end{aligned} \tag{7.53}$$

Since $\dfrac{\mathrm{d}p}{\mathrm{d}\rho} > 0$, we have

$$\rho' = p'\left(\frac{\mathrm{d}p}{\mathrm{d}\rho}\right)^{-1} \text{ and } \frac{\partial\rho}{\partial c} = \frac{\partial p}{\partial c}\left(\frac{\mathrm{d}p}{\mathrm{d}\rho}\right)^{-1}.$$

Hence, introducing the notation $f = p'$, $g = \dfrac{\partial p}{\partial c}$ and

$$\begin{aligned} &k_0 = \left(\frac{\mathrm{d}p}{\mathrm{d}\rho}\right)^{-1}, \qquad k_1 = \rho, \qquad k_2 = p''\left(\frac{\mathrm{d}p}{\mathrm{d}\rho}\right)^{-1}, \qquad k_3 = \rho', \\ &k_4 = \rho'\frac{\mathrm{d}p}{\mathrm{d}\rho}, \qquad\qquad k_5 = \frac{\mathrm{d}G}{\mathrm{d}p}\rho + G(p)\left(\frac{\mathrm{d}p}{\mathrm{d}\rho}\right)^{-1}, \end{aligned}$$

we rewrite the differential equations (7.52) and (7.53), respectively, as

$$-c\,(k_0\,f)' - \mu\,\left[k_1\,f'' + k_2\,f + k_3\,f' + k_4\,(k_0\,f)'\right] = k_5\,f \tag{7.54}$$

with

$$f(z) \xrightarrow[z\to-\infty]{} 0, \quad f(0) = -\frac{c}{\mu_1} \tag{7.55}$$

and

$$-c\,(k_0\,g)' - \mu\,\left[k_1\,g'' + k_2\,g + k_3\,g' + k_4\,(k_0\,g)'\right] = k_5\,g + \rho' \tag{7.56}$$

with

$$g(z) \xrightarrow[z\to-\infty]{} 0, \quad g'(0) = -\frac{1}{\mu_1}. \tag{7.57}$$

Since $f(z) < 0$ for all $z \in (-\infty, 0)$ and $f'(0) < 0$, noting that both $f(z) \to 0$ and $g(z) \to 0$ as $z \to -\infty$ and the right-hand side of the differential equation (7.56) contains the additional term $\rho' < 0$ compared to the right-hand side of the differential equation (7.54), we deduce that $g = \dfrac{\partial p}{\partial c} < 0$, which concludes the proof of Theorem 2. □

Remark 2. *Based on the jump condition* (7.41)*, we expect the travelling-wave solution of Theorem 2 to be unstable if* $\mu_1 > \mu_2$*. In fact, a small perturbation of* $\rho_1(z)$ *that is greater than zero on* $[0, \ell)$ *will propagate with approximate speed* $-\mu_1\,p'(0^+)$*. Noting that when* $\mu_1 > \mu_2$ *the jump condition* (7.41) *gives* $-\mu_1\,p'(0^+) > -\mu_1\,p'(0^-)$*, we deduce that such a perturbation will separate from the rest of the travelling wave* $\rho_1(z)$*.*

7.5.2 Quantitative comparison between individual-based and continuum models

One cell population

We consider the computational simulation results of our individual-based model in the case of one cell population and compare them to numerical solutions of equation (7.1). To ensure consistency, we let $M = 1$ and drop the index h from the functions and from the parameters of the individual-based model. A complete description of the parameter choices and setup of numerical simulations is given in Appendix B.1.1 and Appendix B.2.1. In particular, we define the growth rate G as,

$$G(p) = \frac{1}{2\,\pi} \arctan(\beta\,(P - p)) \quad \text{with} \quad \beta > 0, \tag{7.58}$$

so that the assumptions given by equation (7.2) are satisfied.

Travelling fronts: Figure 7.2 demonstrates that there is an excellent quantitative match between the numerical solutions of equation (7.1) (dashed lines) and the computational simulation results of our individual-based model (solid lines). In agreement with the results established by Theorem 1, the cell density is nonincreasing and connects the homogeneous steady state $\rho \equiv \Pi^{-1}(P)$ to the homogeneous steady state $\rho \equiv 0$. Accordingly, the cell pressure is nonincreasing and connects the homogeneous steady state $p \equiv P$ to the homogeneous steady state $p \equiv 0$.

Higher values of β lead to higher speed of invasion: Figure 7.3 indicates that, as one would expect, increasing the value of the parameter β in the definition of the rate $G(p)$ given by equation (7.58) accelerates the growth of the cell population, thus leading to a faster speed of invasion.

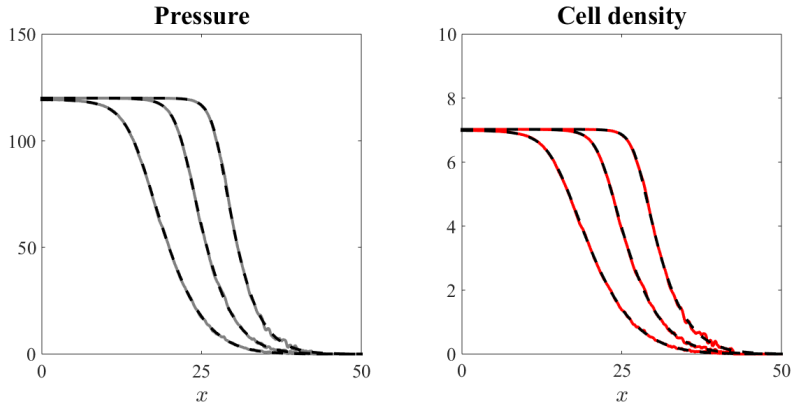

Figure 7.2: Travelling fronts. *Comparison between the computational simulation results of our individual-based model in the case of one population (solid lines) and the numerical solutions of the continuum model given by equation* (7.1) *(dashed lines). The left and right panel display, respectively, the pressure and the cell density at three successive time instants,* i.e. $t = 10$ *(left curves),* $t = 15$ *(middle curves) and* $t = 20$ *(right curves). Values of the pressure and the cell density are in units of* 10^4 *and were taken as an average from three runs of the simulations. Simulations were carried out using a definition for the pressure that satisfies the assumptions given by equation* (7.3)*. The definition of* $G(p)$ *is given by equation* (7.58)*, with the homeostatic pressure* $P = 120 \times 10^4$ *and the coefficient* $\beta = 4 \times 10^{-6}$*. A complete description of the numerical simulation setup is given in Appendix B.1.1 and Appendix B.2.1.*

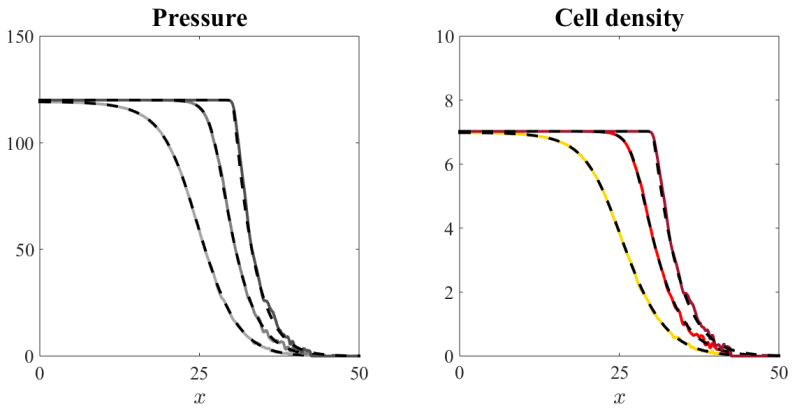

Figure 7.3: Higher values of β lead to higher speed of invasion *Comparison between the computational simulation results of our individual-based model in the case of one cell population (solid lines) and the numerical solutions of the continuum model given by equation* (7.1) *(dashed lines). The left and right panel display, respectively, the pressure and the cell density at the time instant* $t = 15$ *for increasing values of the parameter* β *in the definition of the rate* $G(p)$ *given by equation* (7.58), i.e. $\beta = 1.5 \times 10^{-6}$ *(light grey and yellow lines),* $\beta = 4 \times 10^{-6}$ *(middle grey and red lines) and* $\beta = 4 \times 10^{-5}$ *(dark grey and brown lines). Values of the pressure and the cell density are in units of* 10^4 *and were taken as an average from three runs of the simulations. Simulations were carried out with pressure defined in a way that satisfies the assumptions given by equation* (7.3) *with the homeostatic pressure* $P = 120 \times 10^4$*. A complete description of the numerical simulation setup is given in Appendix B.1.1 and Appendix B.2.1.*

Differences between the outcomes of individual-based and continuum models in the presence of sharp transitions from high to low cell densities: The results presented so far indicate that there is an excellent agreement between the computational simulation results of our individual-based model and the solutions of the corresponding continuum models. However, due to extinction phenomena related to stochasticity effects that occur in the individual-based model for low cell densities, we expect differences between the outcomes of the two modelling approaches to emerge in the presence of sharp transitions from high to low total cell densities. In order to verify this hypothesis, exploiting the asymptotic results of Perthame et al. (2014b), who have shown that under the barotropic relation given by equation (7.4) higher values of the parameter γ lead equation (7.1) to develop sharper invasion fronts, we compare the computational simulation results of our individual-based model in the case of one cell population with the numerical solutions of equation (7.1) under the barotropic relation given by equation (7.4) for increasing values of γ. A complete description of the setup of numerical simulations is given in Appendix B.1.1 and Appendix B.2.1. The results obtained are summarised by Figure 7.4 which shows that larger values of the parameter γ can bring about sharper invasion fronts, which come along with more abrupt variations in the cell density, thus leading to more evident differences between the computational simulation results of the stochastic individual-based model and the numerical solutions of equation (7.1) at the front of invasion. Ultimately, this causes the invasion front of the individual-based model to travel at the same speed but behind the front of the corresponding continuum model. This is further clarified in Figure B.1 in Appendix B, where we compare the PDE and IB models at four consecutive time-steps for the simulations with $\gamma = 2$ whose results are shown in Figure 7.4.

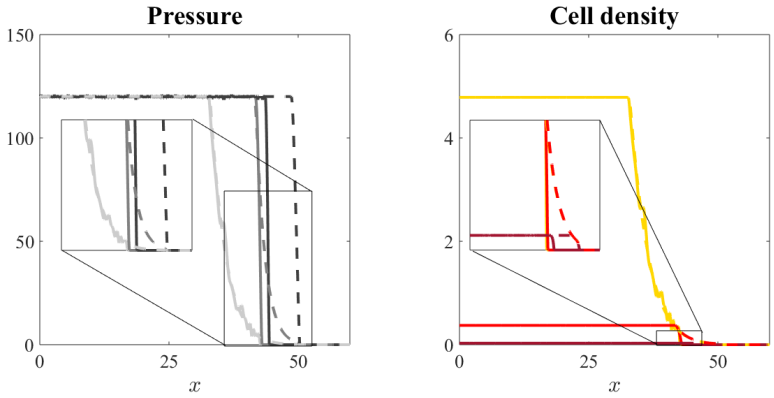

Figure 7.4: Differences in the outcomes of individual-based and continuum models in the presence of sharp transitions from high to low cell densities. *Comparison between the computational simulation results of our individual-based model in the case of one cell population (solid lines) and the numerical solutions of the continuum model given by equation* (7.1) *(dashed lines). The left and right panel display, respectively, the pressure and the cell density at the time instant* $t = 15$ *for increasing values of the parameter* γ *in the barotropic relation given by equation* (7.4), i.e. $\gamma = 1.2$ *(light grey and yellow lines),* $\gamma = 1.5$ *(middle grey and red lines) and* $\gamma = 2$ *(dark grey and brown lines). Values of the pressure and the cell density are in units of* 10^5*. Magnifications of the curves near the invasion fronts are shown in the insets. Simulations were carried out using the definition of* $G(p)$ *given by equation* (7.58)*, with the homeostatic pressure* $P = 120 \times 10^5$ *and the coefficient* $\beta = 4 \times 10^{-5}$*. A complete description of the numerical simulation setup is given in Appendix B.1.1 and Appendix B.2.1.*

Two cell populations

We now turn to the case of two cell populations and we compare computational simulation results of our individual-based model with numerical solutions of the system of equations (7.7). For consistency, we choose $M = 2$, and we set $G_1 \equiv G$ and $G_2 \equiv 0$ in the individual-based model. Full details of the setup of numerical simulations can be found in Appendix B.1.2 and Appendix B.2.2 (for the results reported in Figures 7.5 and 7.6), and Appendix B.1.3 and Appendix B.2.3 (for the results reported in Figures 7.7 and 7.8). In particular, we use the definition of the rate $G(p)$ given by equation (7.58) with the homeostatic pressure $P = 10 \times 10^4$ and we let the population of nonproliferating cells, *i.e.* population 2, be ahead of the population of proliferating cells, *i.e.* population 1, at the initial time $t = 0$.

Figures 7.5 and 7.6 demonstrate that there is an excellent quantitative match between the numerical solutions of the system of equations (7.7) (dashed lines) and the computational simulation results of our individual-based model (solid lines), both in the case where $\mu_1 \leq \mu_2$ and when $\mu_1 > \mu_2$. In both cases, the number of nonproliferating cells, *i.e.* the integral of the cell density ρ_2, is conserved. Over time, the pressure p converges to the homeostatic pressure P while the cell density ρ_1 converges to the corresponding value $\Pi^{-1}(P)$.

Travelling fronts and spatial segregation between the two cell populations: If $\mu_1 \leq \mu_2$, *i.e.* if $\nu_1 \leq \nu_2$, in agreement with the results established by Theorem 2, spatial segregation occurs and the two cell populations remain separated by a sharp interface - see Figure 7.5. The population of nonproliferating cells stays ahead of the population of proliferating cells and, over the regions where they are greater than zero, the cell densities are nonincreasing. The pressure itself is continuous across the interface between the two cell populations, whereas its first derivative jumps from a

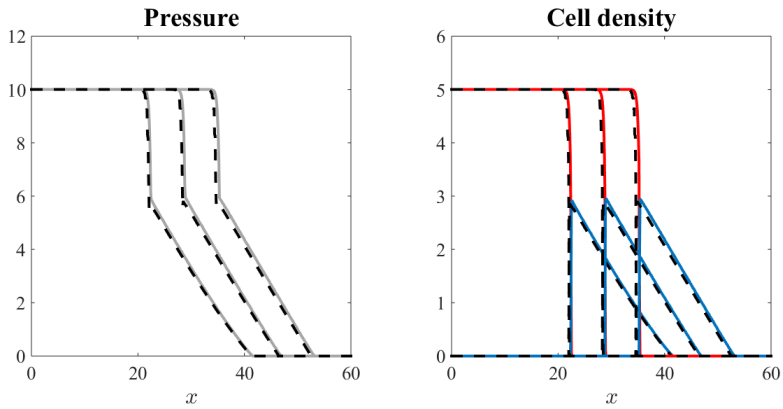

Figure 7.5: Travelling fronts and spatial segregation between the two cell populations. *Comparison between the computational simulation results of our individual-based model in the case of two cell populations (solid lines) and the numerical solutions of the continuum model given by the system of equations* (7.7) *(dashed lines), for* $\mu_1 \leq \mu_2$, i.e. $\nu_1 \leq \nu_2$. *The left and right panel display, respectively, the pressure and the cell densities of population 1 (red lines) and population 2 (blue lines) at three successive time instants,* i.e. $t = 300$ *(left curves),* $t = 450$ *(middle curves) and* $t = 600$ *(right curves). Values of the pressure and the cell densities are in units of* 10^4. *Simulations were carried out using a barotropic relation that satisfies the assumptions given by equation* (7.3) *and the definition of* $G(p)$ *given by equation* (7.58)*, with the homeostatic pressure* $P = 10 \times 10^4$ *and the coefficient* $\beta = 4 \times 10^{-5}$. *A complete description of the numerical simulation setup is given in Appendix B.1.2 and Appendix B.2.2.*

lower negative value to a larger negative value, *i.e.* the sign of the jump coincides with $\text{sgn}(\mu_2 - \mu_1)$ - see the jump condition given by equation (7.41).

Mixing between the two cell populations: If $\mu_1 > \mu_2$, *i.e.* if $\nu_1 > \nu_2$, the cell population 2 is left behind by the cell population 1, which ultimately propagates alone - see Figure 7.6. This is consistent with the heuristic argument provided in Remark 2, which suggests that the travelling-wave solutions of Theorem 2 are unstable in the case where $\mu_1 > \mu_2$.

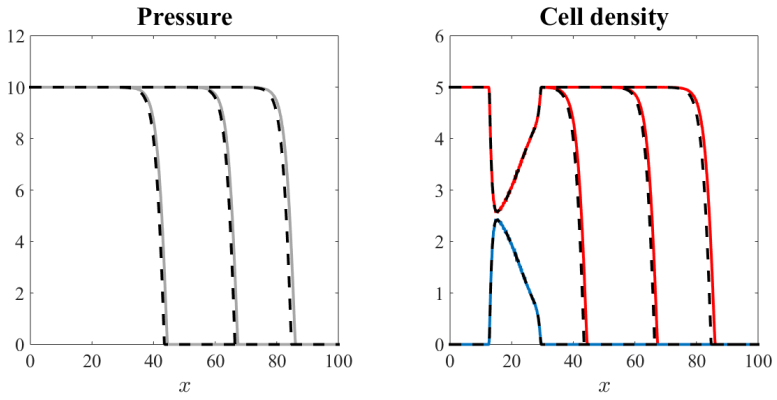

Figure 7.6: Mixing between the two cell populations. *Comparison between the computational simulation results of our individual-based model in the case of two cell populations (solid lines) and the numerical solutions of the continuum model given by the system of equations* (7.7) *(dashed lines), for* $\mu_1 > \mu_2$, i.e. $\nu_1 > \nu_2$. *The left and right panel display, respectively, the pressure and the cell densities of population 1 (red lines) and population 2 (blue lines) at three successive time instants,* i.e. $t = 100$ *(left curves),* $t = 150$ *(middle curves) and* $t = 190$ *(right curves). Values of the pressure and the cell densities are in units of* 10^4. *Simulations were carried out using a barotropic relation that satisfies the assumptions given by equation* (7.3) *and the definition of* $G(p)$ *given by equation* (7.58), *with the homeostatic pressure* $P = 10 \times 10^4$ *and the coefficient* $\beta = 4 \times 10^{-5}$. *A complete description of the numerical simulation setup is given in Appendix B.1.2 and Appendix B.2.2.*

Numerical simulations for more realistic barotropic relations for the definition of the pressure: In this chapter, so far we have focused on barotropic relations defining the local pressure, which satisfy the assumptions given by equation (7.3). However, as mentioned earlier in Section 7.1, more realistic barotropic relations satisfy the following conditions

$$\Pi(\rho) = 0 \ \text{ for } \ \rho \in [0, \rho^*) \quad \text{and} \quad \frac{\partial \Pi}{\partial \rho} > 0 \ \text{ for } \ \rho > \rho^*, \tag{7.59}$$

with $0 < \rho^* < \Pi^{-1}(P)$. Figures 7.7 and 7.8 display the computational simulation results of our stochastic individual-based model and the numerical solutions of the system of equations (7.7) obtained under a barotropic relation that satisfies the more general assumptions given by equation (7.59) - see Appendix B.1.3 and Appendix B.2.3 for a complete description of the numerical simulation setup. These computational results and numerical solutions clearly share the same properties as those of Figures 7.5 and 7.6. This supports the conclusion that the essentials of the results obtained using barotropic relations of the form given by equation (7.3) remain intact even under the more realistic assumptions given by equation (7.59).

7.6 Concluding remarks and discussion

In this chapter, we have developed a simple, yet effective, stochastic individual-based (IB) model for the spatial dynamics of multicellular systems whereby cells undergo pressure-driven movement and pressure-limited population growth. From the construction of our simple IB model, nonlinear partial differential equations (PDEs) commonly used to model the spatial dynamics of growing cell populations can be formally derived. Through comparison of both models we find that the results of

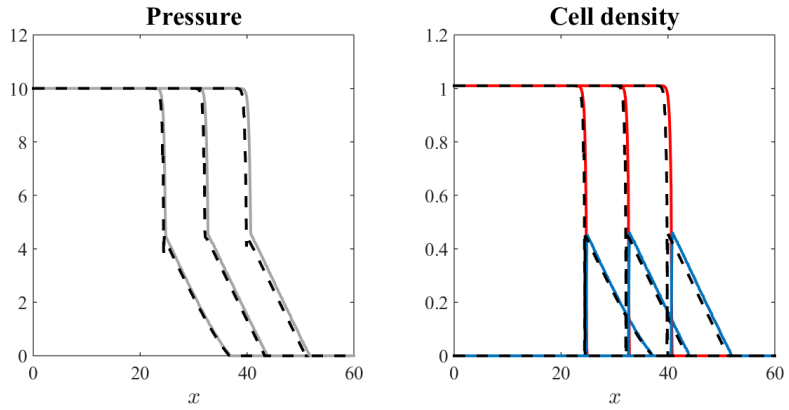

Figure 7.7: Numerical simulations for more realistic barotropic relations. *Comparison between the computational simulation results of our individual-based model in the case of two cell populations (solid lines) and the numerical solutions of the continuum model given by the system of equations* (7.7) *(dashed lines), for* $\mu_1 \leq \mu_2$, i.e. $\nu_1 \leq \nu_2$. *The left and right panel display, respectively, the pressure and the cell densities of population 1 (red lines) and population 2 (blue lines) at three successive time instants,* i.e. $t = 300$ *(left curves),* $t = 450$ *(middle curves) and* $t = 600$ *(right curves). Values of the pressure and the cell densities are in units of* 10^4. *Simulations were carried out using a barotropic relation that satisfies the assumptions given by equation* (7.59) *and the definition of* $G(p)$ *given by equation* (7.58) *with the homeostatic pressure* $P = 10 \times 10^4$ *and the coefficient* $\beta = 4 \times 10^{-5}$. *A complete description of the numerical simulation setup is given in Appendix B.1.3 and Appendix B.2.3.*

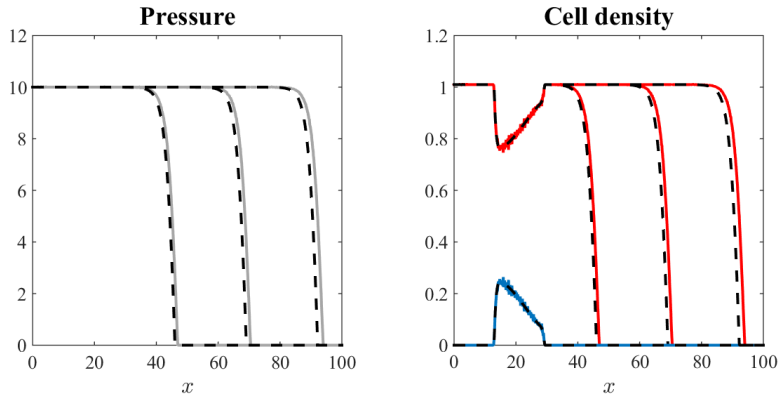

Figure 7.8: Numerical simulations for more realistic barotropic relations. *Comparison between the computational simulation results of our individual-based model in the case of two cell populations (solid lines) and the numerical solutions of the continuum model given by the system of equations* (7.7) *(dashed lines), for* $\mu_1 > \mu_2$, i.e. $\nu_1 > \nu_2$. *The left and right panel display, respectively, the pressure and the cell densities of population 1 (red lines) and population 2 (blue lines) at three successive time instants,* i.e. $t = 100$ *(left curves),* $t = 150$ *(middle curves) and* $t = 200$ *(right curves). Values of the pressure and the cell densities are in units of* 10^4. *Simulations were carried out using a barotropic relation that satisfies the assumptions given by equation* (7.59) *and the definition of* $G(p)$ *given by equation* (7.58) *with the homeostatic pressure* $P = 10 \times 10^4$ *and the coefficient* $\beta = 4 \times 10^{-5}$. *A complete description of the numerical simulation setup is given in Appendix B.1.3 and Appendix B.2.3.*

computational simulations of the individual-based model faithfully mirror the qualitative and quantitative properties of the solutions to the corresponding nonlinear PDEs. This highlights the fact that simple IB models can lead to the emergence of complex spatial patterns of population growth observed in continuum models, *e.g.* travelling waves with composite shapes and sharp interfaces corresponding to spatial segregation between cell populations with different biophysical properties. Although the models described in this chapter have been general in nature, they could be adapted to biologically represent situations of tumour cell growth and invasion into healthy tissue. This could be done by considering the cancer cells as the proliferating cell population and normal healthy tissue to be the nonproliferating cell population. Other possible scenarios such as wound healing and embryonic development are also envisaged.

Chapter 8

Conclusions and potential future directions

In the past decade, the advancement in cell imaging techniques has allowed for insight into the mechanisms that underpin the immune response to solid tumours. Understanding these mechanisms of tumour removal by immune cells, and how tumours can evade this response, has promoted the development of immunotherapy techniques. However, the development of new cancer treatments can be time consuming and expensive. Through the use of mathematical models potential therapy techniques may be tested in a timely and inexpensive manner. In this thesis, we have developed mathematical models to describe tumour-immune competition with the aim to investigate the biological settings which allow for successful immune action.

We began this thesis by describing the key biological processes and mechanisms which have been discovered by experimentalists, historically and in recent years. In particular, we focused on the role of two immune cell types: dendritic cells (DCs) and cytotoxic T lymphocytes (CTLs), where DCs can collect protein antigens from cancer cells and present them to naive CTLs to allow for CTL activation. The CTLs

can then actively target and destroy tumour cells which express the targeted protein antigen. Along with a description of this immune response to cancer, we considered ways in which tumours can evade the immune response and current immunotherapy techniques used to try and restore these processes.

Mathematical modelling techniques have been used extensively in the past to describe cell motion, tumour development and tumour-immune competition. We provided a short review of these techniques and their applications, with a focus on discrete individual-based (IB) models and continuous partial differential equation (PDE) models.

Recent advances in cell imaging technology have allowed for the single cell tracking of immune cells in the tumour microenvironment. In particular, experimental works have highlighted that CTLs, and DCs alter their migration patterns upon exposure to tumour antigens. To describe these movement patterns, mathematically, we have developed a simple individual-based model of immune cell motion using two random walk methods based on a 2D lattice. We chose a Lévy walk to replicate the movement of inactive immune cells, where they can travel in one direction for an extended period of time before choosing a new one. Additionally, for the active immune cells we considered Brownian motion, where at each time instant the cell could move to any neighbouring grid position with equal probability. Results from our computational simulations were able to reproduce qualitatively the spatial trajectories of immune cells observed in the experimental data of single cell tracking. Looking to the future, the T cell experiments completed in Boissonnas et al. (2007) consider cell movement in the z direction as well as x and y directions and therefore it may be appropriate to consider the model in three dimensions. The effects of changing the spatial domain from 2D to 3D on the two forms of random walks, Brownian motion and Lévy walks, would need to be considered. It is probable that

the change of dimension would alter the time it takes for cells moving via either walk to reach their target cells. However the general properties of each walk and their benefits in comparison to each other should be maintained (Bartumeus et al., 2014; Detcheverry, 2017; Wosniack et al., 2017).

Using the modelling strategies to describe immune cell motion, we then developed a spatially stochastic individual-based model describing the spatio-temporal interactions between DCs, CTLs and tumour cells. We included the effects of tumour recognition, immune activation, tumour growth and tumour destruction by the immune system. Simulations of the model were run for the 2D case and parameter settings of potential interest were investigated. The model results suggested that a high density of CTLs within the tumour microenvironment would be beneficial to tumour removal. However increased numbers of DCs could lead to an overcrowding effect. Furthermore, the results of our model highlighted that situations of enhance tumour growth could be control if CTLs had a strong capability of removing tumour cells. However, the model also suggested that altering the activation rate of both immune cells types or the exhaustion rate of the immune cells would not significantly alter the outcome of tumour-immune competition, and therefore are not viable targets for immunotherapy techniques. Immune cell exhaustion was also considered where the immune cells were limited in the number of cells that they could interact with. The results of the model suggested that as long as this limit was not small, *e.g.* an exhaustion limit ≥ 10 cells, then the outcomes of tumour-immune competition would be similar to those where there was no exhaustion limit. The effect of using the switch in cell motion suggested in Chapter 4 was also investigated and it was found that using this switch led to a faster tumour removal time than if Brownian motion was used to describe the motion of all cell types. In this individual-based model, for simplicity, it was assumed that the tumour was homogeneous, *i.e.* all

tumour cells expressed the same tumour antigens. However, tumours can be heterogeneous, where each cell may have a unique antigen profile.

To investigate this further, we extended the individual-based model to include the effects of heterogeneity within and between tumour cells. Each tumour cell was characterised by an antigen profile, which described the expression levels of the eleven MAGE antigens expressed by the cell. Initially, the antigen profiles of tumour cells were dependent on the total level of heterogeneity within the tumour. The antigen profile of each cell was additionally allowed to vary over time due to the occurrence of epimutations. The antigen expression of each tumour cell subsequently shaped the cellular immune response, and ultimately determined the receptors produced by the CTLs. Successful destruction of tumour cells by the CTLs then depended on the level of antigen expressed by the tumour cell corresponding to the CTL's T cell receptor. Once again, simulations of the model were run for the 2D case and parameter settings of potential interest were investigated. Computational simulations of this model clarified the conditions for the emergence of tumour clearance, dormancy or escape, and allowed us to assess the impact of antigenic heterogeneity of cancer cells on the efficacy of immune action. The model results also suggested that a diverse T cell population, where multiple antigen receptors are produced, would be advantageous in removal of the tumour. Furthermore, the model results indicated that increasing the frequency of epimutations may be a beneficial approach to treat cancer.

Ultimately, the results from both tumour-immune individual-based models highlighted the complex interplay between spatial interactions and adaptive mechanisms that underpin the immune response against solid tumours, and suggests how this may be exploited to further develop cancer immunotherapies. Looking to the future, these individual-based models could be extended further by considering the

effects of division and decay of the immune cells types or through describing processes where tumour cells directly attack the lymphocytes. Normally Fas ligand from the lymphocyte binds to the Fas receptor on the tumour cell surface, they aggregate to form a Fas associated death domain which activates a caspase cascade resulting in apoptosis of the tumour cell (Hersey and Zhang, 2001). However, tumour cells can also produce FasL and activate apoptosis of the CTLs through their Fas receptors (Stewart and Abrams, 2008). Furthermore, we have only described tumour-immune competition in 2D, and therefore extending the model into 3D could bring further understanding of the biological mechanisms underpinning the immune response to solid tumours and the phenomena observed in the 2D model, such as overcrowding.

As mentioned previously, individual-based models can be limited by their lack of amenability to mathematical analysis techniques. To overcome this we aim to derive the continuum counterparts of the individual-based models described previously. However, due to the inclusion of a Lévy walk and other complex mechanisms, we considered a simpler biological situation. We developed an individual-based model describing a cell population, where cells were able to undergo pressure-driven movement and pressure-dependent proliferation. From the discrete random branching walk that underlies the individual-based model we formally derived nonlinear partial differential equations which have been commonly used to model the spatial dynamics of growing cell populations. We subsequently carried out a systematic comparison between the individual-based model and its continuum counterparts, both in the case of one single cell population and in the case of multiple cell populations with different biophysical properties. The outcomes of our comparative study demonstrated that the results of computational simulations of the individual-based model we able to faithfully mirror the qualitative and quantitative properties of the

solutions to the corresponding nonlinear partial differential equations. This is of potential use when working on biologically motivated models, as the individual-based approach may be easier to describe to biologists and other nonmathematicians, however through the continuum model a level of mathematical analysis can be retained. Ultimately, these results illustrated how the simple rules governing the dynamics of single cells in our individual-based model can lead to the emergence of complex spatial patterns of population growth observed in continuum models. Similar methods could be used in the future to derive the corresponding continuum models of more complex individual-based models, such as those we have developed to describe tumour-immune competition. In this regard, many previous continuous models have been used to describe Lévy flights. However, in the case of Lévy walks there is a gap in the literature and this form of random walk is not well described in the context of systems of equations.

Our cell population migration and growth model could be extended into higher dimensions or used to describe biological situations such as cancer invasion. In this regard, it would be interesting to use our stochastic individual-based model to further investigate the formation of finger-like patterns of invasion observed for the two population system of PDEs posed on a two dimensional spatial domain (Lorenzi et al., 2017). Such spatial patterns resemble infiltrating patterns of cancer-cell invasion commonly observed in breast tumours (Wang et al., 2012). An additional development of our study would be to compare the results presented here with those obtained from equivalent models defined on irregular (non-uniform) lattices, as well as to investigate how our modelling approach could be related to off-lattice models of growing cell populations (Drasdo, 2005; Motsch and Peurichard, 2018; Van Liedekerke et al., 2015). Cell population models have also be used to consider other modes of cell migration, for example chemotaxis, whereby cells follow

a chemical signal. The continuum limit of stochastic chemotactic models has been considered (Erban and Othmer, 2004; Stevens, 2000) and in a similar way our model could be adapted to consider chemotaxis, whereby cells move up the chemoattractant gradient, rather than down the pressure gradient.

Appendix A

Appendix for Chapter 5

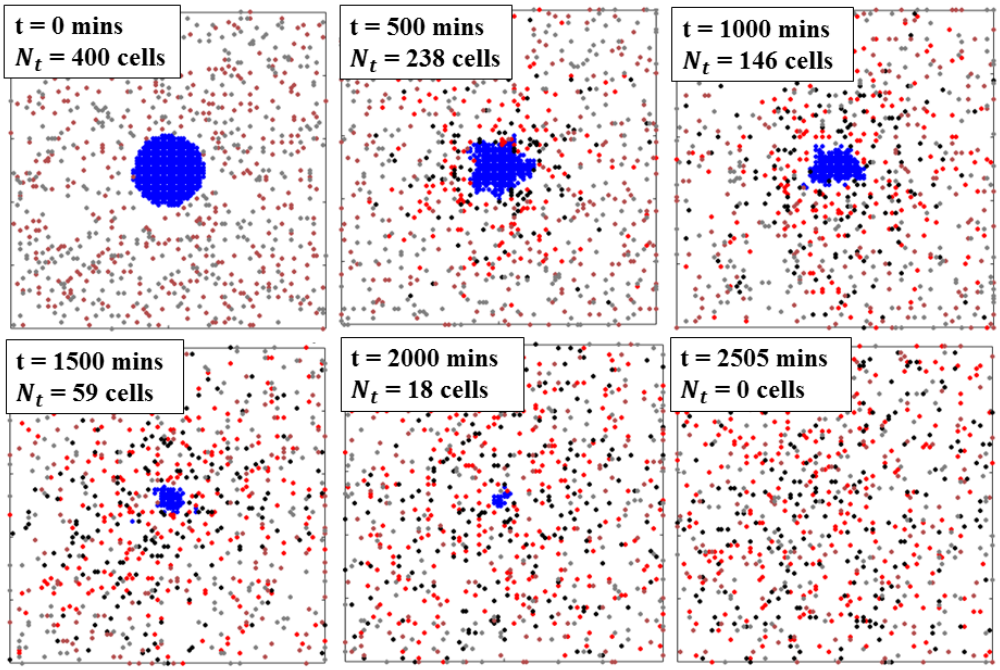

Figure A.1: Example of spatial distributions of cells over time for a case of tumour elimination. *Initially, the simulations begin with 400 tumour cells (blue) situated in the centre of the domain surrounded by inactive cytotoxic T lymphocytes, CTLS, (pink) and inactive dendritic cells, DCs, (grey). Throughout the simulations the DCs and CTLs can become activated (black and red, respectively) and interact with tumour cells. In the parameter setting used here the tumour cell number reduces until all cells are removed from the system at time* $t = 2505$*. For this simulation we use the parameter values given in Table 5.2 with an exhaustion limit of 5 cells.*

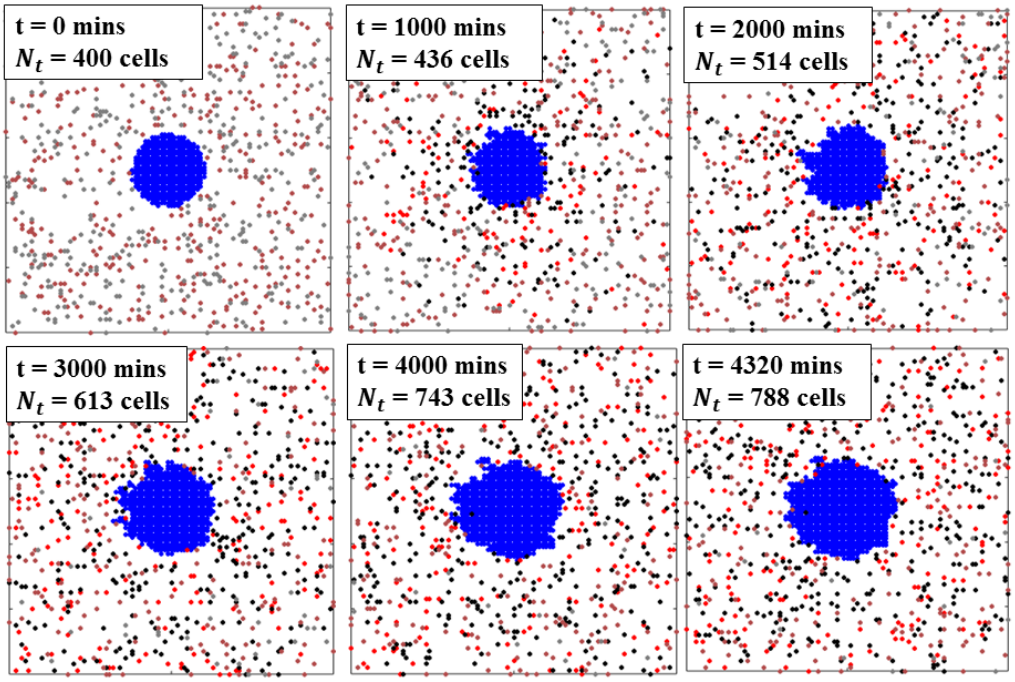

Figure A.2: Example of spatial distributions of cells over time for a case of tumour persistence. *Initially, the simulations begin with 400 tumour cells (blue) situated in the centre of the domain surrounded by inactive cytotoxic T lymphocytes, CTLS, (pink) and inactive dendritic cells, DCs, (grey). Throughout the simulations the DCs and CTLs can become activated (black and red, respectively) and interact with tumour cells. In the parameter setting used here the tumour cell number increases over the simulation time and the tumour increases in size. For this simulation we use the parameter values given in Table 5.2 with an exhaustion limit of 1 cell.*

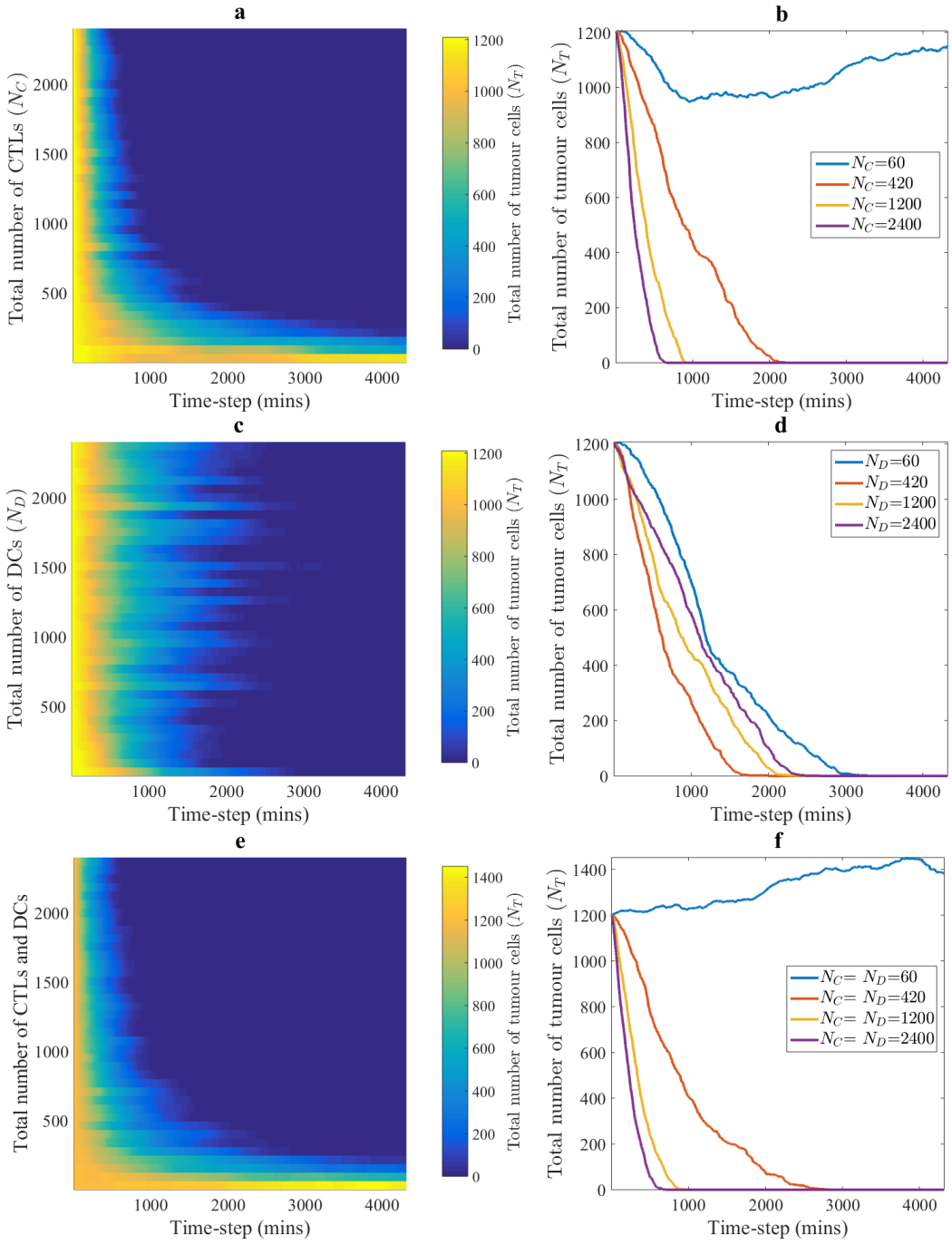

Figure A.3: Increasing the number of DCs can lead to longer tumour removal times. *The heat maps show the evolution of the tumour cell number over time for each given value of N_C and/or N_D (left panels). We select four simulation results for cell numbers, of* 60, 420, 1200 *and* 2400 *cells, and compare the tumour cell number over time for each parameter setting (right panels). In each case, we begin the simulations with* 1200 *tumour cells and test for varying values of:* ***a,b*** *N_C only,* ***c,d*** *N_D only and* ***e,f*** *N_C and N_D. All values were averaged over three simulation runs.*

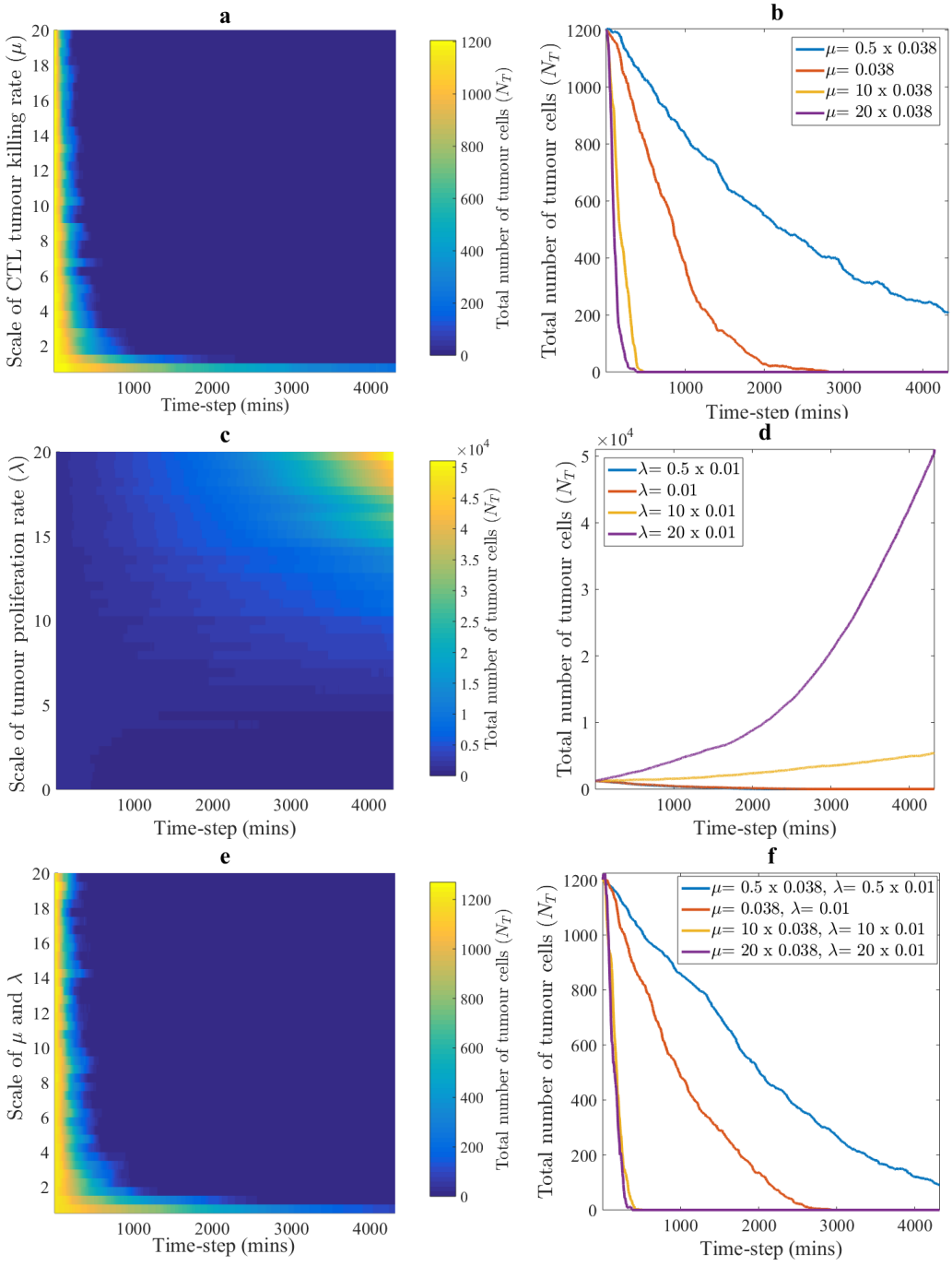

Figure A.4: The ratio between the removal rate of tumour cells by CTLs and the tumour cell division rate is a crucial parameter in tumour removal. *The heat maps show the evolution of the tumour cell number over time for each given value of μ and/or λ (left panels). We select four values of μ and/or λ and compare the tumour cell number over time for each parameter setting (right panels). In each case, we begin the simulations with 1200 tumour cells and test for varying values of:* ***a,b*** *μ only,* ***c,d*** *λ only and* ***e,f*** *μ and λ. All values were averaged over three simulation runs*

Appendix B

Appendix for Chapter 7

B.1 Details of numerical simulations of the individual-based model

We use a uniform discretisation of the interval $[0, 100]$ that consists of 1001 points as the spatial domain, *i.e.* the grid-step is $\chi = 0.1$, and we choose the time-step $\tau = 2 \times 10^{-3}$. We implement zero-flux boundary conditions to prevent cells from moving out of the spatial domain. For all simulations, we use the definition of the rate G given by equation (7.44) and we perform numerical computations in MATLAB. Further details for each specific situation considered are provided in the next subsections.

B.1.1 Setup of numerical simulations for the case of one cell population

For consistency with equation (7.1), we set $M = 1$ and we drop the index $h = 1$ both from the functions and from the parameters of the individual-based model.

We define the rate G in equations (7.9)-(7.11) according to equation (7.44). We set the homeostatic pressure $P = 120 \times 10^4$ for the simulation results reported in Figure 7.2 and Figure 7.3, while we choose $P = 120 \times 10^5$ for the simulation results of Figure 7.4. Moreover, we choose $\beta = 4 \times 10^{-6}$ for the simulation results reported in Figure 7.2, $\beta = 4 \times 10^{-5}$ for the simulation results of Figure 7.4, and $\beta \in \{1.5 \times 10^{-6}, 4 \times 10^{-6}, 4 \times 10^{-5}\}$ for the simulation results of Figure 7.3. We set $\nu = 0.02$ in equations (7.13)-(7.15) and we define the pressure p_i^k according to the following barotropic relation

$$\Pi(\rho_i^k) = K_\gamma \, (\rho_i^k)^\gamma \quad \text{with} \quad K_\gamma = \frac{\gamma + 1}{\gamma} \quad \text{and} \quad \gamma > 1,$$

which satisfies the conditions given by equation (7.2). We let $\gamma \in \{1.2, 1.5, 2\}$ for the simulation results of Figure 7.4, while we choose $\gamma = 1.2$ for the simulation results reported in Figure 7.2 and Figure 7.3. We impose compact support by using the initial cell density

$$\rho_i^0 = \begin{cases} A \, \exp\left(-b \, x_i^2\right) \text{ for } x_i \leq 50 \\ 0 \text{ for } x_i > 50 \end{cases} \quad \text{with} \quad A = 2 \times 10^4 \quad \text{and} \quad b = 4 \times 10^{-3}.$$

The results presented in Figure 7.2 and Figure 7.3 correspond to the average over three simulations of our individual-based model, while the results in Figure 7.4 correspond to one single simulation when $\gamma = 1.5$ or $\gamma = 2$ and the average over two simulations when $\gamma = 1.2$.

B.1.2 Setup of numerical simulations for the case of two cell populations

For consistency with the system of equations (7.7), we choose $M = 2$, and we set $G_1 \equiv G$ and $G_2 \equiv 0$ in equations (7.9)-(7.11), where G is defined according to equation (7.44) with the homeostatic pressure $P = 10 \times 10^4$ and the factor $\beta = 4 \times 10^{-5}$. We set $\nu_1 = 0.01$ and $\nu_2 = 0.5$ in equations (7.13)-(7.15) for the simulation results reported in Figure 7.5, while we consider $\nu_1 = 0.5$ and $\nu_2 = 0.01$ for the simulation results of Figure 7.6. We define the pressure p_i^k according to the following simplified barotropic relation

$$\Pi(\rho_i^k) = K\,\rho_i^k \quad \text{with} \quad K = 2,$$

which satisfies the conditions given by equation (7.2). Here, we choose $\gamma = 1$ as the results displayed in Section 7.5.2 and Figure 7.4 highlight that for large γ there can be disagreement between the discrete and continuum models. We make use of the initial cell densities

$$\rho_{1i}^0 = A_1 \exp\left(-b_1\, x_i^2\right) \quad \text{and} \quad \rho_{2i}^0 = \begin{cases} 0, & \text{for } x_i \leq 13, \\ A_2 \exp\left(-b_2 (x_i - 14)^2\right), & \text{for } x_i \in (13, 29), \\ 0, & \text{for } x_i \geq 29, \end{cases} \tag{B.1}$$

where

$$A_1 = 1.25 \times 10^4, \quad b_1 = 0.06, \quad A_2 = 2.5 \times 10^4 \quad \text{and} \quad b_2 = 6 \times 10^{-3}.$$

The results presented in Figure 7.5 and Figure 7.6 correspond to one single simulation of our individual-based model.

B.1.3 Setup of numerical simulations for the case of two populations with a redefined pressure function

For consistency with the system of equations (7.7), we choose $M = 2$, and we set $G_1 \equiv G$ and $G_2 \equiv 0$ in equations (7.9)-(7.11), where G is defined according to equation (7.44) with the homeostatic pressure $P = 10 \times 10^4$ and the factor $\beta = 4 \times 10^{-5}$. We set $\nu_1 = 0.01$ and $\nu_2 = 0.5$ in equations (7.13)-(7.15) for the simulation results reported in Figure 7.7, while we consider $\nu_1 = 0.5$ and $\nu_2 = 0.01$ for the simulation results of Figure 7.8. We define the pressure p_i^k according to the following barotropic relation

$$\Pi(\rho_i^k) = q\,(\rho_i^k - \rho^*)_+ \quad \text{where} \quad q = 10 \quad \text{and} \quad \rho^* = r\,P \;\; \text{with} \;\; r = 10^{-3},$$

which satisfies the conditions given by equation (7.45). We choose this definition of the pressure function as we now only depend on a linear function of the cell density which may be a more biologically realistic description of cellular pressure. We make use of the initial cell densities given by equation (B.1) with

$$A_1 = 12.5 \times 10^4, \quad b_1 = 0.06, \quad A_2 = 25 \times 10^4 \quad \text{and} \quad b_2 = 6 \times 10^{-3}.$$

The results presented in Figure 7.8 and Figure 7.7 correspond to one single simulation of our individual-based model.

B.2 Details of numerical simulations of the continuum models

We let $x \in [0, 100]$ and we construct numerical solutions for equation (7.1) and for the system of equations (7.7) complemented with zero Neumann boundary conditions. We use a finite volume method based on a time-splitting between the conservative and nonconservative parts. For the conservative parts, transport terms are approximated through an upwind scheme whereby the cell edge states are calculated by means of a high-order extrapolation procedure (LeVeque, 2002), while the forward Euler method is used to approximate the nonconservative parts. We consider a uniform discretisation of the interval $[0, 100]$ that consists of 1001 points and we perform numerical computations in MATLAB. For all simulations, we use the definition of the rate G given by equation (7.44). Further details for each specific situation considered are provided in the next subsections.

B.2.1 Setup of numerical simulations for the case of one cell population

The rate G is defined according to equation (7.44) with the homeostatic pressure $P = 120 \times 10^4$ for the numerical solutions reported in Figure 7.2 and Figure 7.3, while we choose $P = 120 \times 10^5$ for the numerical solutions of Figure 7.4. Moreover, we choose $\beta = 4 \times 10^{-6}$ for the numerical solutions reported in Figure 7.2, $\beta = 4 \times 10^{-5}$ for the numerical solutions of Figure 7.4, and $\beta \in \{1.5 \times 10^{-6}, 4 \times 10^{-6}, 4 \times 10^{-5}\}$ for the numerical solutions reported in Figure 7.3. We define the pressure p according

to the following barotropic relation

$$\Pi(\rho) = K_\gamma \, \rho^\gamma \quad \text{with} \quad K_\gamma = \frac{\gamma + 1}{\gamma} \quad \text{and} \quad \gamma > 1,$$

which satisfies the conditions given by equation (7.2). We let $\gamma \in \{1.2, 1.5, 2\}$ for the numerical solutions of Figure 7.4, while we choose $\gamma = 1.2$ for the numerical solutions reported in Figure 7.2 and Figure 7.3. Given the parameter values used for the individual-based model in the case of one single cell population, we choose the mobility $\mu = 4.166 \times 10^{-7}$ for the numerical solutions reported in Figure 7.2 and Figure 7.3, while we set $\mu = 4.166 \times 10^{-8}$ for the numerical solutions of Figure 7.4. In this way, both values of μ satisfy the condition given by equation (7.21) for $h = 1$. We impose the initial condition

$$\rho(0, x) = \begin{cases} A \, \exp\left(-b \, x^2\right) \text{ for } x \geq 50 \\ 0 \text{ for } x < 50 \end{cases} \qquad \text{with} \quad A = 2 \times 10^4 \quad \text{and} \quad b = 4 \times 10^{-3}.$$

B.2.2 Setup of numerical simulations for the case of two populations

The rate G is defined according to equation (7.44) with the homeostatic pressure $P = 10 \times 10^4$ and $\beta = 4 \times 10^{-5}$. Given the parameter values used for the individual-based model in the case of two cell populations, we choose the mobilities $\mu_1 = 2.5 \times 10^{-7}$ and $\mu_2 = 1.25 \times 10^{-5}$ for the numerical solutions reported in Figure 7.5, and the mobilities $\mu_1 = 1.25 \times 10^{-5}$ and $\mu_2 = 2.5 \times 10^{-7}$ for the numerical solutions of Figure 7.6. This guarantees that the conditions given by equation (7.21) for $h = 1, 2$ are satisfied. We define the pressure p according to the following simplified

barotropic relation

$$\Pi(\rho) = K\,\rho \quad \text{with} \quad K = 2,$$

which satisfies the conditions given by equation (7.2). Again, we choose $\gamma = 1$ as the results displayed in Section 7.5.2 and Figure 7.4 highlight that for large γ there can be disagreement between the discrete and continuum models. We impose the initial conditions

$$\rho_1^0(0,x) = A_1 \exp\left(-b_1\,x^2\right) \quad \text{and} \quad \rho_2^0 = \begin{cases} 0, & \text{for } x \leq 13, \\ A_2 \exp\left(-b_2(x-14)^2\right), & \text{for } x \in (13,29), \\ 0, & \text{for } x \geq 29, \end{cases} \tag{B.2}$$

where

$$A_1 = 1.25 \times 10^4, \quad b_1 = 0.06, \quad A_2 = 2.5 \times 10^4 \quad \text{and} \quad b_2 = 6 \times 10^{-3}.$$

B.2.3 Setup of numerical simulations for the case of two populations with a redefined pressure function

The rate G is defined according to equation (7.58) with the homeostatic pressure $P = 10 \times 10^4$ and $\beta = 4 \times 10^{-5}$. Given the parameter values used for the individual-based model in the case of two cell populations, we choose the mobilities $\mu_1 = 2.5 \times 10^{-7}$ and $\mu_2 = 1.25 \times 10^{-5}$ for the numerical solutions reported in Figure 7.7, and the mobilities $\mu_1 = 1.25 \times 10^{-5}$ and $\mu_2 = 2.5 \times 10^{-7}$ for the numerical solutions of Figure 7.8. This guarantees that the conditions given by equation (7.21) for $h = 1, 2$

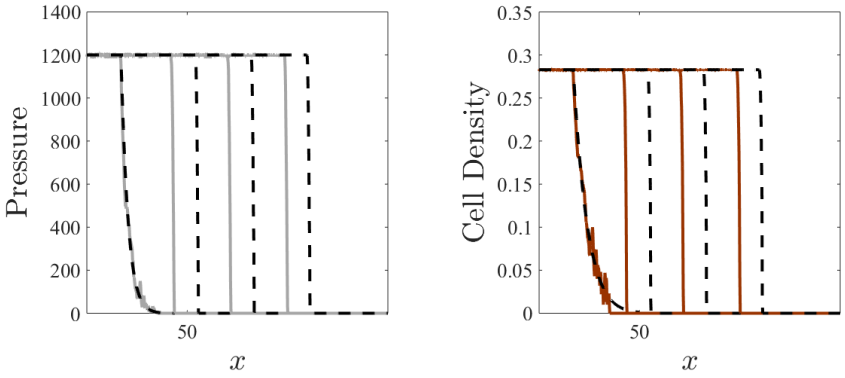

Figure B.1: The invasion front of the individual-based model travels at the same speed but behind the front of the corresponding continuum model. *The left and right panel display, respectively, the pressure and the cell density at the time instants* $t = 10$, $t = 50$, $t = 150$ *and* $t = 250$. *Values of the pressure and the cell density are in units of* 10^4. *Simulations were carried out using the same parameter values as the results for* $\gamma = 2$ *displayed in Figure 7.4. A complete description of the numerical simulation setup is given in Appendix B.1.1 and Appendix B.2.1.*

are satisfied. We define the pressure p according to the following barotropic relation

$$\Pi(\rho) = q\,(\rho - \rho^*)_+ \quad \text{where} \quad q = 10 \quad \text{and} \quad \rho^* = r\,P \;\; \text{with} \;\; r = 10^{-3},$$

which satisfies the conditions given by equation (7.45). We impose the initial conditions given by equation (B.2) with

$$A_1 = 12.5 \times 10^4, \quad b_1 = 0.06, \quad A_2 = 25 \times 10^4 \quad \text{and} \quad b_2 = 6 \times 10^{-3}.$$

Bibliography

Agliari, E., Biselli, E., De Ninno, A., Schiavoni, G., Gabriele, L., Gerardino, A., Mattei, F., Barra, A., and Businaro, L. (2014). Cancer-driven dynamics of immune cells in a microfluidic environment. *Sci Rep*, 4:6639.

Agrawal, S. and Kishore, M. C. (2000). MHC class I gene expression and regulation. *J Hematother Stem Cell Res*, 9(6):795–812.

Aguirre-Ghiso, J. A. (2007). Models, mechanisms and clinical evidence for cancer dormancy. *Nat Rev Cancer*, 7(11):834–846.

Ahmed, M. D., Bae, Y. S., et al. (2014). Dendritic cell-based therapeutic cancer vaccines: Past, present and future. *Clin Exp Vaccine Res*, 3(2):113–116.

Al-Tameemi, M., Chaplain, M. A. J., and d'Onofrio, A. (2012). Evasion of tumours from the control of the immune system: Consequences of brief encounters. *Biol Direct*, 7:31–31.

Albers, J. J., Ammon, T., Gosmann, D., Audehm, S., Thoene, S., Winter, C., Secci, R., Wolf, A., Stelzl, A., Steiger, K., et al. (2019). Gene editing enables T-cell engineering to redirect antigen specificity for potent tumor rejection. *Life Sci Alliance*, 2(2):e201900367.

Alemani, D., Pappalardo, F., Pennisi, M., Motta, S., and Brusic, V. (2012). Combining cellular automata and lattice Boltzmann method to model multiscale avascular tumor growth coupled with nutrient diffusion and immune competition. *J Immunol Methods*, 376(1-2):55–68.

Algarra, I., Cabrera, T., and Garrido, F. (2000). The HLA crossroad in tumor immunology. *Human Immunol*, 61(1):65–73.

Ambrosi, D., Duperray, A., Peschetola, V., and Verdier, C. (2009). Traction patterns of tumor cells. *J Math Biol*, 58(1-2):163–181.

Ambrosi, D., Gamba, A., and Serini, G. (2004). Cell directional and chemotaxis in vascular morphogenesis. *Bull Math Biol*, 66(6):1851–1873.

Ambrosi, D. and Mollica, F. (2002). On the mechanics of a growing tumor. *Int J Eng Sci*, 40(12):1297–1316.

Ambrosi, D. and Preziosi, L. (2002). On the closure of mass balance models for tumor growth. *Math Mod Meth Appl Sci*, 12(05):737–754.

Ambrosi, D. and Preziosi, L. (2009). Cell adhesion mechanisms and stress relaxation in the mechanics of tumours. *Biomech Model Mechanobiol*, 8(5):397–413.

American Cancer Soceity (2018). Cancer immunotherapy. `www.cancer.org/treatment/treatments-and-side-effects/treatment-types/immunotherapy`. Accessed 7th February 2018.

An, G., Mi, Q., Dutta-Moscato, J., and Vodovotz, Y. (2009). Agent-based models in translational systems biology. *Wiley Interdiscip Rev Syst Biol Med*, 1(2):159–171.

Anagnostou, V., Smith, K. N., Forde, P. M., Niknafs, N., Bhattacharya, R., White, J., Zhang, T., Adleff, V., Phallen, J., Wali, N., et al. (2017). Evolution of neoantigen landscape during immune checkpoint blockade in non-small cell lung cancer. *Cancer Discov*, 7(3):264–276.

Andersen, R., Donia, M., Ellebaek, E., Borch, T. H., Kongsted, P., Iversen, T. Z., et al. (2016). Long-lasting complete responses in patients with metastatic melanoma after adoptive cell therapy with tumor-infiltrating lymphocytes and an attenuated IL-2 regimen. *Clin Cancer Res*, 22(15):3734–3745.

Anderson, A. R. A. and Chaplain, M. A. J. (1998). Continuous and discrete mathematical models of tumor-induced angiogenesis. *Bull Math Biol*, 60(5):857–899.

Anderson, A. R. A., Weaver, A. M., Cummings, P. T., and Quaranta, V. (2006). Tumor morphology and phenotypic evolution driven by selective pressure from the microenvironment. *Cell*, 127(5):905–915.

Araujo, R. P. and McElwain, D. L. S. (2004). A history of the study of solid tumour growth: The contribution of mathematical modelling. *Bull Math Biol*, 66(5):1039–1091.

Arciero, J. C., Jackson, T. L., and Kirschner, D. E. (2004). A mathematical model of tumor-immune evasion and siRNA treatment. *Discrete Contin Dyn Syst Ser B*, 4(1):39–58.

Ariel, G., Rabani, A., Benisty, S., Partridge, J. D., Harshey, R. M., and Be'Er, A. (2015). Swarming bacteria migrate by Lévy walk. *Nat Comm*, 6:8396.

Armstrong, N. J., Painter, K. J., and Sherratt, J. A. (2006). A continuum approach to modelling cell-cell adhesion. *J Theor Biol*, 243(1):98–113.

Asatryan, A. D. and Komarova, N. L. (2016). Evolution of genetic instability in heterogeneous tumors. *J Theor Biol*, 396:1–12.

Baar, M., Coquille, L., Mayer, H., Holzel, M., Rogava, M., Tuting, T., and Bovier, A. (2016). A stochastic model for immunotherapy of cancer. *Sci Rep*, 6:24169.

Babbs, C. F. (2012). Predicting success or failure of immunotherapy for cancer: Insights from a clinically applicable mathematical model. *Am J Cancer Res*, 2(2):204–213.

Bachelier, L. (1900). Théorie de la spéculation. In *Annales scientifiques de l'École normale supérieure*, volume 17, pages 21–86.

Bakunin, O. G. (2003). Mysteries of diffusion and labyrinths of destiny. *Physics-Uspekhi*, 46(3):309–313.

Balachandran, V. P., Łuksza, M., Zhao, J. N., Makarov, V., Moral, J. A., Remark, R., et al. (2017). Identification of unique neoantigen qualities in long-term survivors of pancreatic cancer. *Nature*, 551:512–516.

Balea, S., Halanay, A., Jardan, D., Neamţu, M., and Safta, C. (2014). Stability analysis of a feedback model for the action of the immune system in leukemia. *Math Model Nat Phenom*, 9(1):108–132.

Bartumeus, F., Raposo, E. P., Viswanathan, G. M., and da Luz, M. G. E. (2014). Stochastic optimal foraging: tuning insensitive and extensive dynamics in random searches. *PLoS one*, 9(9):e106373.

Basan, M., Risler, T., Joanny, J.-F., Sastre-Garau, X., and Prost, J. (2009). Homeostatic competition drives tumor growth and metastasis nucleation. *HFSP Journal*, 3(4):265–272.

Basu, R., Whitlock, B. M., Husson, J., Le Floch, A., Jin, W., Oyler-Yaniv, A., Dotiwala, F., Giannone, G., Hivroz, C., Biais, N., et al. (2016). Cytotoxic T cells use mechanical force to potentiate target cell killing. *Cell*, 165(1):100–110.

Bauer, A. L., Jackson, T. L., and Jiang, Y. (2007). A cell-based model exhibiting branching and anastomosis during tumor-induced angiogenesis. *Biophys J*, 92(9):3105–3121.

Beatty, G. L. and Moon, E. K. (2014). Chimeric antigen receptor T cells are vulnerable to immunosuppressive mechanisms present within the tumor microenvironment. *Oncoimmunol*, 3(11):e970027.

Bellomo, N. and Delitala, M. (2008). From the mathematical kinetic, and stochastic game theory to modelling mutations, onset, progression and immune competition of cancer cells. *Phys Life Rev*, 5(4):183–206.

Bernoulli, J. (1713). *Ars conjectandi, opus posthumum. Accedit Tractatus de seriebus infinitis, et epistola Gallice scripta De ludo pilae reticularis*. impensis Thurnisiorum, fratrum.

Besse, A., Clapp, G. D., Bernard, S., Nicolini, F. E., Levy, D., and Lepoutre, T. (2018). Stability analysis of a model of interaction between the immune system and cancer cells in chronic myelogenous leukemia. *Bull Math Biol*, 80(5):1084–1110.

Bialkowski, L., van Weijnen, A., Van der Jeught, K., Renmans, D., Daszkiewicz, L., Heirman, C., Stangé, G., Breckpot, K., Aerts, J. L., and Thielemans, K. (2016). Intralymphatic mRNA vaccine induces CD8 T-cell responses that inhibit the growth of mucosally located tumours. *Sci Rep*, 6:22509.

Bianca, C., Chiacchio, F., Pappalardo, F., and Pennisi, M. (2012). Mathematical modeling of the immune system recognition to mammary carcinoma antigen. *BMC Bioinformatics*, 13(17 Supplement):S21.

Billingham, R. E., Brent, L., and Medawar, P. B. (1954). Quantitative studies on tissue transplantation immunity. II. The origin, strength and duration of actively and adoptively acquired immunity. *Proc R Soc Lond B*, 143(910):58–80.

Binder, B. J. and Landman, K. A. (2009). Exclusion processes on a growing domain. *J Theor Biol*, 259(3):541–551.

Boes, M., Cerny, J., Massol, R., den Brouw, M. O. P., Kirchhausen, T., Chen, J., and Ploegh, H. L. (2002). T-cell engagement of dendritic cells rapidly rearranges MHC class II transport. *Nature*, 418(6901):983.

Boissonnas, A., Fetler, L., Zeelenberg, I. S., Hugues, S., and Amigorena, S. (2007). In vivo imaging of cytotoxic T cell infiltration and elimination of a solid tumor. *J Exp Med*, 204(2):345–356.

Bonini, C. and Mondino, A. (2015). Adoptive T-cell therapy for cancer: The era of engineered T cells. *Eur J Immunol*, 45(9):2457–2469.

Boon, T., Coulie, P. G., Van den Eynde, B. J., and van der Bruggen, P. (2006). Human T cell responses against melanoma. *Annu Rev Immunol*, 24:175–208.

Bouchnita, A., Belmaati, F., Aboulaich, R., Koury, M. J., and Volpert, V. (2017). A hybrid computation model to describe the progression of multiple myeloma and its intra-clonal heterogeneity. *Computation*, 5(1):16.

Bray, F., Ferlay, J., Soerjomataram, I., Siegel, R. L., Torre, L. A., and Jemal, A. (2018). Global cancer statistics 2018: GLOBOCAN estimates of incidence and mortality worldwide for 36 cancers in 185 countries. *CA Cancer J Clin*, 68(6):394–424.

Brenner, D., Krammer, P. H., and Arnold, R. (2008). Concepts of activated T cell death. *Crit Rev Oncol Hematol*, 66(1):52–64.

Brentjens, R. J., Davila, M. L., Riviere, I., Park, J., Wang, X., Cowell, L. G., Bartido, S., Stefanski, J., Taylor, C., Olszewska, M., et al. (2013). CD19-targeted T cells rapidly induce molecular remissions in adults with chemotherapy-refractory acute lymphoblastic leukemia. *Sci Transl Med*, 5(177):177ra38–177ra38.

Bresch, D., Colin, T., Grenier, E., Ribba, B., and Saut, O. (2010). Computational modeling of solid tumor growth: The avascular stage. *SIAM J Sci Comput*, 32(4):2321–2344.

Brown, R. (1828). On the existence of molecules. *Philos Mag*, 4:161–173.

Brown, S. D., Warren, R. L., Gibb, E. A., Martin, S. D., Spinelli, J. J., Nelson, B. H., and Holt, R. A. (2014). Neo-antigens predicted by tumor genome meta-analysis correlate with increased patient survival. *Genome Res*, 24(5):743–750.

Brú, A., Albertos, S., Subiza, J. L., García-Asenjo, J. L., and Brú, I. (2003). The universal dynamics of tumor growth. *Biophys. J.*, 85(5):2948–2961.

Bunimovich-Mendrazitsky, S., Byrne, H., and Stone, L. (2008). Mathematical model of pulsed immunotherapy for superficial bladder cancer. *Bull Math Biol*, 70(7):2055–2076.

Bunimovich-Mendrazitsky, S., Halachmi, S., and Kronik, N. (2015). Improving bacillus calmette-guérin (BCG) immunotherapy for bladder cancer by adding interleukin 2 (IL-2): A mathematical model. *Math Med Biol*, 33(2):159–188.

Burden, T. N., Ernstberger, J., and Fister, K. R. (2004). Optimal control applied to immunotherapy. *Discrete Contin Dyn Syst Ser B*, 4(1):135–146.

Buttenschoen, A., Hillen, T., Gerisch, A., and Painter, K. J. (2018). A space-jump derivation for non-local models of cell–cell adhesion and non-local chemotaxis. *J Math Biol*, 76(1-2):429–456.

Butterfield, L. H. (2013). Dendritic cells in cancer immunotherapy clinical trials: Are we making progress? *Front Immunol*, 4:454.

Byrne, H. M. (2010). Dissecting cancer through mathematics: From the cell to the animal model. *Nat Rev Cancer*, 10(3):221.

Byrne, H. M. and Chaplain, M. A. J. (1995). Growth of nonnecrotic tumors in the presence and absence of inhibitors. *Math Biosci*, 130(2):151–181.

Byrne, H. M. and Chaplain, M. A. J. (1996). Growth of necrotic tumors in the presence and absence of inhibitors. *Math Biosci*, 135(2):187–216.

Byrne, H. M. and Chaplain, M. A. J. (1997). Free boundary value problems associated with the growth and development of multicellular spheroids. *Eur J Appl Math*, 8(6):639–658.

Byrne, H. M. and Drasdo, D. (2009). Individual-based and continuum models of growing cell populations: A comparison. *J Math Biol*, 58(4-5):657.

Byrne, H. M., King, J. R., McElwain, D. L. S., and Preziosi, L. (2003). A two-phase model of solid tumour growth. *Appl Math Lett*, 16(4):567–573.

Byrne, H. M. and Preziosi, L. (2003). Modelling solid tumour growth using the theory of mixtures. *Math Med Biol*, 20(4):341–366.

Calzone, L., Tournier, L., Fourquet, S., Thieffry, D., Zhivotovsky, B., Barillot, E., and Zinovyev, A. (2010). Mathematical modelling of cell-fate decision in response to death receptor engagement. *PLoS Comput Biol*, 6(3):e1000702.

Cancer Research UK (2018). Cancer research statistics for the UK. `www.cancerresearchuk.org/health-professional/cancer-statistics-for-the-uk`. Accessed 7th February 2018.

Cappuccio, A., Elishmereni, M., and Agur, Z. (2006). Cancer immunotherapy by interleukin-21: Potential treatment strategies evaluated in a mathematical model. *Cancer Res*, 66(14):7293–7300.

Carelle, N., Piotto, E., Bellanger, A., Germanaud, J., Thuillier, A., and Khayat, D. (2002). Changing patient perceptions of the side effects of cancer chemotherapy. *Cancer*, 95(1):155–163.

Carreno, B. M., Magrini, V., Becker-Hapak, M., Kaabinejadian, S., Hundal, J., Petti, A. A., Ly, A., Lie, W. R., Hildebrand, W. H., Mardis, E. R., et al. (2015). A dendritic cell vaccine increases the breadth and diversity of melanoma neoantigen-specific T cells. *Science*, 348(6236):803–808.

Casal, A., Sumen, C., Reddy, T. E., Alber, M. S., and Lee, P. P. (2005). Agent-based modeling of the context dependency in T cell recognition. *J Theor Biol*, 236(4):376–391.

Cattani, C. and Ciancio, A. (2012). Separable transition density in the hybrid model for tumor-immune system competition. *Comput Math Methods Med*, 2012:6101024.

Cattani, C., Ciancio, A., and d'Onofrio, A. (2010). Metamodeling the learning–hiding competition between tumours and the immune system: A kinematic approach. *Math Comput Model*, 52(1-2):62–69.

Celli, S., Day, M., Muller, A. J., Molina-Paris, C., Lythe, G., and Bousso, P. (2012). How many dendritic cells are required to initiate a T-cell response? *Blood*, 120(19):3945–3948.

Chalitchagorn, K., Shuangshoti, S., Hourpai, N., Kongruttanachok, N., Tangkijvanich, P., Thongngam, D., Voravud, N., Sriuranpong, V., and Mutirangura, A. (2004). Distinctive pattern of LINE-1 methylation level in normal tissues and the association with carcinogenesis. *Oncogene*, 23(54):8841.

Champagnat, N., Ferrière, R., and Méléard, S. (2006). Unifying evolutionary dynamics: from individual stochastic processes to macroscopic models. *Theor Pop Biol*, 69(3):297–321.

Champiat, S., Dercle, L., Ammari, S., Massard, C., Hollebecque, A., Postel-Vinay, S., Chaput, N., Eggermont, A. M., Marabelle, A., Soria, J. C., et al. (2016). Hyperprogressive disease (HPD) is a new pattern of progression in cancer patients treated by anti-PD-1/PD-L1. *Clin Cancer Res*, 23(8):1920–1928.

Chaplain, M. A. J. (1995). Reaction-diffusion prepatterning and its potential role in tumour invasion. *J Biol Syst*, 3(4):929–936.

Chaplain, M. A. J., Ganesh, M., and Graham, I. G. (2001). Spatio-temporal pattern formation on spherical surfaces: Numerical simulation and application to solid tumour growth. *J Math Biol*, 42(5):387–423.

Chaplain, M. A. J., Graziano, L., and Preziosi, L. (2006). Mathematical modelling of the loss of tissue compression responsiveness and its role in solid tumour development. *Math Med Biol*, 23(3):197–229.

Chaplain, M. A. J. and Lolas, G. (2006). Mathematical modelling of cancer invasion of tissue: Dynamic heterogeneity. *Netw Heterog Media*, 1(3):399–439.

Chaplain, M. A. J., Lorenzi, T., and Macfarlane, F. R. (2019). Bridging the gap between individual-based and continuum models of growing cell populations. *J Math Biol*, doi:10.1007/s00285–019–01391–y.

Chaplin, D. D. (2010). Overview of the immune response. *J Allergy Clin Immunol*, 2 Suppl 2(125):S3–S23.

Chen, C., Byrne, H., and King, J. (2001). The influence of growth-induced stress from the surrounding medium on the development of multicell spheroids. *J Math Biol*, 43(3):191–220.

Chen, D. S. and Mellman, I. (2017). Elements of cancer immunity and the cancer-immune set point. *Nature*, 541:321–330.

Chen, L. and Flies, D. B. (2013). Molecular mechanisms of T cell co-stimulation and co-inhibition. *Nat Rev Immunol*, 13(4):227.

Chinnasamy, N., Wargo, J. A., Yu, Z., Rao, M., Frankel, T. L., Riley, J. P., Hong, J. J., Parkhurst, M. R., Feldman, S. A., Schrump, D. S., et al. (2011). A TCR targeting the HLA-A* 0201–

restricted epitope of MAGE-A3 recognizes multiple epitopes of the MAGE-A antigen superfamily in several types of cancer. *J Immunol*, 186(2):685–696.

Chisholm, R. H., Lorenzi, T., Desvillettes, L., and Hughes, B. D. (2016). Evolutionary dynamics of phenotype-structured populations: From individual-level mechanisms to population-level consequences. *Z Angew Math Phys*, 67(4):100.

Chisholm, R. H., Lorenzi, T., Lorz, A., Larsen, A. K., Almeida, L., Escargueil, A., and Clairambault, J. (2015). Emergence of drug tolerance in cancer cell populations: An evolutionary outcome of selection, non-genetic instability and stress-induced adaptation. *Cancer Res*, 75(6):930–939.

Cho, H. and Levy, D. (2017). Modeling the dynamics of heterogeneity of solid tumours in response to chemotherapy. *Bull Math Biol*, 79(12):2986–3012.

Chowdhury, D., Sahimi, M., and Stauffer, D. (1991). A discrete model for immune surveillance, tumor immunity and cancer. *J Theor Biol*, 152(2):263–270.

Christophe, C., Müller, S., Rodrigues, M., Petit, A. E., Cattiaux, P., Dupré, L., Gadat, S., and Valitutti, S. (2015). A biased competition theory of cytotoxic T lymphocyte interaction with tumor nodules. *PloS one*, 10(3):e0120053.

Chupeau, M., Bénichou, O., and Voituriez, R. (2015). Cover times of random searches. *Nat Phys*, 11:844–847.

Ciarletta, P., Foret, L., and Amar, M. B. (2011). The radial growth phase of malignant melanoma: multi-phase modelling, numerical simulations and linear stability analysis. *J R Soc Interface*, 8(56):345–368.

Coates, A., Abraham, S., Kaye, S. B., Sowerbutts, T., Frewin, C., Fox, R. M., and Tattersall, M. H. N. (1983). On the receiving end-patient perception of the side-effects of cancer chemotherapy. *Eur J Canc Clin Oncol*, 19(2):203–208.

Coico, R. and Sunshine, G. (2015). Overview of the immune system. In *Immunology: A short course 7th Edition*, chapter 1, pages 1–11. John Wiley & Sons.

Condamin, S., Bénichou, O., Tejedor, V., Voituriez, R., and Klafter, J. (2007). First-passage times in complex scale-invariant media. *Nature*, 450(7166):77.

Connerotte, T., Van Pel, A., Godelaine, D., Tartour, E., Schuler-Thurner, B., Lucas, S., Thielemans, K., Schuler, G., and Coulie, P. G. (2008). Functions of anti-MAGE T-cells induced in melanoma patients under different vaccination modalities. *Cancer Res*, 68(10):3931–3940.

Coulie, P. G., Van den Eynde, B. J., Van Der Bruggen, P., and Boon, T. (2014). Tumour antigens recognized by T lymphocytes: At the core of cancer immunotherapy. *Nat Rev Cancer*, 14(2):135.

Dancer, E. N., Hilhorst, D., Mimura, M., and Peletier, L. A. (1999). Spatial segregation limit of a competition–diffusion system. *Eur J Appl Math*, 10(2):97–115.

Davila, M. L., Riviere, I., Wang, X., Bartido, S., Park, J., Curran, K., Chung, S. S., Stefanski, J., Borquez-Ojeda, O., Olszewska, M., et al. (2014). Efficacy and toxicity management of 19-28z CAR T cell therapy in B cell acute lymphoblastic leukemia. *Sci Transl Med*, 6(224):224ra25–224ra25.

Davis, M. M., Boniface, J. J., Reich, Z., Lyons, D., Hampl, J., Arden, B., and Chien, Y. (1998). Ligand recognition by $\alpha\beta$ T cell receptors. *Annu Rev Immunol*, 16(1):523–544.

Davydov, B. I. (1934). Uravnenie Fokkera Planka i vremya relaksatsii Maksvellovskogo raspredeleniya (Fokker Planck equation and Maxwellian distribution relaxation time). In *Dokl Akad Nauk SSSR*, volume 2, page 212.

De Boer, R. J., Hogeweg, P., Dullens, H. F., De Weger, R. A., and Den Otter, W. (1985). Macrophage T lymphocyte interactions in the anti-tumor immune response: A mathematical model. *J Immunol*, 134(4):2748–2758.

de Pillis, L. G., Gu, W., and Radunskaya, A. E. (2006a). Mixed immunotherapy and chemotherapy of tumors: Modeling, applications and biological interpretations. *J Theor Biol*, 238(4):841–862.

de Pillis, L. G., Mallet, D. G., and Radunskaya, A. E. (2006b). Spatial tumor-immune modeling. *Comput Math Methods Med*, 7(2-3):159–176.

de Pillis, L. G. and Radunskaya, A. E. (2003). A mathematical model of immune response to tumour invasion. In *Second MIT Conference on Computational Fluid and Solid Mechanics*, pages 1661–1668. Elsevier.

de Pillis, L. G., Radunskaya, A. E., and Wiseman, C. L. (2005). A validated mathematical model of cell-mediated immune response to tumor growth. *Cancer Res*, 65(17):7950–7958.

de Pillis, L. G., Renee Fister, K., Gu, W., Collins, C., Daub, M., Gross, D., Moore, J., and Preskill, B. (2009). Mathematical model creation for cancer chemo-immunotherapy. *Comput Math Meth Med*, 10(3):165–184.

De Smet, C., De Backer, O., Faraoni, I., Lurquin, C., Brasseur, F., and Boon, T. (1996). The activation of human gene MAGE-1 in tumor cells is correlated with genome-wide demethylation. *Proc Nat Acad Sci*, 93(14):7149–7153.

Deisboeck, T. S., Wang, Z., Macklin, P., and Cristini, V. (2011). Multiscale cancer modeling. *Annu Rev Biomed Eng*, 13:127–155.

Delbridge, A. R. D., Grabow, S., Strasser, A., and Vaux, D. L. (2016). Thirty years of Bcl-2: Translating cell death discoveries into novel cancer therapies. *Nat Rev Cancer*, 16(2):99–109.

Delitala, M., Dianzani, U., Lorenzi, T., and Melensi, M. (2013). A mathematical model for immune and autoimmune response mediated by T-cells. *Comput Math Appl*, 66(6):1010–1023.

Delitala, M. and Lorenzi, T. (2013). Recognition and learning in a mathematical model for immune response against cancer. *Discrete Contin Dyn Syst Ser B*, 18(4):891–914.

Deroulers, C., Aubert, M., Badoual, M., and Grammaticos, B. (2009). Modeling tumor cell migration: From microscopic to macroscopic models. *Phys Rev E*, 79(3):031917.

Detcheverry, F. (2017). Generalized run-and-turn motions: From bacteria to Lévy walks. *Phys Rev E*, 96(1):012415.

Dhodapkar, M. V., Dhodapkar, K. M., and Palucka, A. K. (2008). Interactions of tumor cells with dendritic cells: Balancing immunity and tolerance. *Cell Death Differ*, 15(1):39.

d'Onofrio, A. (2005). A general framework for modeling tumor-immune system competition and immunotherapy. *Physica D*, 208(3-4):220–235.

d'Onofrio, A. and Ciancio, A. (2011). Simple biophysical model of tumor evasion from immune system control. *Phys Rev E*, 84(3):031910.

Dranoff, G. (2004). Cytokines in cancer pathogenesis and cancer therapy. *Nat Rev Cancer*, 4(1):11.

Drasdo, D. (2005). Coarse graining in simulated cell populations. *Adv Complex Syst*, 8(02n03):319–363.

Drasdo, D. and Hoehme, S. (2012). Modeling the impact of granular embedding media, and pulling versus pushing cells on growing cell clones. *New J Phys*, 14(5):055025.

Dritschel, H., Waters, S. L., Roller, A., and Byrne, H. M. (2018). A mathematical model of cytotoxic and helper T cell interactions in a tumour microenvironment. *Lett Biomath*, 5(sup1):S36–S68.

Dudley, M. E., Wunderlich, J., Nishimura, M. I., Yu, D., Yang, J. C., Topalian, S. L., Schwartzentruber, D. J., Hwu, P., Marincola, F. M., Sherry, R., et al. (2001). Adoptive transfer of cloned melanoma-reactive T lymphocytes for the treatment of patients with metastatic melanoma. *J Immunother*, 24(4):363–373.

Dybiec, B. and Gudowska-Nowak, E. (2017). Lévy flights versus Lévy walks in bounded domains. *Phys Rev E*, 95(5):052102.

Dyson, L., Maini, P. K., and Baker, R. E. (2012). Macroscopic limits of individual-based models for motile cell populations with volume exclusion. *Phys Rev E*, 86(3):031903.

Eftimie, R., Bramson, J. L., and Earn, D. J. D. (2011). Interactions between the immune system and cancer: A brief review of non-spatial mathematical models. *Bull Math Biol*, 73(1):2–32.

Ehrlich, M. (2002). DNA methylation in cancer: Too much, but also too little. *Oncogene*, 21(35):5400.

Einstein, A. (1905). Uber die von der molekularkinetischen theorie der warme geforderte bewegung von in ruhenden flussigkeiten suspendierten teilchen. *Annal Phys*, 322(8):549–560.

Einstein, M. H., Baron, M., Levin, M. J., Chatterjee, A., Edwards, R. P., Zepp, F., Carletti, I., Dessy, F. J., Trofa, A. F., Schuind, A., et al. (2009). Comparison of the immunogenicity and safety of cervarix and gardasil human papillomavirus (HPV) cervical cancer vaccines in healthy women aged 18-45 years. *Hum Vaccin*, 5(10):705–719.

Eissing, T., Conzelmann, H., Gilles, E. D., Allgöwer, F., Bullinger, E., and Scheurich, P. (2004). Bistability analyses of a caspase activation model for receptor-induced apoptosis. *J Biol Chem*, 279(35):36892–36897.

Enderling, H., Anderson, A. R. A., Chaplain, M. A. J., Beheshti, A., Hlatky, L., and Hahnfeldt, P. (2009). Paradoxical dependencies of tumor dormancy and progression on basic cell kinetics. *Cancer Res*, 69(22):8814–8821.

Engelhardt, J. J., Boldajipour, B., Beemiller, P., Pandurangi, P., Sorensen, C., Werb, Z., Egeblad, M., and Krummel, M. F. (2012). Marginating dendritic cells of the tumor microenvironment cross-present tumor antigens and stably engage tumor-specific T cells. *Cancer Cell*, 21(3):402–417.

Erban, R. and Othmer, H. G. (2004). From individual to collective behavior in bacterial chemotaxis. *SIAM J Appl Math*, 65(2):361–391.

Fedotov, S. (2016). Single integrodifferential wave equation for a Lévy walk. *Phys Rev E*, 93(2):020101.

Fedotov, S. and Korabel, N. (2017). Emergence of Lévy walks in systems of interacting individuals. *Phys Rev E*, 95(1):030107.

Fehres, C. M., Unger, W. W. J., Garcia-Vallejo, J. J., and van Kooyk, Y. (2014). Understanding the biology of antigen cross-presentation for the design of vaccines against cancer. *Front Immunol*, 5:149.

Feinberg, A. P. (2004). The epigenetics of cancer etiology. In *Seminars in Cancer Biology*, volume 14, pages 427–432. Elsevier.

Feinberg, A. P. and Tycko, B. (2004). The history of cancer epigenetics. *N Rev Cancer*, 4(2):143.

Feng, K., Guo, Y., Dai, H., Wang, Y., Li, X., Jia, H., and Han, W. (2016). Chimeric antigen receptor-modified T cells for the immunotherapy of patients with EGFR-expressing advanced relapsed/refractory non-small cell lung cancer. *Sci China Life Sci*, 59(5):468–479.

Ferlay, J., Colombet, M., Soerjomataram, I., Mathers, C., Parkin, D., Piñeros, M., Znaor, A., and Bray, F. (2018). Estimating the global cancer incidence and mortality in 2018: GLOBOCAN sources and methods. *Int J Cancer*, 144(8):1941–1953.

Ferlay, J., Ervik, M., Lam, F., Colombet, M., Mery, L., Piñeros, M., Znaor, A., Soerjomataram, I., and Bray, F. (2019). Global Cancer Observatory: Cancer Today. Lyon, France: International Agency for Research on Cancer. `https://gco.iarc.fr/today`. Accessed March 2019.

Fernando, A. E., Landman, K. A., and Simpson, M. J. (2010). Nonlinear diffusion and exclusion processes with contact interactions. *Phys Rev E*, 81(1):011903.

Ferreira, S. C., Martins, M. L., and Vilela, M. J. (2002). Reaction-diffusion model for the growth of avascular tumor. *Phys Rev E*, 65(2):021907.

Fesnak, A. D., June, C. H., and Levine, B. L. (2016). Engineered T cells: The promise and challenges of cancer immunotherapy. *Nat Rev Cancer*, 16(9):566.

Fishman, M. A. and Perelson, A. S. (1993). Modeling T cell-antigen presenting cell interactions. *J Theor Biol*, 160(3):311–342.

Fozard, J. A., Byrne, H. M., Jensen, O. E., and King, J. R. (2010). Continuum approximations of individual-based models for epithelial monolayers. *Math Med Biol*, 27(1):39–74.

Frascoli, F., Flood, E., and Kim, P. S. (2016). A model of the effects of cancer cell motility and cellular adhesion properties on tumour-immune dynamics. *Math Med Biol*, 34(2):215–240.

Frascoli, F., Kim, P. S., Hughes, B. D., and Landman, K. A. (2014). A dynamical model of tumour immunotherapy. *Math Biosci*, 253:50–62.

Fricke, G. M., Letendre, K. A., Moses, M. E., and Cannon, J. L. (2016). Persistence and adaptation in immunity; T cells balance the extent and thoroughness of search. *PLoS Comput Biol*, 12(3):e1004818.

Frigault, M. J. and Maus, M. V. (2016). Chimeric antigen receptor-modified T cells strike back. *Int Immunol*, 28(7):355–363.

Furth, R. (1920). The Brownian motion with consideration of the longevity of the direction of movement. *Z Phys*, 2:244–256.

Fussenegger, M., Bailey, J. E., and Varner, J. (2000). A mathematical model of caspase function in apoptosis. *Nat Biotechnol*, 18(7):768–774.

Gajewski, T. F., Schreiber, H., and Fu, Y. (2013). Innate and adaptive immune cells in the tumor microenvironment. *Nat Immunol*, 14(10):1014–1022.

Galante, A., Tamada, K., and Levy, D. (2012). B7-h1 and a mathematical model for cytotoxic T cell and tumor cell interaction. *Bull Math Biol*, 74(1):91–102.

Gan, W., Tian, C., and Zhu, P. (2015). Hopf bifurcation in a fractional diffusion food-limited model with feedback control. *J Math Chem*, 53(6):1393–1411.

Garg, A. D., Coulie, P. G., Van den Eynde, B. J., and Agostinis, P. (2017). Integrating next-generation dendritic cell vaccines into the current cancer immunotherapy landscape. *Trends in Immunology*, 1392:1–17.

Garrido, F., Cabrera, T., and Aptsiauri, N. (2010). Hard and soft lesions underlying the HLA class I alterations in cancer cells: Implications for immunotherapy. *Int J Cancer*, 127(2):249–256.

Gatenby, R. A. and Gawlinski, E. T. (1996). A reaction-diffusion model of cancer invasion. *Cancer Res*, 56(24):5745–5753.

Gerdemann, U., Katari, U., Christin, A. S., Cruz, C. R., Tripic, T., Rousseau, A., Gottschalk, S. M., Savoldo, B., Vera, J. F., Heslop, H. E., et al. (2011). Cytotoxic T lymphocytes simultaneously targeting multiple tumor-associated antigens to treat EBV negative lymphoma. *Mol Ther*, 19(12):2258–2268.

Ghaffarizadeh, A., Heiland, R., and Friedman, S. H. (2018). PhysiCell: An open source physics-based cell simulator for 3-D multicellular systems. *PLoS Comput Biol*, 14:e1005991.

Gnedenko, B. V. and Kolmogorov, A. N. (1954). Limit theorems for sums of independent random variables Addison-Wesley. *Am J Math*, 105.

Golovin, A. A., Matkowsky, B. J., and Volpert, V. A. (2008). Turing pattern formation in the Brusselator model with superdiffusion. *SIAM J Appl Math*, 69(1):251–272.

Gomis, R. R. and Gawrzak, S. (2017). Tumor cell dormancy. *Mol Oncol*, 11(1):62–78.

Gong, C., Milberg, O., and Wang, B. (2017). A computational multiscale agent-based model for simulating spatio-temporal tumour immune response to PD-1 and PD-L1 inhibition. *J R Soc Interface*, 14(134):20170320.

Gotwals, P., Cameron, S., Cipolletta, D., Cremasco, V., Crystal, A., Hewes, B., Mueller, B., Quaratino, S., Sabatos-Peyton, C., Petruzzelli, L., et al. (2017). Prospects for combining targeted and conventional cancer therapy with immunotherapy. *Nat Rev Cancer*, 17(5):286–301.

Goya, G. F., Marcos-Campos, I., Fernandez-Pacheco, R., Saez, B., Godino, J., Asin, L., Lambea, J., Tabuenca, P., Mayordomo, J. I., Larrad, L., et al. (2008). Dendritic cell uptake of iron-based magnetic nanoparticles. *Cell Biol Int*, 32(8):1001–1005.

Graff-Dubois, S., Faure, O., Gross, D. A., Alves, P., Scardino, A., Chouaib, S., Lemonnier, F. A., and Kosmatopoulos, K. (2002). Generation of CTL recognizing an HLA-A* 0201-restricted epitope shared by MAGE-A1,-A2,-A3,-A4,-A6,-A10, and-A12 tumor antigens: implication in a broad-spectrum tumor immunotherapy. *J Immunol*, 169(1):575–580.

Greenspan, H. (1976). On the growth and stability of cell cultures and solid tumors. *J. Theor. Biol.*, 56(1):229–242.

Grimm, V. and Railsback, S. F. (2005). Individual-based models and ecology. In *Princeton Series in Theoretical and Computational Biology*. Princeton University Press.

Gross, G. and Eshhar, Z. (2016). Therapeutic potential of T cell chimeric antigen receptors (CARs) in cancer treatment: Counteracting off-tumor toxicities for safe CAR T cell therapy. *Annu Rev Pharmacol Toxicol*, 56:59–83.

Grupp, S. A., Kalos, M., Barrett, D., Aplenc, R., Porter, D. L., Rheingold, S. R., Teachey, D. T., Chew, A., Hauck, B., Wright, J. F., et al. (2013). Chimeric antigen receptor–modified T cells for acute lymphoid leukemia. *N Engl J Med*, 368(16):1509–1518.

Halle, S., Keyser, K. A., Stahl, F. R., Busche, A., Marquardt, A., Zheng, X., Galla, M., Heissmeyer, V., Heller, K., Boelter, J., et al. (2016). In vivo killing capacity of cytotoxic T cells is limited and involves dynamic interactions and T cell cooperativity. *Immunity*, 44(2):233–245.

Hanahan, D. and Weinberg, R. A. (2011). Hallmarks of cancer: The next generation. *Cell*, 144(5):646–674.

Hanert, E. (2012). Front dynamics in a two-species competition model driven by Lévy flights. *J Theor Biol*, 300:134–142.

Harris, T. H., Banigan, E. J., Christian, D. A., Konradt, C., Wojno, E. D. T., Norose, K., Wilson, E. H., John, B., Weninger, W., Luster, A. D., et al. (2012). Generalized Lévy walks and the role of chemokines in migration of effector CD8+ T cells. *Nature*, 486(7404):545–548.

Harshyne, L. A., Watkins, S. C., Gambotto, A., and Barratt-Boyes, S. M. (2001). Dendritic cells acquire antigens from live cells for cross-presentation to CTL. *J Immunol*, 166(6):3717–3723.

Harshyne, L. A., Zimmer, M. I., Watkins, S. C., and Barratt-Boyes, S. M. (2003). A role for class A scavenger receptor in dendritic cell nibbling from live cells. *J Immunol*, 170(5):2302–2309.

Hartmann, S., Brisam, M., Rauthe, S., Driemel, O., Brands, R. C., Rosenwald, A., Kübler, A. C., and Müller-Richter, U. D. (2016). Contrary melanoma-associated antigen-A expression at the tumor front and center: A comparative analysis of stage I and IV head and neck squamous cell carcinoma. *Oncol Lett*, 12(4):2942–2947.

Hersey, P. and Zhang, X. (2001). How melanoma cells evade trail-induced apoptosis. *Nat Rev Cancer*, 1(2):142–150.

Hillen, T. and Othmer, H. G. (2000). The diffusion limit of transport equations derived from velocity-jump processes. *SIAM J Appl Math*, 61(3):751–775.

Hillen, T. and Painter, K. J. (2009). A user's guide to PDE models for chemotaxis. *J Math Biol*, 58(1-2):183.

Hu, W. Y., Zhong, W. R., Wang, F. H., Li, L., and Shao, Y. Z. (2012). In silico synergism and antagonism of an anti-tumour system intervened by coupling immunotherapy and chemotherapy: A mathematical modelling approach. *Bull Math Biol*, 74(2):434–452.

Hua, F., Cornejo, M. G., Cardone, M. H., Stokes, C. L., and Lauffenburger, D. A. (2016). Effects of Bcl-2 levels on Fas signaling-induced caspase-3 activation: Molecular genetic tests of computational model predictions. *J Immunol*, 175(2):985–995.

Huang, A. C., Postow, M. A., Orlowski, R. J., Mick, R., Bengsch, B., Manne, S., Xu, W., Harmon, S., Giles, J. R., Wenz, B., et al. (2017). T-cell invigoration to tumour burden ratio associated with anti-PD-1 response. *Nature*, 545(1):60–65.

Hui, E., Cheung, J., Zhu, J., Su, X., Taylor, M. J., Wallweber, H. A., Sasmal, D. K., Huang, J., Kim, J. M., Mellman, I., et al. (2017). T cell costimulatory receptor CD28 is a primary target for PD-1–mediated inhibition. *Science*, 355(6332):1428–1433.

Humphries, N. E., Weimerskirch, H., and Sims, D. W. (2013). A new approach for objective identification of turns and steps in organism movement data relevant to random walk modelling. *Methods Ecol Evol*, 4(10):930–938.

Igney, F. H. and Krammer, P. H. (2002). Immune escape of tumors: Apoptosis resistance and tumor counterattack. *J Leukoc Biol*, 71(6):907–920.

Ikeda, H. (2016). T-cell adoptive immunotherapy using tumor-infiltrating T cells and genetically engineered TCR-T cells. *Int Immunol*, 28(7):349–353.

Joglekar, A. V., Leonard, M. T., Jeppson, J. D., Swift, M., Li, G., Wong, S., Peng, S., Zaretsky, J. M., Heath, J. R., Ribas, A., et al. (2019). T cell antigen discovery via signaling and antigen-presenting bifunctional receptors. *Nat Methods*, 16(2):191.

John, L. B., Devaud, C., Duong, C. M., Yong, C., Beavis, P. A., Haynes, N. M., Chow, M. T., Smyth, M. J., Kershaw, M. H., and Darcy, P. K. (2013). Anti-PD-1 antibody therapy potently enhances the eradication of established tumors by gene-modified T cells. *Clin Cancer Res*, 19(20):5636–5646.

Johnson, L. A., Scholler, J., Ohkuri, T., Kosaka, A., Patel, P. R., McGettigan, S. E., Nace, A. K., Dentchev, T., Thekkat, P., Loew, A., et al. (2015). Rational development and characterization of humanized anti–EGFR variant III chimeric antigen receptor T cells for glioblastoma. *Sci Transl Med*, 7(275):275ra22.

Johnston, M. D., Edwards, C. M., Bodmer, W. F., Maini, P. K., and Chapman, S. J. (2007). Mathematical modeling of cell population dynamics in the colonic crypt and in colorectal cancer. *Proc Nat Acad Sci*, 104(10):4008–4013.

Johnston, S. T., Baker, R. E., McElwain, D. L. S., and Simpson, M. J. (2017). Co-operation, competition and crowding: A discrete framework linking allee kinetics, nonlinear diffusion, shocks and sharp-fronted travelling waves. *Sci Rep*, 7:42134.

Johnston, S. T., Simpson, M. J., and Baker, R. E. (2012). Mean-field descriptions of collective migration with strong adhesion. *Phys Rev E*, 85(5):051922.

Joshi, B., Wang, X., Banerjee, S., Tian, H., Matzavinos, A., and Chaplain, M. A. J. (2009). On immunotherapies and cancer vaccination protocols: A mathematical modelling approach. *J Theor Biol*, 259(4):820–827.

Kageyama, S., Ikeda, H., Miyahara, Y., Imai, N., Ishihara, M., Saito, K., Sugino, S., Ueda, S., Ishikawa, T., Kokura, S., et al. (2015). Adoptive transfer of MAGE-A4 T-cell receptor gene-transduced lymphocytes in patients with recurrent esophageal cancer. *Clin Cancer Res*, 21(10):2268–2277.

Kalos, M., Levine, B. L., Porter, D. L., Katz, S., Grupp, S. A., Bagg, A., and June, C. H. (2011). T cells with chimeric antigen receptors have potent antitumor effects and can establish memory in patients with advanced leukemia. *Sci Transl Med*, 3(95):95ra73.

Kather, J. N., Poleszczuk, J., and Suarez-Carmona, M. (2017). In silico modeling of immunotherapy and stroma-targeting therapies in human colorectal cancer. *Cancer Res*, 77:6442–6452.

Kato, S., Goodman, A. M., Walavalkar, V., Barkauskas, D. A., Sharabi, A., and Kurzrock, R. (2017). Hyper-progressors after immunotherapy: Analysis of genomic alterations associated with accelerated growth rate. *Clin Cancer Res*, page 3133.

Keir, M. E., Butte, M. J., Freeman, G. J., and Sharpe, A. H. (2008). PD-1 and its ligands in tolerance and immunity. *Annu Rev Immunol*, 26:677–704.

Kenney, J. F. and Keeping, E. S. (1962). *Mathematics of Statistics Pt. 1.* Princeton, NJ: Van Nostrand.

Kershaw, M. H., Westwood, J. A., Parker, L. L., Wang, G., Eshhar, Z., Mavroukakis, S. A., White, D. E., Wunderlich, J. R., Canevari, S., Rogers-Freezer, L., et al. (2006). A phase I study on adoptive immunotherapy using gene-modified T cells for ovarian cancer. *Clin Cancer Res*, 12(20):6106–6115.

Kim, I. and Požár, N. (2018). Porous medium equation to Hele-Shaw flow with general initial density. *Trans Amer Math Soc*, 370(2):873–909.

Kim, I. C., Perthame, B., and Souganidis, P. E. (2016). Free boundary problems for tumor growth: A viscosity solutions approach. *Nonlinear Anal*, 138:207–228.

Kim, P. S. and Lee, P. P. (2012). Modeling protective anti-tumor immunity via preventative cancer vaccines using a hybrid agent-based and delay differential equation approach. *PLoS Comput Biol*, 8(10):e1002742.

Kirschner, D. and Panetta, J. C. (1998). Modeling immunotherapy of the tumor–immune interaction. *J Math Biol*, 37(3):235–252.

Klafter, J. and Zumofen, G. (1994). Lévy statistics in a hamiltonian system. *Phys Rev E*, 49(6):4873.

Klebanoff, C. A., Gattinoni, L., and Restifo, N. P. (2006). CD8+ T-cell memory in tumor immunology and immunotherapy. *Immunol Rev*, 211(1):214–224.

Kolev, M. (2003). Mathematical modeling of the competition between acquired immunity and cancer. *Int J Appl Math Comput Sci*, 13:289–296.

Kolev, M., Nawrocki, S., and Zubik-Kowal, B. (2013). Numerical simulations for tumor and cellular immune system interactions in lung cancer treatment. *Commun Nonlinear Sci Numer Simul*, 18(6):1473–1480.

Konstorum, A., Vella, A. T., Adler, A. J., and Laubenbacher, R. (2017). Addressing current challenges in cancer immunotherapy with mathematical and computational modeling. *J Royal Soc Interface*, 14(131):20170150.

Koren, T., Lomholt, M. A., Chechkin, A. V., Klafter, J., and Metzler, R. (2007). Leapover lengths and first passage time statistics for Lévy flights. *Phys Rev Lett*, 99(16):160602.

Köse, E., Moore, S., Ofodile, C., Radunskaya, A., Swanson, E. R., and Zollinger, E. (2017). Immuno-kinetics of immunotherapy: Dosing with DCs. *Lett Biomath*, 4(1):39–58.

Kranz, L. M., Diken, M., Haas, H., et al. (2016). Systemic RNA delivery to dendritic cells exploits antiviral defence for cancer immunotherapy. *Nature*, 534:396–401.

Krummel, M. F., Bartumeus, F., and Gérard, A. (2016). T-cell migration, search strategies and mechanisms. *Nat Rev Immunol*, 16(3):193–201.

Kuznetsov, V. A. and Knott, G. D. (2001). Modeling tumor regrowth and immunotherapy. *Math Comput Model*, 33(12):1275–1287.

Kuznetsov, V. A., Makalkin, I. A., Taylor, M. A., and Perelson, A. S. (1994). Nonlinear dynamics of immunogenic tumors: Parameter estimation and global bifurcation analysis. *Bull Math Biol*, 56(2):295–321.

Landman, K. A. and Fernando, A. E. (2011). Myopic random walkers and exclusion processes: Single and multispecies. *Physica A Stat Mech Appl*, 390(21-22):3742–3753.

Laoui, D., Keirsse, J., Morias, Y., Van Overmeire, E., Geeraerts, X., Elkrim, Y., Kiss, M., Bolli, E., Lahmar, Q., Sichien, D., et al. (2016). The tumour microenvironment harbours ontogenically distinct dendritic cell populations with opposing effects on tumour immunity. *N Comm*, 7:13720.

Larkin, J., Chiarion-Sileni, V., Gonzalez, R., Grob, J. J., Cowey, L. C., Lao, C. D., Schadendorf, D., Dummer, R., Smylie, M., Rutkowski, P., et al. (2015). Combined nivolumab and ipilimumab or monotherapy in untreated melanoma. *N Engl J Med*, 373(1):23–34.

Lawrence, B. P. (2016). Cytotoxic T lymphocytes. In *Encyclopedia of Immunotoxicology*, pages 246–249. Springer.

Legewie, S., Blüthgen, N., and Herzel, H. (2006). Mathematical modeling identifies inhibitors of apoptosis as mediators of positive feedback and bistability. *PLoS Comput Biol*, 2(9):e120.

Lejeune, O., Chaplain, M. A. J., and El Akili, I. (2008). Oscillations and bistability in the dynamics of cytotoxic reactions mediated by the response of immune cells to solid tumours. *Math Comp Model*, 47(5):649–662.

Leone, P., Shin, E., Perosa, F., Vacca, A., Dammacco, F., and Racanelli, V. (2013). MHC class I antigen processing and presenting machinery: Organization, function, and defects in tumor cells. *J Natl Cancer Inst*, 105(16):1172–1187.

Levandowsky, M., White, B. S., and Schuster, F. L. (1997). Random movements of soil amebas. *Acta Protozool*, 4(36).

LeVeque, R. J. (2002). *Finite volume methods for hyperbolic problems*, volume 31. Cambridge University Press.

Leverson, J. D. (2016). Abstract IA34: Clinical proof of concept for the first-in-class Bcl-2-selective inhibitor venetoclax (ABT-199/GDC-0199). *Cancer Res*, 76(3 Supplement):IA34.

Lévy, P. (1937). Calcul des probabilités (Gauthier-Villars, Paris, 1925). *Théorie de l addition des variables aléatoires*.

Li, L., Nørrelykke, S. F., and Cox, E. C. (2008). Persistent cell motion in the absence of external signals: A search strategy for eukaryotic cells. *PLoS one*, 3(5):e2093.

Li, X., Yang, A., Huang, H., Zhang, X., Town, J., Davis, B., Cockcroft, D. W., and Gordon, J. R. (2010). Induction of type 2 T helper cell allergen tolerance by IL-10–differentiated regulatory dendritic cells. *Am J Respir Cell Mol Biol*, 42(2):190–199.

Lim, D. S., Kim, J. H., Lee, D. S., Yoon, C. H., and Bae, Y. S. (2007). DC immunotherapy is highly effective for the inhibition of tumor metastasis or recurrence, although it is not efficient for the eradication of established solid tumors. *Cancer Immunol Immunother*, 56(11):1817–1829.

Lin Erickson, A. H., Wise, A., Fleming, S., Baird, M., Lateef, Z., Molinaro, A., Teboh-Ewungkem, M., and de Pillis, L. G. (2009). A preliminary mathematical model of skin dendritic cell trafficking and induction of T cell immunity. *Discrete Contin Dyn Syst Ser B*, 12:323–336.

Linette, G. P., Stadtmauer, E. A., Maus, M. V., Rapoport, A. P., Levine, B. L., Emery, L., Litzky, L., Bagg, A., Carreno, B. M., Cimino, P. J., et al. (2013). Cardiovascular toxicity and titin cross-reactivity of affinity enhanced T cells in myeloma and melanoma. *Blood*, 122(6):863–871.

Littman, D. R. (2015). Releasing the brakes on cancer immunotherapy. *Cell*, 162(6):1186–1190.

Liu, Z. and Li, Z. (2014). Molecular imaging in tracking tumor-specific cytotoxic T lymphocytes (CTLs). *Theranostics*, 4(10):990–1001.

Ljunggren, H., Stam, N. J., Öhlén, C., Neefjes, J. J., Höglund, P., Heemels, M., Bastin, J., Schumacher, T. N. M., Townsend, A., Kärre, K., et al. (1990). Empty MHC class I molecules come out in the cold. *Nature*, 346(6283):476.

Lorenzi, T., Chisholm, R. H., and Clairambault, J. (2016). Tracking the evolution of cancer cell populations through the mathematical lens of phenotype-structured equations. *Biol Direct*, 11(1):43.

Lorenzi, T., Chisholm, R. H., Melensi, M., Lorz, A., and Delitala, M. (2015). Mathematical model reveals how regulating the three phases of T-cell response could counteract immune evasion. *Immunology*, 146(2):271–280.

Lorenzi, T., Lorz, A., and Perthame, B. (2017). On interfaces between cell populations with different mobilities. *Kinet Relat Mod*, 10(1):299–311.

Lorz, A., Lorenzi, T., Clairambault, J., Escargueil, A., and Perthame, B. (2015). Modeling the effects of space structure and combination therapies on phenotypic heterogeneity and drug resistance in solid tumours. *Bull Math Biol*, 77(1):1–22.

Lowengrub, J. S., Frieboes, H. B., Jin, F., Chuang, Y. L., Li, X., Macklin, P., Wise, S. M., and Cristini, V. (2009). Nonlinear modelling of cancer: Bridging the gap between cells and tumours. *Nonlinearity*, 23(1):R1.

Lu, Y., Parker, L., Lu, T., Zheng, Z., Yao, X., Robbins, P. F., van der Bruggen, P., Klebanoff, C. A., Hinrichs, C. S., and Goff, S. (2015). A phase I study of an HLA-DPB1* 0401-restricted T cell receptor targeting MAGE-A3 for patients with metastatic cancers. *J Immunother Cancer*, 3(S2):158.

Łuksza, M., Riaz, N., Makarov, V., Balachandran, V. P., Hellmann, M. D., Solovyov, A., Rizvi, N. A., Merghoub, T., Levine, A. J., Chan, T. A., et al. (2017). A neoantigen fitness model predicts tumour response to checkpoint blockade immunotherapy. *Nature*, 551(7681):517–520.

Lushnikov, P. M., Chen, N., and Alber, M. (2008). Macroscopic dynamics of biological cells interacting via chemotaxis and direct contact. *Phys Rev E*, 78(6):061904.

Macfarlane, F. R., Chaplain, M. A. J., and Lorenzi, T. (2019). A stochastic individual-based model to explore the role of spatial interactions and antigen recognition in the immune response against solid tumours. *Submitted to J Theor Biol, Pending Revisions*.

Macfarlane, F. R., Lorenzi, T., and Chaplain, M. A. J. (2018). Modelling the immune response to cancer: An individual-based approach accounting for the difference in movement between inactive and activated T cells. *Bull Math Biol*, 80(6):1539–1564.

Mackensen, A., Meidenbauer, N., Vogl, S., Laumer, M., Berger, J., and Andreesen, R. (2006). Phase I study of adoptive T-cell therapy using antigen-specific CD8+ T cells for the treatment of patients with metastatic melanoma. *J Clin Oncol*, 24(31):5060–5069.

Macklin, P. and Edgerton, M. E. (2010). Discrete cell modeling. In Cristini, V. and Lowengrub, J. S., editors, *Multiscale modelling of cancer: An integrated experimental and mathematical modeling approach*, pages 88–122. Cambridge University Press.

Mallet, D. G. and de Pillis, L. G. (2006). A cellular automata model of tumor-immune system interactions. *J Theor Biol*, 239(3):334–350.

Mandelbrot, B. B. (1982). *The fractal geometry of nature*, volume 2. WH Freeman New York.

Manem, V. S. K., Kohandel, M., Komarova, N. L., and Sivaloganathan, S. (2014). Spatial invasion dynamics on random and unstructured meshes: Implications for heterogeneous tumor populations. *J Theor Biol*, 349:66–73.

Manjili, M. H. (2018). A theoretical basis for the efficacy of cancer immunotherapy and immunogenic tumor dormancy: The adaptation model of immunity. *Advances in Cancer Res*, 137:17–36.

Masoudi-Nejad, A. and Wang, E. (2015). Cancer modeling and network biology: Accelerating toward personalized medicine. In *Semin Cancer Biol*, volume 30, pages 1–3. Elsevier.

Matthäus, F., Mommer, M. S., Curk, T., and Dobnikar, J. (2011). On the origin and characteristics of noise-induced Lévy walks of E. coli. *PloS one*, 6(4):e18623.

Matzavinos, A. and Chaplain, M. A. J. (2004). Travelling-wave analysis of a model of the immune response to cancer. *C R Biol*, 327(11):995–1008.

Matzavinos, A., Chaplain, M. A. J., and Kuznetsov, V. A. (2004). Mathematical modelling of the spatio-temporal response of cytotoxic T-lymphocytes to a solid tumour. *Math Med Biol*, 21(1):1–34.

Maude, S. L., Frey, N., Shaw, P. A., Aplenc, R., Barrett, D. M., Bunin, N. J., Chew, A., Gonzalez, V. E., Zheng, Z., Lacey, S. F., et al. (2014). Chimeric antigen receptor T cells for sustained remissions in leukemia. *N Engl J Med*, 371(16):1507–1517.

McGuire, M. F., Enderling, H., Wallace, D. I., Batra, J., Jordan, M., Kumar, S., Panetta, J. C., and Pasquier, E. (2013). Formalizing an integrative, multidisciplinary cancer therapy discovery workflow. *Cancer Res*, 73(20):6111–6117.

Mckeithan, T. W. (1995). Kinetic proofreading in T-cell receptor signal transduction. *Proc Nat Acad Sci*, 92(11):5042–5046.

Mellet, A., Perthame, B., and Quiros, F. (2017). A Hele–Shaw problem for tumor growth. *J Funct Anal*, 273(10):3061–3093.

Messerschmidt, J. L., Prendergast, G. C., and Messerschmidt, G. L. (2016). How cancers escape immune destruction and mechanisms of action for the new significantly active immune therapies: Helping non-immunologists decipher recent advances. *Oncologist*, 21(2):233–243.

Metzcar, J., Wang, Y., Heiland, R., and Macklin, P. (2019). A review of cell-based computational modeling in cancer biology. *JCO Clin Cancer Informatics*, 3:1–13.

Miller, M., Wei, S., Parker, I., and Cahalan, M. (2002). Two-photon imaging of lymphocyte motility and antigen response in intact lymph node. *Science*, 296(5574):1869–1873.

Mimura, M., Sakaguchi, H., and Matsushita, M. (2000). Reaction–diffusion modelling of bacterial colony patterns. *Physica A Stat Mech Appl*, 282(1-2):283–303.

Modiano, J. F. and Bellgrau, D. (2016). Fas ligand based immunotherapy: A potent and effective neoadjuvant with checkpoint inhibitor properties, or a systemically toxic promoter of tumor growth? *Discov Med*, 21(114):109–116.

Montroll, E. W. and Weiss, G. H. (1965). Random walks on lattices. II. *J Math Phys*, 6(2):167–181.

Moreno, B. H., Parisi, G., Robert, L., and Ribas, A. (2015). Anti–PD-1 therapy in melanoma. In *Semin Oncol*, volume 42, pages 466–473. Elsevier.

Morgan, R. A., Chinnasamy, N., Abate-Daga, D. D., Gros, A., Robbins, P. F., Zheng, Z., Feldman, S. A., Yang, J. C., Sherry, R. M., Phan, G. Q., et al. (2013). Cancer regression and neurologic toxicity following anti-MAGE-A3 TCR gene therapy. *J Immunother*, 36(2):133.

Morgan, R. A., Johnson, L. A., Davis, J. L., Zheng, Z., Woolard, K. D., Reap, E. A., Feldman, S. A., Chinnasamy, N., Kuan, C., Song, H., et al. (2012). Recognition of glioma stem cells by genetically modified T cells targeting EGFRvIII and development of adoptive cell therapy for glioma. *Human Gene Ther*, 23(10):1043–1053.

Morgan, R. A., Yang, J. C., Kitano, M., Dudley, M. E., Laurencot, C. M., and Rosenberg, S. A. (2010). Case report of a serious adverse event following the administration of T cells transduced with a chimeric antigen receptor recognizing ERBB2. *Mol Ther*, 18(4):843–851.

Motsch, S. and Peurichard, D. (2018). From short-range repulsion to Hele-Shaw problem in a model of tumor growth. *J Math Biol*, 76(1-2):205–234.

Müller-Richter, U. D. A., Dowejko, A., Reuther, T., Kleinheinz, J., Reichert, T. E., and Driemel, O. (2009). Analysis of expression profiles of MAGE-A antigens in oral squamous cell carcinoma cell lines. *Head Face Med*, 5(1):10.

Murray, P. J., Edwards, C. M., Tindall, M. J., and Maini, P. K. (2009). From a discrete to a continuum model of cell dynamics in one dimension. *Phys Rev E*, 80(3):031912.

Murray, P. J., Edwards, C. M., Tindall, M. J., and Maini, P. K. (2012). Classifying general nonlinear force laws in cell-based models via the continuum limit. *Phys Rev E*, 85(2):021921.

Nani, F. and Freedman, H. I. (2000). A mathematical model of cancer treatment by immunotherapy. *Math Biosci*, 163(2):159–199.

Nava-Sedeno, J. M., Hatzikirou, H., Klages, R., and Deutsch, A. (2017). Cellular automaton models for time-correlated random walks: Derivation and analysis. *Sci Reports*, 7(1):16952.

Oey, H. and Whitelaw, E. (2014). On the meaning of the word "epimutation". *Trends Genet*, 30(12):519–520.

O'Rourke, D. M., Nasrallah, M., Morrissette, J. J., Melenhorst, J. J., Lacey, S. F., Mansfield, K., Martinez-Lage, M., Desai, A. S., Brem, S., Maloney, E., et al. (2016). Pilot study of T cells redirected to EGFRvIII with a chimeric antigen receptor in patients with EGFRvIII+ glioblastoma. *J Clin Oncol*, 34(15):2067.

Othmer, H. G., Dunbar, S. R., and Alt, W. (1988). Models of dispersal in biological systems. *J Math Biol*, 26(3):263–298.

Othmer, H. G. and Hillen, T. (2002). The diffusion limit of transport equations II: Chemotaxis equations. *SIAM J Appl Math*, 62(4):1222–1250.

Ott, P. A., Hu, Z., Keskin, D. B., Shuklka, S. A., Sun, J., et al. (2017). An immunogenic personal neoantigen vaccine for patients with melanoma. *Nature*, 547(7662):217–221.

Oxford University Press (2019). Cancer. In *The Oxford English Dictionary*. Oxford University Press.

Painter, K. J. and Hillen, T. (2015). Navigating the flow: Individual and continuum models for homing in flowing environments. *J R Soc Interface*, 12(112):20150647.

Painter, K. J. and Sherratt, J. A. (2003). Modelling the movement of interacting cell populations. *J Theor Biol*, 225(3):327–339.

Pappalardo, F., Musumeci, S., and Motta, S. (2008). Modeling immune system control of atherogenesis. *Bioinformatics*, 24(15):1715–1721.

Parlato, S., De Ninno, A., Molfetta, R., Toschi, E., Salerno, D., Mencattini, A., Romagnoli, G., Fragale, A., Roccazzello, L., Buoncervello, M., et al. (2017). 3D microfluidic model for evaluating immunotherapy efficacy by tracking dendritic cell behaviour toward tumor cells. *Sci Rep*, 7(1):1093.

Pearson, K. (1905). The problem of the random walk. *Nature*, 72(1867):342.

Peltomäki, P. (2012). Mutations and epimutations in the origin of cancer. *Exp Cell Res*, 318(4):299–310.

Peng, L., Trucu, D., Lin, P., Thompson, A., and Chaplain, M. A. J. (2017). A multiscale mathematical model of tumour invasive growth. *Bull Math Biol*, 79(3):389–429.

Penington, C. J., Hughes, B. D., and Landman, K. A. (2011). Building macroscale models from microscale probabilistic models: A general probabilistic approach for nonlinear diffusion and multispecies phenomena. *Phys Rev E*, 84(4):041120.

Penington, C. J., Hughes, B. D., and Landman, K. A. (2014). Interacting motile agents: Taking a mean-field approach beyond monomers and nearest-neighbor steps. *Phy Rev E*, 89(3):032714.

Perez, C., Jukica, A., Listopad, J. J., Anders, K., Kühl, A. A., Loddenkemper, C., Blankenstein, T., and Charo, J. (2015). Permissive expansion and homing of adoptively transferred T cells in tumor-bearing hosts. *Int J Cancer*, 137(2):359–371.

Perthame, B. (2014). Some mathematical aspects of tumor growth and therapy. In *ICM 2014-International Congress of Mathematicians*.

Perthame, B., Quirós, F., Tang, M., and Vauchelet, N. (2014a). Derivation of a Hele–Shaw type system from a cell model with active motion. *Interface Free Bound*, 16(4):489–508.

Perthame, B., Quirós, F., and Vázquez, J. L. (2014b). The Hele–Shaw asymptotics for mechanical models of tumor growth. *Arch Ration Mech Anal*, 212(1):93–127.

Phan, G. Q. and Rosenberg, S. A. (2013). Adoptive cell transfer for patients with metastatic melanoma: The potential and promise of cancer immunotherapy. *Cancer Control*, 20(4):289–297.

Poleszczuk, J., Macklin, P., and Enderling, H. (2016). Agent-based modeling of cancer stem cell driven solid tumor growth. *Meth Mol Biol*, 1516:335–346.

Porter, D. L., Hwang, W., Frey, N. V., Lacey, S. F., Shaw, P. A., Loren, A. W., Bagg, A., Marcucci, K. T., Shen, A., Gonzalez, V., et al. (2015). Chimeric antigen receptor T cells persist and induce sustained remissions in relapsed refractory chronic lymphocytic leukemia. *Sci Transl Med*, 7(303):303ra139.

Postow, M. A., Chesney, J., Pavlick, A. C., Robert, C., Grossmann, K., McDermott, D., Linette, G. P., Meyer, N., Giguere, J. K., Agarwala, S. S., et al. (2015). Nivolumab and ipilimumab versus ipilimumab in untreated melanoma. *N Engl J Med*, 372(21):2006–2017.

Preziosi, L. (2003). *Cancer modelling and simulation*. CRC Press.

Radunskaya, A., de Pillis, L. G., and Gallegos, A. (2013). A model of dendritic cell therapy for melanoma. *Front Oncol*, 3:56.

Raichlen, D. A., Wood, B. M., Gordon, A. D., Mabulla, A. Z. P., Marlowe, F. W., and Pontzer, H. (2014). Evidence of Lévy walk foraging patterns in human hunter–gatherers. *Proc Nat Acad Sci*, 111(2):728–733.

Raman, M. C. C., Rizkallah, P. J., Simmons, R., Donnellan, Z., Dukes, J., Bossi, G., Le Provost, G. S., Todorov, P., Baston, E., Hickman, E., et al. (2016). Direct molecular mimicry enables off-target cardiovascular toxicity by an enhanced affinity TCR designed for cancer immunotherapy. *Sci Rep*, 6:18851.

Ramis-Conde, I., Drasdo, D., Anderson, A. R. A., and Chaplain, M. A. J. (2008). Modeling the influence of the E-cadherin-β-catenin pathway in cancer cell invasion: A multiscale approach. *Biophys J*, 95(1):155–165.

Ranft, J., Basan, M., Elgeti, J., Joanny, J.-F., Prost, J., and Jülicher, F. (2010). Fluidization of tissues by cell division and apoptosis. *Proc Natl Acad Sci USA*, 107(49):20863–20868.

Rapoport, A. P., Stadtmauer, E. A., Binder-Scholl, G. K., Goloubeva, O., Vogl, D. T., Lacey, S. F., Badros, A. Z., Garfall, A., Weiss, B., Finklestein, J., et al. (2015). NY-ESO-1–specific TCR–engineered T cells mediate sustained antigen-specific antitumor effects in myeloma. *Nat Med*, 21(8):914.

Rayleigh, L. (1880). On the resultant of a large number of vibrations of the same pitch and of arbitrary phase. *The London, Edinburgh, and Dublin Philosophical Magazine and Journal of Science*, 10(60):73–78.

Ren, J., Liu, X., Fang, C., Jiang, S., June, C. H., and Zhao, Y. (2017). Multiplex genome editing to generate universal CAR-T cells resistant to PD-1 inhibition. *Clin Cancer Res*, 23(9):2255–2266.

Restifo, N. P., Smyth, M. J., and Snyder, A. (2016). Acquired resistance to immunotherapy and future challenges. *Nat Rev Cancer*, 16(2):121–126.

Rhee, I., Shin, M., Hong, S., Lee, K., Kim, S. J., and Chong, S. (2011). On the Lévy-walk nature of human mobility. *IEEE/ACM Transact Netw*, 19(3):630–643.

Richardson, L. F. (1926). Atmospheric diffusion shown on a distance-neighbour graph. *Proc R Soc Lond Ser A*, 110(756):709–737.

Robbins, F., Kassim, S. H., Tran, T. L. N., Crystal, J. S., Morgan, R. A., Feldman, S. A., Yang, J. C., Dudley, M. E., Wunderlich, J. R., Sherry, R. M., et al. (2015). A pilot trial using lymphocytes genetically engineered with an NY-ESO-1–reactive T-cell receptor: Long-term follow-up and correlates with response. *Clin Cancer Res*, 21(5):1019–1027.

Robbins, P. F., Morgan, R. A., Feldman, S. A., Yang, J. C., Sherry, R. M., Dudley, M. E., Wunderlich, J. R., Nahvi, A. V., Helman, L. J., Mackall, C. L., et al. (2011). Tumor regression in patients with metastatic synovial cell sarcoma and melanoma using genetically engineered lymphocytes reactive with NY-ESO-1. *J Clin Oncol*, 29(7):917.

Roch, N., Kutup, A., Vashist, Y., Yekebas, E., Kalinin, V., and Izbicki, J. R. (2010). Coexpression of MAGE-A peptides and HLA class I molecules in hepatocellular carcinoma. *Anticancer Res*, 30(5):1617–1623.

Rodgers, D. T., Mazagova, M., Hampton, E. N., Cao, Y., Ramadoss, N. S., Hardy, I. R., Schulman, A., Du, J., Wang, F., Singer, O., et al. (2016). Switch-mediated activation and retargeting of CAR-T cells for B-cell malignancies. *Proc Nat Acad Sci*, 113(4):E459–E468.

Rohrs, J. A., Wang, P., and Finley, S. D. (2019). Understanding the dynamics of T-cell activation in health and disease through the lens of computational modeling. *JCO Clin Cancer Inform*, 3:1–8.

Roose, T., Chapman, S. J., and Maini, P. K. (2007). Mathematical models of avascular tumor growth. *SIAM Rev*, 49(2):179–208.

Rozenberg, G. (2011). B4: Lymphocytes. In *Microscopic Haematology: A Practical Guide for the Laboratory*, page 106. Elsevier Australia.

Sadelain, M., Brentjens, R., and Rivière, I. (2013). The basic principles of chimeric antigen receptor design. *Cancer Discov*, 3(4):388–398.

Sadikovic, B., Al-Romaih, K., Squire, J. A., and Zielenska, M. (2008). Cause and consequences of genetic and epigenetic alterations in human cancer. *Curr Genomics*, 9(6):394–408.

Sahin, U., Derhovanessian, E., Miller, M., Kloke, B., Simon, P., et al. (2017). Personalized RNA mutanome vaccines mobilize poly-specific therapeutic immunity against cancer. *Nature*, 547(7662):222–226.

Schmid, D. A., Irving, M. B., Posevitz, V., Hebeisen, M., Posevitz-Fejfar, A., Sarria, J. C. F., Gomez-Eerland, R., Thome, M., Schumacher, T. N. M., Romero, P., et al. (2010). Evidence for a TCR affinity threshold delimiting maximal CD8 T cell function. *J Immunol*, 184(9):4936–4946.

Scholler, J., Brady, T. L., Binder-Scholl, G., Hwang, W., Plesa, G., Hege, K. M., Vogel, A. N., Kalos, M., Riley, J. L., Deeks, S. G., et al. (2012). Decade-long safety and function of retroviral-modified chimeric antigen receptor T cells. *Sci Transl Med*, 4(132):132ra53.

Schreibelt, G., Bol, K. F., Westdorp, H., Wimmers, F., Aarntzen, E. H. J. G., Duiveman-de Boer, T., van de Rakt, M. W. M. M., Scharenborg, N. M., de Boer, A. J., Pots, J. M., et al. (2016). Effective clinical responses in metastatic melanoma patients after vaccination with primary myeloid dendritic cells. *Clin Cancer Res*, 22(9):2155–2166.

Schueler-Furman, O., Elber, R., and Margalit, H. (1998). Knowledge-based structure prediction of MHC class I bound peptides: A study of 23 complexes. *Fold Des*, 3(6):549–564.

Schumacher, T. N. and Hacohen, N. (2016). Neoantigens encoded in the cancer genome. *Curr Opinion Immunol*, 41:98–103.

Sharma, P. and Allison, J. P. (2015). The future of immune checkpoint therapy. *Science*, 348(6230):56–61.

Shay, J. W., Zou, Y., Hiyama, E., and Wright, W. E. (2001). Telomerase and cancer. *Hum Mol Gen*, 10(7):677–685.

Sherratt, J. A. and Chaplain, M. A. J. (2001). A new mathematical model for avascular tumour growth. *J Math Biol*, 43(4):291–312.

Shlesinger, M. F., Klafter, J., and West, B. J. (1986). Lévy walks with applications to turbulence and chaos. *Phys A Stat Mech Appl*, 140(1-2):212–218.

Shlesinger, M. F., Klafter, J., and Wong, Y. M. (1982). Random walks with infinite spatial and temporal moments. *J Stat Phys*, 27(3):499–512.

Simpson, M. J., Landman, K. A., and Hughes, B. D. (2010). Cell invasion with proliferation mechanisms motivated by time-lapse data. *Physica A Stat Mech Appl*, 389(18):3779–3790.

Simpson, M. J., Merrifield, A., Landman, K. A., and Hughes, B. D. (2007). Simulating invasion with cellular automata: Connecting cell-scale and population-scale properties. *Phys Rev E*, 76(2):021918.

Slansky, J. E. and Jordan, K. R. (2010). The Goldilocks model for TCR: Too much attraction might not be best for vaccine design. *PLoS Biol*, 8(9):e1000482.

Smith, S. N., Wang, Y., Baylon, J. L., Singh, N. K., Baker, B. M., Tajkhorshid, E., and Kranz, D. M. (2014). Changing the peptide specificity of a human T cell receptor by directed evolution. *Nature Comm*, 5:5223.

Sotolongo-Costa, O., Molina, L. M., Perez, D. R., Antoranz, J., and Reyes, M. (2003). Behavior of tumors under nonstationary therapy. *Physica D*, 178(3):242–253.

Spranger, S. (2016). Mechanisms of tumor escape in the context of the T-cell-inflamed and the non-T-cell-inflamed tumor microenvironment. *Int Immunol*, 28(8):383–391.

Spranger, S. and Gajewski, T. F. (2018). Impact of oncogenic pathways on evasion of antitumour immune responses. *Nat Rev Cancer*, 18(3):139.

Stage, H., Fedotov, S., and Méndez, V. (2016). Proliferating Lévy walkers and front propagation. *Math Model Nat Phenom*, 11(3):157–178.

Stevens, A. (2000). The derivation of chemotaxis equations as limit dynamics of moderately interacting stochastic many-particle systems. *SIAM J Appl Math*, 61(1):183–212.

Stevens, A. and Othmer, H. G. (1997). Aggregation, blowup, and collapse: The abc's of taxis in reinforced random walks. *SIAM J Appl Math*, 57(4):1044–1081.

Stewart, T. J. and Abrams, S. I. (2008). How tumours escape mass destruction. *Oncogene*, 27(45):5894–5903.

Stone, J. D., Chervin, A. S., and Kranz, D. M. (2009). T-cell receptor binding affinities and kinetics: Impact on T-cell activity and specificity. *Immunology*, 126(2):165–176.

Takayanagi, T. and Ohuchi, A. (2001). A mathematical analysis of the interactions between immunogenic tumor cells and cytotoxic T lymphocytes. *Microbiol Immunol*, 45(10):709–715.

Tan, M. P., Gerry, A. B., Brewer, J. E., Melchiori, L., Bridgeman, J. S., Bennett, A. D., Pumphrey, N. J., Jakobsen, B. K., Price, D. A., Ladell, K., et al. (2015). T cell receptor binding affinity governs the functional profile of cancer-specific CD8+ T cells. *Clin Exp Immunol*, 180(2):255–270.

Tang, M., Vauchelet, N., Cheddadi, I., Vignon-Clementel, I., Drasdo, D., and Perthame, B. (2014). Composite waves for a cell population system modeling tumor growth and invasion. In *Partial Differential Equations: Theory, Control and Approximation*, pages 401–429. Springer.

Taylor, G. I. (1922). Diffusion by continuous movements. *Proc Lond Math Soc*, 2(1):196–212.

Tejedor, V., Bénichou, O., and Voituriez, R. (2009). Global mean first-passage times of random walks on complex networks. *Phys Rev E*, 80(6):065104.

Tel, J., Aarntzen, E. H. J. G., Baba, T., Schreibelt, G., Schulte, B. M., Benitez-Ribas, D., Boerman, O. C., Croockewit, S., Oyen, W. J. G., van Rossum, M., et al. (2013). Natural human plasmacytoid dendritic cells induce antigen-specific T-cell responses in melanoma patients. *Cancer Res*, 73(3):1063–1075.

Teng, M. W. L., Swann, J. B., Koebel, C. M., Schreiber, R. D., and Smyth, M. J. (2008). Immune-mediated dormancy: An equilibrium with cancer. *J Leukocyte Biol*, 84(4):988–993.

Tomasetti, C. and Levy, D. (2010). An elementary approach to modeling drug resistance in cancer. *Math Biosci Eng*, 7(4):905.

Tong, J. C., Tan, T. W., and Ranganathan, S. (2004). Modeling the structure of bound peptide ligands to major histocompatibility complex. *Protein Sci*, 13(9):2523–2532.

Urosevic, M., Braun, B., Willers, J., Burg, G., and Dummer, R. (2005). Expression of melanoma-associated antigens in melanoma cell cultures. *Exp Dermatol*, 14(7):491–497.

Van Liedekerke, P., Palm, M., Jagiella, N., and Drasdo, D. (2015). Simulating tissue mechanics with agent-based models: Concepts, perspectives and some novel results. *Comput Part Mech*, 2(4):401–444.

Van Tongelen, A., Loriot, A., and De Smet, C. (2017). Oncogenic roles of DNA hypomethylation through the activation of cancer-germline genes. *Cancer Lett*, 396:130–137.

VanSeggelen, H., Tantalo, D. G. M., Afsahi, A., Hammill, J. A., and Bramson, J. L. (2015). Chimeric antigen receptor-engineered T cells as oncolytic virus carriers. *Mol Ther Oncolytics*, 2:15014.

Verdegaal, E. M. E., De Miranda, N. F. C. C., Visser, M., Harryvan, T., Van Buuren, M. M., Andersen, R. S., Hadrup, S. R., Van Der Minne, C. E., Schotte, R., Spits, H., et al. (2016). Neoantigen landscape dynamics during human melanoma-T cell interactions. *Nature*, 536(7614):91.

Walker, R. and Enderling, H. (2016). From concept to clinic: Mathematically informed immunotherapy. *Curr Probl Cancer*, 40(11):68–83.

Walker, R., Navas, P. E., Friedman, S. H., Galliani, S., Karolak, A., Macfarlane, F. R., Noble, R., Poleszczuk, J., Russell, S., Rejniak, K. A., et al. (2016). Enhancing synergy of CAR T cell therapy and oncolytic virus therapy for pancreatic cancer. *bioRxiv*, page 055988.

Wang, S. and Lin, S. (2013). Tumor dormancy: Potential therapeutic target in tumor recurrence and metastasis prevention. *Exp Hematology & Oncol*, 2(1):29.

Wang, Y.-Y., Lehuédé, C., Laurent, V., Dirat, B., Dauvillier, S., Bochet, L., Le Gonidec, S., Escourrou, G., Valet, P., and Muller, C. (2012). Adipose tissue and breast epithelial cells: A dangerous dynamic duo in breast cancer. *Cancer Lett*, 324(2):142–151.

Wang, Z., Butner, J. D., Kerketta, R., Cristini, V., and Deisboeck, T. S. (2015). Simulating cancer growth with multiscale agent-based modeling. In *Semin Cancer Biol*, volume 30, pages 70–78. Elsevier.

Ward, J. P. and King, J. R. (1997). Mathematical modelling of avascular-tumour growth. *Math Med Biol*, 14(1):39–69.

Ward, J. P. and King, J. R. (1999). Mathematical modelling of avascular-tumour growth II: Modelling growth saturation. *Math Med Biol*, 16(2):171–211.

Weinberg, R. A. (2007a). Crowd control: Tumour immunology and immunotherapy. In Weinberg, R. A., editor, *The Biology of Cancer*, chapter 15, pages 655–724. Garland Science, U.S.A.

Weinberg, R. A. (2007b). Moving out: Invasion and metastasis. In Weinberg, R. A., editor, *The Biology of Cancer*, chapter 14, pages 587–654. Garland Science, U.S.A.

Weninger, W., Biro, M., and Jain, R. (2014). Leukocyte migration in the interstitial space of non-lymphoid organs. *Nat Rev Immunol*, 14(4):232–246.

Wilgenhof, S., Corthals, J., Heirman, C., van Baren, N., Lucas, S., Kvistborg, P., Thielemans, K., and Neyns, B. (2016). Phase II study of autologous monocyte-derived mRNA electroporated dendritic cells (TriMixDC-MEL) plus ipilimumab in patients with pretreated advanced melanoma. *J Clin Oncol*, 34(12):1330–1338.

Wilgenhof, S., Van Nuffel, A. M. T., Corthals, J., Heirman, C., Tuyaerts, S., Benteyn, D., De Coninck, A., Van Riet, I., Verfaillie, G., Vandeloo, J., et al. (2011). Therapeutic vaccination with an autologous mRNA electroporated dendritic cell vaccine in patients with advanced melanoma. *J Immunother*, 34(5):448–456.

Wilkie, K. P. and Hahnfeldt, P. (2013). Mathematical models of immune-induced cancer dormancy and the emergence of immune evasion. *Interface Focus*, 3(4):20130010.

Wischnewski, F., Pantel, K., and Schwarzenbach, H. (2006). Promoter demethylation and histone acetylation mediate gene expression of MAGE-A1,-A2,-A3, and-A12 in human cancer cells. *Mol Cancer Res*, 4(5):339–349.

Wolf, K., Muller, R., Borgmann, S., Bröcker, E. B., and Friedl, P. (2003). Amoeboid shape change and contact guidance: T-lymphocyte crawling through firbrillar collagen is independent of matrix remodelling by MMPs and other proteases. *Blood*, 102(9):3262–3269.

Wolfram, S. (1983). Statistical mechanics of cellular automata. *Rev Mod Phys*, 55(3):601.

Wosniack, M. A., Santos, M. C., Raposo, E. P., Viswanathan, G. M., and da Luz, M. G. E. (2017). The evolutionary origins of Lévy walk foraging. *PLoS Comput Biol*, 13(10):e1005774.

Wu, A., Liao, D., Kirilin, V., Lin, K., Torga, G., Qu, J., Liu, L., Sturm, J. C., Pienta, K., and Austin, R. (2018). Cancer dormancy and criticality from a game theory perspective. *Cancer Convergence*, 2(1):1.

Wu, C., Roybal, K. T., Puchner, E. M., Onuffer, J., and Lim, W. A. (2015). Remote control of therapeutic T cells through a small molecule–gated chimeric receptor. *Science*, 350(6258):aab4077.

Yarchoan, M., Johnson, B. A., Lutz, E. R., Laheru, D. A., and Jaffee, E. M. (2017). Targeting neoantigens to augment antitumour immunity. *Nat Rev Cancer*, 17(4):209–222.

Ye, Q., Loisiou, M., Levine, B. L., Suhoski, M. M., Riley, J. L., June, C. H., Coukos, G., and Powell, D. J. (2011). Engineered artificial antigen presenting cells facilitate direct and efficient expansion of tumor infiltrating lymphocytes. *J Transl Med*, 9(1):131.

Yeh, A. C. and Ramaswamy, S. (2015). Mechanisms of cancer cell dormancy? Another hallmark of cancer? *Cancer Res*, 75(23):5014–5022.

Yokoi, C., Hernández-Machado, A., and Ramírez-Piscina, L. (1990). Some exact results for the lattice covering time problem. *Phys Lett A*, 145(2):82–86.

Yong, C. S. M., Dardalhon, C. D., Taylor, N., Darcy, P., and Kershaw, M. H. (2017). CAR-T-cell therapy of solid tumors. *Immunol Cell Biol*, 95(4):356–363.

Zaburdaev, V., Denisov, S., and Klafter, J. (2015). Lévy walks. *Rev Mod Phys*, 87(2):483.

Zaburdaev, V. Y., Biais, N., Schmiedeberg, M., Eriksson, J., Jonsson, A. B., Sheetz, M. P., and Weitz, D. A. (2014). Uncovering the mechanism of trapping and cell orientation during Neisseria Gonorrhoeae twitching motility. *Biophys J*, 107(7):1523–1531.

Zaburdaev, V. Y. and Chukbar, K. V. (2002). Enhanced superdiffusion and finite velocity of Lévy flights. *J Exp Theor Phys*, 94(2):252–259.

Zajac, P., Schultz-Thater, E., Tornillo, L., Sadowski, C., Trella, E., Mengus, C., Iezzi, G., and Spagnoli, G. C. (2017). MAGE-A antigens and cancer immunotherapy. *Front Med*, 4:18.

Zhang, Y., Chaux, P., Stroobant, V., Eggermont, A. M. M., Corthals, J., Maillère, B., Thielemans, K., Marchand, M., Boon, T., and van der Bruggen, P. (2003). A MAGE-3 peptide presented by HLA-DR1 to CD4+ T cells that were isolated from a melanoma patient vaccinated with a MAGE-3 protein. *J Immunol*, 171(1):219–225.

Zhang, Y., Stroobant, V., Russo, V., Boon, T., and Van der Bruggen, P. (2002). A MAGE-A4 peptide presented by HLA-B37 is recognized on human tumors by cytolytic T lymphocytes. *Tissue Antigens*, 60(5):365–371.

Zumofen, G. and Klafter, J. (1993). Scale-invariant motion in intermittent chaotic systems. *Phys Rev E*, 47(2):851.